The Effect of Ageing on the Clean-up of Dusts and Soils after a Nuclear Contamination Event

Gemma Louise Woodward

Submitted in accordance with the requirements for the degree of
Doctor of Philosophy

The University of Leeds
School of Earth and Environment

June 2018

The candidate confirms that the work submitted is her own, except where work which has formed part of jointly-authored publications has been included. The contribution of the candidate and the other authors to this work has been explicitly indicated below. The candidate confirms that appropriate credit has been given within the thesis where reference has been made to the work of others.

The work presented in Chapter 4 of this thesis is submitted for publication: **Woodward, G. L.,** Peacock, C. L., Otero-Fariña, A., Thompson, O. R., Brown, A. P., and Burke, I. T. (in press) A universal uptake mechanism for cobalt(II) on soil constituents: ferrihydrite, kaolinite, humic acid, and organo-mineral composites. *Geochimica et Cosmochimica Acta*

Candidate's contribution (G.L. Woodward) – Developed the concept, prepared the manuscript, conducted batch sorption experiments, interpreted data, developed EQLFOR model, gathered, interpreted and fitted Co EXAFS spectra. Caroline Peacock - Formed initial concept, aided data interpretation, aided in model development, commented on the manuscript. Alba Otero-Fariña - provided experiment methodology, provided humic acid, commented on manuscript. Olivia R Thompson - Formed initial concept, commented on manuscript. Andrew P Brown - assisted with STEM, EDS, and EELS data collection and analysis, commented on manuscript. Ian T Burke - Formed initial concept, assisted in data interpretation, trained candidate in EXAFS fitting and analysis, commented on the manuscript.

Acknowledgements

I would like to massively thank my supervisors, Ian Burke and Caroline Peacock, who first of all gave me this unexpected opportunity and then supported me throughout my PhD by sharing their knowledge and advice. I'd also like to thank Olivia Thompson at the NNL for her support.

This thesis would have been impossible without collaborating with a number of extremely talented individuals. Therefore, I'd like to thank Alba Otero-Fariña for being my source of Spanish humic acid and helping me when I was a nervous first year, Andy Brown for his help on the TEM and answering my ridiculously basic questions, and Giannantonio Cibin, Steve Parry, and Andy Dent for their expertise on beamline B18 at Diamond Light Source.

My research would not have gone as smoothly as it did without Andy Connelly managing the Cohen labs and being a friendly face, for which I'm extremely grateful. I'd also like to thank Fiona Keay for her help whenever I panicked and thought I'd broke something. Thanks go to Stephen Reid for ICP analysis and Lesley Neve for her help on the XRD.

I'd also like to thank all of the members of the Cohen Geochemistry group over my four years here for their advice, support, and being there to moan about lab work with. I couldn't have found a friendlier group of people to share labs with and you'll all be missed when I leave. Especially Daniela and Josie for being my casual therapists at various times throughout the four years; your support when times got rough helped me carry on despite everything. Also, Aislinn, Dave, and Emma – Ian's random radioactivity conferences would not have been as fun without you.

Another big thank you goes to Lizane Pamer, without whom I would have given up from pH electrode problems less than 6 months into the PhD. I owe my understanding of pH probes to her, as well as hours of entertainment that probably ended up with me procrastinating more than I should have.

To the Leeds University Pokémon raid group – Liam, Owen, Lucy, Melanie, Ping, Draper, Mat, Katie, Lauren, Charlotte and the others – I would have finished my thesis a lot sooner if it hadn't been for you guys

I would like to thank my parents, Carol and John, who have supported all of my academic achievements and goals throughout the years, even when the most they understood of my research was “something about soils and she gets to travel a lot”. I would also like to thank my brother, Nick, for taking no interest in my PhD whatsoever and I’m sure he’ll take great pleasure in reminding me that I’ll always be his little sister no matter how many qualifications I get.

And to George, for sticking with me through panic attacks and when I was just being a little crazy. Your support has meant the world to me and the last two and a half years wouldn’t have gone so smoothly without you by my side.

Abstract

Cobalt is a waste product in many industrial processes and its most common radioactive isotope – ^{60}Co – is a by-product of nuclear reactors. If released into the environment, cobalt would cause much harm as its stable isotope is toxic to plants and animals in large quantities and the radioactive isotope decays via gamma radiation. This thesis investigates the sorption of Co onto the surfaces of common soil constituents and composites of these, as well as several natural soils, to help aid decontamination procedures.

The key findings of this thesis were with regard to Co sorption behaviour to substances commonly found in soils. At high pH, Cobalt was found to form binuclear bidentate inner-sphere complexes with ferrihydrite, kaolinite, humic acid, as well as composites of the minerals with humic acid. At low pH, Co sorbed to kaolinite, humic acid, and the kaolinite-humic acid composite via outer-sphere complexes. STEM analysis showed that Co sorbed to one face of the kaolinite particles where high affinity AlOH sites are located. Above pH 5, humic acid behaves colloidally and Co bound to these colloidal particles are mobile. A surface complexation model was developed based on this information that was capable of modelling Co sorption to the end-member phases. However, Co sorption to the composite phases cannot be modelled assuming linear additivity of the end-member phases.

This model was further tested with Co sorption to soils with a range of constituents and carbon contents. Co sorption to peat was high across the entire pH range and the model produced a good fit to this. Sorption to the agricultural soil and sediment was low below pH 6, but increased to 100% by pH 8. Model fits to these replicated the overall behaviour but did not make accurate detailed predictions.

Co sorption to ferrihydrite and humic acid were not found to increase with ageing, though sorption to sorption to kaolinite increased up to 28 days. Co became incorporated into ferrihydrite with longer sorption periods, thus decreasing the amount of Co desorbed, and desorption by citric acid or HCl were the most effective due to dissolution of the ferrihydrite releasing incorporated Co. EDTA was the most effective at desorbing Co from kaolinite and humic acid as it

desorbed Co via chelation. The most efficient method of decontamination based on these experiments would be to wash with EDTA within 7 days of the contamination event, as after this period of time EDTA removed from ferrihydrite similar amounts of Co as citric acid and HCl.

The findings of this thesis mark a significant advance in understanding the fundamental processes governing the sorption and desorption of Co in the environment. Particularly, it shows that while Co sorption to soils can be modelled assuming parameters based on sorption to pure phases, these models are missing the complexity required to fully model sorption to soils. Therefore it is essential for future work to further constrain the sorption processes controlling Co behaviour to soil phases. Furthermore, decontamination techniques are affected by the length of the sorption equilibrium period for iron oxides. This suggests that for soils with high Fe contents decontamination should be attempted as soon as possible.

Table of Contents

List of Tables

List of Figures

Chapter 1: Introduction

1.1 Background context and rationale

Cobalt-60 was chosen to study because a large number of industries use it as a radioactive source, therefore it is possible that it would be the radionuclide of choice in a radiological dispersion device (RDD) (Luckey and Kansas, 2003). ^{60}Co is a synthetic radionuclide and is also one of the most highly radioactive sources for an RDD; it has a half-life of 5.27 years and 1 g of cobalt-60 has an activity of 44 TBq. As it decays through gamma radiation it is not easily contained through shelding. It is a major radionuclide generated in the civil nuclear industry as a by-product of nuclear fission reactions and is present in low-level liquid waste. Therefore there is an interest in understanding its behaviour in the environment should there be an unexpected event wherein it is released into the surface and sub-surface. Most radionuclides formed in nuclear reactors have low solubility, and so accumulate in the upper soil layers or interstitial system of sediments in aquatic systems (Igwe et al., 2005). For example, Smith et al. (2008) found that 98 % of ^{60}Co remained in the upper 15 cm of soil after 1 year. As ^{60}Co has a half-life of 5.27 years, it is essential to efficiently decontaminate an area to prevent dangerous doses of radiation affecting life, as the amount present will not naturally decay quickly.

Soils are rarely made up of just 1 or 2 components, and so it is necessary to understand how Co interacts with soil constituents on their own and as a mixture as this knowledge will assist in determining the most effective decontamination technique. This mechanistic understanding can be input to surface complexation models to test whether current knowledge is accurate and compare how well the model predicts sorption compared to macroscopic data of the systems being tested. By combining models of sorption to a number of soil components, the knowledge gained from these can then be used to predict how Co would react in a natural soil. It is possible to test these models by sorbing Co to a number of different soils and comparing the predicted sorption to the collected data. This process allows us to test whether our understanding gained from the simple

systems fully explains cobalt's sorption behaviour in a more complex natural system.

After a nuclear contamination event, the initial response is not to immediately decontaminate the affected area. First, the nature of the incident needs to be assessed, the exact radionuclides involved need to be determined, and it needs to be decided whether clean-up is necessary and, if so, which would be the most appropriate decontamination method. This is likely to result in the radionuclide being in the environment for a period of time, and this could affect the efficiency of any decontamination techniques that are put into place.

In the case of there being a time delay, it is essential to know whether there is an ageing period past which decontamination becomes significantly less efficient. Knowing about a potential critical ageing period could influence decisions made in the aftermath of a contamination event, and potentially increase the priority of remediation. In particular, this would prevent a waste of resources if - without this understanding - decontamination would be attempted after the critical ageing period has passed resulting in ineffective remediation.

1.2 Aims and objectives

The overarching aim of this thesis was to understand the sorption behaviour of Co to substances commonly found in soils and how this affects the mobility of Co^{2+}. To fulfil this aim, a number of specific objectives were tested:

- Determine the macroscopic sorption behaviour of Co with ferrihydrite, kaolinite, humic acid, and ferrihydrite-humic acid and kaolinite-humic acid composites. Establish whether the behaviour was affected by ionic strength of the system or (in the case of the organo-mineral composites) the carbon content of the composites,
- Use EXAFS spectroscopy to determine the local environment of Co sorption to the sorption phases,
- Input the knowledge gained from EXAFS into a thermodynamic surface complexation model to be able to predict Co sorption to the organo-mineral composites,

- Determine whether Co sorption to natural soils is comparable to that of Co sorption to ferrihydrite, kaolinite, humic acid, or composites of ferrihydrite-humic acid or kaolinite-humic acid,
- Observe whether Co sorption to ferrihydrite, kaolinite, and humic acid changes over time,
- Determine the most effective desorption agent to release Co back into solution after several different sorption equilibration times.

1.3 Thesis Structure

This thesis is structured to first give an overview of the project in Chapter 1. Each chapter then intends to inform the reader of knowledge that will lead to a final understanding of the stated objectives.

Chapter 2 presents a detailed review of the literature, including discussion of the structure of soils and the chemistry and mineralogy of key minerals discussed in this work, sorption theory, the geochemical behaviour of Co, and current decontamination methods.

Chapter 3 of this thesis presents a detailed description of the materials and methods employed in the research of this work. Detailed relevant background to the techniques used is also given.

Chapter 4 is the first results chapter and presents an investigation of Co sorption to ferrihydrite, kaolinite, humic acid, and organo-mineral composites. The objectives for this investigation were addressed by a detailed experimental programme with a range of Co concentrations (10^{-5} – 10^{-3} mol L^{-1}), and ionic strengths (10^{-3} – 10^{-1} mol L^{-1}). The experiments were conducted across the pH range 3.5 – 8.5. The EXAFS results were interpreted using the Demeter package (Ravel and Newville, 2005), and the macroscopic and EXAFS results were input to the EQLFOR surface complexation model (Sherman et al., 2008; Sherman, 2009). High-resolution TEM was used to supplement the microscopic EXAFS data and to gain an image of the location of Co sorbed to ferrihydrite, kaolinite, and humic acid.

Chapter 5 builds on this work by exploring the Co sorption behaviour to 3 soils of different origins and C contents. Batch sorption experiments were used and the

over the pH range 3.5 to 8.5 for the 3 soils and the results were again input to EQLFOR.

Chapter 6 then focusses on the effect of ageing and desorption on Co sorption to ferrihydrite, kaolinite, and humic acid. Batch sorption experiments were carried out at pH 8 and left to equilibrate for either 1, 7, 28 or 84 days, before the supernatant was replaced by one of 4 desorption agents: DIW, EDTA, citric acid, or HCl. These were shaken for 1 day before being sampled to determine how much Co was in solution.

Finally, Chapter 7 summarises the conclusions from this work together with an overall discussion of the results.

Chapter 2 : Literature Review

2.1 Sources of Cobalt

Cobalt is a naturally occurring element that is found widely in rocks, soils, water, and vegetation (Gál et al., 2008). Easily weathered minerals – such as olivine, hornblende, and augite (Mitchell, 1967) – often contain Co^{2+} up to 8% (Young, 1957) as it is incorporated into the crystal lattice by substituting with Fe^{2+} and Mg^{2+} because they have similar ionic radii (Co^{2+} = 8.2 nm, Mg^{2+} = 7.8 nm, and Fe^{2+} = 8.3 nm) (Smith and Paterson, 1995). The concentration of Co in sedimentary rocks is related to the composition of the material that was originally weathered, and so its concentration can vary from 0.06 ppm in quartz to 14 ppm in shales (Tatsumoto, 1957; Carr and Turekian, 1961; Mitchell, 1967).

Co ores (such as cobaltite – CoAsS – and linnaeite – Co_3S_4) are found in a number of countries including Canada, Russia and Democratic Republic of Congo, where it is mined and refined for use in industry. Co is also commonly extracted as a by-product of copper and nickel mining because Co ores are rare and small in size compared to the mining fields of copper and nickel (Mudd et al., 2013). Industrial uses vary widely, as they include the use of Co compounds as paint pigments, as well as creating corrosion- and wear-resistant alloys when combined with iron and nickel (Jacobs and Walter, 2005).

Many forms of anthropogenic activity release Co into the environment. Coal power plants release Co that is associated with fine particulate matter, fly ash, and bottom ash (Reddy et al., 2005). The amount of Co emitted is dependent on its concentration in the initial fuel (Reddy et al., 2005) with concentrations ranging from 2.1 (Coles et al., 1979) to 9.6 $\mu g\ g^{-1}$ (Raask, 1985) in coals. Vehicle exhausts are also known to emit Co, with concentrations increasing from 0.15 ng m^{-3} at roof top level to 0.47 ng m^{-3} at street level (Johansson et al., 2009). Cobalt emissions have also been associated with cement plants (Chen et al., 2010), glassworks (Jandová et al., 2005), and the petroleum industry (Silva et al., 2015).

Cobalt can also exist as a radioactive isotope, of which ^{60}Co has the longest half-life (~5 years). Cobalt-60 is produced as a low-level liquid waste from nuclear power reactors (Bangash et al., 1992) and is present in the cooling waters of nuclear reactors (Motojima et al., 1978). ^{60}Co is created artificially by the activation of stable ^{59}Co by bombarding it with neutrons. The ^{59}Co absorbs a neutron, converting it to ^{60}Co (Ward Whicker and Schultz, 1982). This then decays by gamma and beta radiation to the stable ^{60}Ni (King, 1994):

$$^{59}_{27}Co + ^{1}_{0}n \rightarrow ^{60}_{27}Co \xrightarrow[t_{\frac{1}{2}}=5.27\ years]{} ^{60}_{28}Ni + ^{0}_{-1}\beta + \gamma \quad (2.1)$$

2.2 Health Effects

Cobalt is a bioessential nutrient due to its compounds assisting in the formation of haemoglobin (Aubert and Pinta, 1977) and being a central atom in vitamin B_{12} (Bruland, 1983). Vitamin B_{12} is a coenzyme involved in many biological reactions, such as DNA synthesis (Andres et al., 2004), meaning that a lack of Co could cause serious harm if there is a deficiency. In plants, Co was found to be important in N_2 fixation as increasing the supply of Co resulted in an increase in rhizobial growth, N_2 fixation, and production of vitamin B_{12} (Kliewer and Evans, 1963). In leguminous plants (e.g sweet lupin) a Co deficiency was found to delay the onset of N_2 fixation by several weeks (Dilworth et al., 1979). Fauna suffering from a Co deficiency show symptoms such as a loss of appetite, lack of growth, and low fertility (Mengel and Kirkby, 1978). A deficiency of vitamin B_{12} in humans can result in disturbances in the nervous system, and leads to the blood disease pernicious anemia, which causes the deterioration of cells in bone marrow that are responsible for replacing blood (Enghag, 2004).

On the other hand, a surplus of Co can also be damaging to lifeforms. In plants, Co toxicity alters the structure and number of chloroplasts in a leaf and in some plants it inhibits enzymes involved in the fixation of CO_2 (Palit et al., 1994). This results in leaf fall, inhibition of greening, and reduced shoot weight (Palit et al., 1994). Excessive intake of Co in animals can cause heart disease, and in cases where this resulted in death the Co concentration was an order of magnitude greater than average (Tokaz et al., 2013).

Radioactive ^{60}Co decays producing beta/gamma radiation, which can have harmful effects on living organisms if they receive a high doses. At high doses of radiation functional cells (as opposed to structural cells) of an organ die (Mettler and Voelz, 2002). However, this may not cause harm if the cells are not essential for survival. But if a large number of cells die, or those that are affected are critical to survival, then symptoms such as vomiting, fatigue, and fever can occur in humans (the severity of which are dependent on the dose of radiation received) (Anno et al., 1989).

In contrast, plants have been shown to benefit from exposure to gamma radiation. Irradiating hard wheat and chickpea seeds with a low dose of radiation (≤25 Gy) was found to increase the root number and root length (Melki and Sallami, 2008; Melki and Marouani, 2010) while irradiating tomato seeds with up to 10 Gy caused early ripening of

the fruits, and consequently increases in the number and weight of ripe fruit (Sidrak and Suess, 1973).

Too high of an exposure to radiation can inhibit plant growth. Bartlett pears that were subjected to 3000 – 4000 Gy did not ripen even when all other factors benefitted ripening (Maxie et al., 1966). The mean survival rate of *Curcuma alismatifolia* decreased from 63% at a dose of 20 Gy to 7% at 30 Gy and then to 2% at 40 Gy (Lee Abdullah et al., 2009). As well as a decreasing survival rate with increased doses of radioactivity, Lee Abdullah et al. (2009) found that the height of the plants and number of leaves decreased.

Therefore, while low concentration levels of Co are essential for living organisms to function, and even low doses of gamma radiation can be beneficial to plants, high amounts are poisonous to plant and animals. This results in the removal of Co and its radioactive isotopes to be necessary in order to prevent harm to people and the environment.

2.3 Geochemical Behaviour of Cobalt

Metallic Co is not reactive with air, only forming Co_3O_4 when heated and if the reaction occurs above 900°C, cobalt(II) oxide, CoO, is formed. Cobalt metal does react directly with halogens to form a variety of cobalt(II) salts, including $CoBr_2$, $CoCl_2$, and CoI_2. Additionally, cobalt dissolves in sulfuric acid to form solutions containing aqueous Co^{2+} (Jacobs and Walter, 2005).

Cobalt has four oxidation states: Co^{4+}, Co^{3+}, Co^{2+}, and Co^{1+}, although Co^{3+} and Co^{2+} are the most common (Ma and Hooda, 2010). Co^{3+} is not stable in aqueous solution (Baes and Mesmer, 1976), and so it often precipitates as sulphides, or is adsorbed by or incorporated into hydrous oxide minerals such as Mn(III, IV) oxides as these oxides precipitate in the same Eh-pH conditions that Co^{3+} is present (Kabata-Pendias, 2011; Swanner et al., 2014). It can be stabilised by forming a complex with a ligand (e.g. EDTA or NH_3) and may then be present in aqueous solutions (Krupka and Serne, 2002). In contrast, Co^{2+} is stable in aqueous solution and is mobile in oxidising acidic environments (Fig. 2.1) (Kabata-Pendias, 2011). Despite this, Co^{2+} mobility is limited in

oxidising environments because it is strongly associated with manganese and iron oxides found in soils and sediments (Wasserman et al., 2001). Under specific conditions – such as transient waterlogging – Mn and Fe can become reduced, which causes the release of Co^{2+} that is then able to leach deeper into the soil layers (Baize, 1997). This results in a higher rate of weathering in poorly drained environments and these soils will have a higher concentration of available Co^{2+} which would cause more being taken up by plants and so entering the food chain (Mengel and Kirkby, 1978).

In aqueous solutions, Co^{2+} is octahedrally coordinated with six water molecules, however octahedral and tetrahedral stereochemistries are often in equilibrium and so there is usually some tetrahedral $Co(OH_2)_4^{2+}$ present (King, 1994; Collins and Kinsela, 2010).

Figure 2.1: Eh-pH diagram for the system Co-S-C-O-H. Assumed activites for dissolved species are: Co 10^{-6}; C 10^{-1}; S 10^{-3}. Co^{3+} is only present at extremely low Eh values and so is not located on the diagram (Swanner et al., 2014). From Brookins (1988).

Despite this, Co^{2+} preferentially forms solid compounds in a tetrahedral structure, especially when binding to anionic ligands (Dunitz, 1957; Sacconi et al., 1962; King, 1994). In contrast, Co^{3+} complexes are almost exclusively octahedrally coordinated, with few 5-coordinated complexes that take the form of square pyramidal geometry (such as the vitamin B_{12} complex) (King, 1994).

Co^{2+} has a similar ionic radius to that of Cu^{2+}, Fe^{2+}, Fe^{3+},Mn^{2+}, Mg^{2+}, Ni^{2+}, ad Zn^{2+}, giving it the potential to be isomorphously substituted into oxides, silicate, and sulphide minerals that contain these ions. For example, Co is known to substitute for Ni in many copper-nickel-iron sulphide orebodies (Young, 1957) .

In basaltic rocks (such as gabbros, norites, and andesites) Co is commonly found in association with Fe and Mg (Carr and Turekian, 1961). In some Caledonian basaltic and dioritic rocks, the Co/Mg ratio was approximately constant with varying concentrations of the two metals (Nockolds and Mitchell, 1948), and log/log plots of Co and Mg show a positive trend (Carr and Turekian, 1961). A similar positive trend occurs between Co and Mg in granites, though in this case there is less scatter and the positive trend is stronger. In alkali and calcalkali, the Co/Mg and Co/Fe ratios were found to be constant (Nockolds and Allen, 1953; 1954). As with Co and Mg, log/log plots of Co and Fe in basaltic rocks show a positive trend (Carr and Turekian, 1961). These suggest some relationship between Co and Fe and Mg during the formation of igneous rocks.

In the pore waters of marine sediments, Co concentrations increase with depth. Cobalt was found to be undetectable in the shallow, oxic zone sediments on the east and west coast of North America, but concentrations increased to 50 nmol kg^{-1} in the manganese reduction zones at ~8 – 10 cm depth (Heggle and Lewis, 1984). This is likely due to adsorbed Co being released from the Mn oxides when they are reduced. Below this depth, Co concentrations in the pore waters began to decrease again as a result of the precipitation of insoluble cobalt sulphides (Heggle and Lewis, 1984). However, in other regions, such as Maizurur Bay, Japan, the Co concentration was found to remain relatively stable with increases in depth (Kurata, 1974). This suggests that the behaviour of Co in sediments is highly dependent on the mineralogy of the sediments and chemistry of the porewaters.

2.4 Soils and their constituents

Soil is a mixture of organic matter, minerals, gases, liquids, and organisms that together support life. Depending on the location, what makes up a soil can vary drastically. In sandy soils over 99% consists of mineral matter, but this can drop to as low as 5% in soils

high in organic matter, such as peat (Jackson, 1969). The distribution of minerals present in soils is dependent on those inherited from the parent rock and by soil forming processes that may destroy some minerals and selectively accumulate others (Jackson, 1969). The amount of organic matter in a soil is controlled by 5 factors: climate, time, vegetation, parent material, and topography (Jenny, 1941). These factors vary in different locations, and therefore for different soils. This results in organic matter accumulating at different rates and in varying quantities (Sparks, 1995).

Despite the varying amounts of each soil constituent in soils, there are three minerals that contribute the most to the geochemical behaviour due to their high surface area and abundance in natural soil systems– clay minerals, iron oxides, and organic matter – and therefore this review will focus on these.

2.4.1 Iron Oxides

Iron oxides are not found in as large quantities as clays in soils, but play an important role in many soil processes because of their large surface area and high reactivity (Sparks, 1995).

The basic structural unit of all Fe oxides is the octahedron, where each Fe atom is surrounded by six oxygen atoms (Sparks, 1995). Iron is most commonly found in its trivalent Fe(III) form in the iron oxides, however there are three compounds that contain divalent Fe(II) – FeO, $Fe(OH)_2$ and Fe_3O_4 (Schwertmann and Cornell, 2003).

Hematite (Fe_2O_3) and goethite (FeOOH) are the most common iron oxides and the most thermodynamically stable (Sparks, 1995). They are found in soils, often present as films on the surfaces of soil grains to give them a red/ brown colour (Jackson, 1969).

Ferrihydrite is a hydrated semicrystalline material that exists as a poorly ordered mineral. It is made up of nano-crystals that are typically 4 – 6 nm in size (Schwertmann and Cornell, 1991, 2003). These small particles pack together and form aggregates that are greater than 0.1 μm, and this aggregation results in ferrihydrite being microporous.

Ferrihydrite is widespread in surface environments, but transforms into a more stable iron oxide unless stabilised in some way (Schwertmann and Cornell, 2003). Stabilization can occur by ferrihydrite binding with organic ligands (e.g. alizarin; Yuwono et al., 2012) and metal cations (Liu et al., 2016), and coprecipitation with humic substances (Angelico et al., 2014).This can cause changes in particle-particle interactions and surface charge, or may slow the transformation into a single crystal from the mesocrystal state (Yuwono et al., 2012). The structure of ferrihydrite has been difficult to define due to its low degree of order, and the composition of it appears to be variable, especially regarding the

amounts of OH and H_2O (Schwertmann and Cornell, 2003). However, the simple formula $Fe_5O_8H.H_2O$ is generally used to represent this mineral (Towe and Bradley, 1967).

The surface area of ferrihydrite (ranging from as low as 175 $m^2 g^{-1}$ to 599 $m^2 g^{-1}$; Zhu et al., 2010, and Rout et al., 2012, respectively) is much higher than that of other iron oxides, such as goethite (~45 $m^2 g^{-1}$; Sherman et al., 2008) and hematite (~28 $m^2 g^{-1}$; Christl and Kretzschmar, 2001). This makes ferrihydrite much more reactive than other iron oxides that are more prevalent in soils. The large range in measured surface areas of ferrihydrite is because of its aggregated structure and interparticle porosity, which means the internal area can be inaccessible to some measurement techniques, such as the BET surface area method. This method uses N_2 adsorption to measure the surface area of the solid and if the interior of the ferrihydrite aggregates is inaccessible to the N_2 then the measured surface area will be lower than the true surface area (Schwertmann and Cornell, 2003; Ona-Nguema et al., 2005).

The surface functional groups of iron oxides are hydroxyls (OH). They can react with acids and bases through reactions 2.2 and 2.3 due to their double pair of electrons and dissociable hydrogen atom. This means they are amphoteric and their charge changes with pH (Schwertmann and Cornell, 2003).

$$\equiv FeOH_2^+ \leftrightarrow \equiv FeOH + H^+ \quad (2.2)$$

$$\equiv FeOH \leftrightarrow \equiv FeO^- + H^+ \quad (2.3)$$

Due to its amphoteric nature, the charge of ions that will be attracted to the iron oxides changes with the pH of the system. At acidic pH values the surface sites will be in the $\equiv FeOH_2^+$ form and will attract anions, but at basic pH values cations will be attracted due to the surface site being present as $\equiv FeO^-$.

2.4.2 Clay Minerals

The clay distribution in soils may change with depth depending on the age of the soil (Barshad, 1964). In young soils with a uniform alluvial parent material, there is no change in clay content with depth, whereas in a moderately weathered soil the clay content is highest at the surface and decreases with depth, and in well-developed soils the clay content increases with depth until it reaches a maximum, below which the clay content either stays constant or decreases.

Clay minerals play a large role in the chemistry of soils. They often determine the physical properties of a soil, such as plasticity and structure, as well as the chemical

properties (e.g. cation exchange, ion release, and ion fixation) (Jackson, 1969). This is often due to the abundance of clay minerals in the soil rather than it being particularly influential, as the surface areas are generally low: 39.8 $m^2 g^{-1}$ for bentonite (Aylmore et al., 1970), 12.2 $m^2 g^{-1}$ for kaolinite (Peacock and Sherman, 2005) and 43 $m^2 g^{-1}$ for illite (Helios Rybicka et al., 1995) . For example, as the percentage of clay in a soil increases, the ability for it to hold water increases (Keen and Raczkowski, 1921).

Clays are formed of layers of silica tetrahedral and alumina octahedral sheets. A 1 :1 clay mineral (Fig. 2.2) occurs when one tetrahedral sheet binds to an octahedral sheet via the oxygen atoms at the tip of the tetrahedral sheet, and when two tetrahedral sheets are bound to an octahedral sheet, a 2 : 1 clay is created (Grim, 1968; Sparks, 1995). In the interlayer space between the sheets cations can be octahedrally coordinated with hydroxyl groups, or may be present as individual cations (Sparks, 1995).

During the formation of a mineral an atom in the crystal lattice can be substituted for by another atom of a similar size. This can result in the charge changing from neutral to a net negative or positive charge, which is then balanced by ions near the surface of the clay (Sparks, 1995). In clays, the Si^{4+} in the tetrahedral sheet is often replaced by Al^{3+} and sometimes P, while the central ion in the octahedral sheet (Al^{3+}, Mg^{2+}, Fe^{2+}) can be replaced by Fe^{2+}, Fe^{3+}, Mg^{2+}, Ni^{2+}, Zn^{2+}, or Cu^{2+} (Sparks, 1995). When a trivalent ion occupies the central space, the clay is referred to as a dioctahedral structure because only two of the three octahedral positions are filled, but when a divalent ion is the central atom all three of the octahedral positions are filled and it is a trioctahedral structure (Jackson, 1969).

Figure 2.2: The structure of kaolinite. From Barani and Kalantari (2017).

Kaolinite ($Al_2Si_2O_5(OH)_4$) is a 1 : 1 dioctahedral clay (Fig. 2.2) that contains little isomorphic substitution (Sparks, 1995). There is no interlayer space as the silica and alumina sheets share a common plane of oxygen atoms and repeating layers are bound via hydrogen bonds, which prevents kaolinite from expanding in water, which 2 : 1 clays such as montmorillonite do (Jackson, 1969). This structure also leads to the silica/ oxygen and alumina/ hydroxyl sheets being exposed, allowing them to interact with other soil species (Grim, 1968).

Despite having little isomorphic substitution, Al^{3+} typically substitutes for Si^{4+} in the tetrahedral sheet (van Olphen, 1977). This creates a permanent negative charge on the basal surface that results in the attraction of cations in solution throughout the entire pH range. Kaolinite also has a hydroxyl surface where the OH groups can act as proton donors and form H-bonds with foreign molecules (Tunega et al., 2002). However, these are less reactive than the pH-dependent surface sites and do not contribute to the sorption capacity of the mineral (Brady et al., 1996; Liu et al., 2013).

The pH-dependent charge of kaolinite is due to the presence of ≡AlOH and ≡SiOH groups found at the edges of the octahedral and tetrahedral sheets, respecitively. The ≡SiOH groups are found at the edge of the tetrahedral sheet and only contribute towards the negative charge by deprotonation to $\equiv SiO^-$ through the same reaction as equation 2.3, where Fe is replaced with Si (Sposito, 1984; Sparks, 1995; Huertas et al., 1998). In contrast, the ≡AlOH are amphoteric and becomes protonated and deprotonated through equations 2.2 and 2.3 where Fe is replaced with Al (Sparks, 1995).

2.4.3 Organic Matter

Soil organic matter is an important constituent in soils as it can control the uptake and availability of plant nutrients by having a high surface area (800 – 900 $m^2\ g^{-1}$) and a cation exchange capacity of 150 – 300 $cmol\ kg^{-1}$ (Sparks, 1995). This high surface area and cation exchange capacity means that soil organic matter is capable of sorbing macro- and micro-nutrients, heavy metals, and pesticides, thereby controlling their mobility in the soil (Sparks, 1995).

The main elemental constituents of soil organic matter are carbon, oxygen, hydrogen, and nitrogen, with phosphorus and sulphur being less abundant (Sparks, 1995). The ratio of these elements to each other stays similar in drastically different soil types that contain different amounts of each of the chemical species (Kononova, 1966; Stevenson, 1994).

Soil organic matter can be split into 2 groups: non-humic and humic substances. Non-humic substances only exist in the soil briefly because they are attacked by

microorganisms. They include carbohydrates, proteins, peptides, amino acids, fats, waxes, and low-molecular-weight acids (Sparks, 1995).

The decomposition of plant, animal, and microbial material produces acidic, complex organic molecules that make up humic substances (Tipping, 2002). Humic substances can be subdivided into humic acid, fulvic acid, and humin, which are defined based on the conditions under which they are soluble / insoluble. Fulvic acid is soluble in both acid and alkali solutions, humic acid is insoluble in acid and soluble in alkali, and humin is insoluble in acid and alkali solutions (Sparks, 1995). The elemental composition of the three phases are similar and often overlap due to different sources of the soil (for example, the relative C content ranges for humic acid, fulvic acid and humin are 52 – 65%, 40.7 – 60.4% and 55.9 – 56.3%, respectively), humic acid has the largest range and therefore the possibility to have the lowest O content (24.8 – 41.7%) compared to humin (31- 36.5) and fulvic acid (39.7 – 49.8%) (Tipping, 2002). However, the molecular weights of the phases are dramatically different, with fulvic acid generally having a range of 1,000 to 3,900, humic acid can have molecular weights up to 200,000 (Beckett et al., 1987; Tipping, 2002), and humin having the largest molecular weights at 100,000 – 10,000,000 (Pettit, 2004; Calace et al., 2007; Helal et al., 2011).

All three sub-categories of humic substances consist of functional groups that may contain carbon, oxygen, hydrogen, or nitrogen in a range of structures (Stevenson, 1994). These functional groups contribute to the high cation exchange capacity by becoming deprotonated as pH increases; this then allows cations to bind to the functional groups as they now have a negative charge. The functional groups that deprotonate at pH values commonly found in soils (<5) are carboxyls (R-COOH), quinones (Ar=O), and phenolic OH groups (Ar-OH) (Sparks, 1995). Therefore, these are the functional groups that are most important for interactions between humic substances and cations. Humic acids are characterised as being dominated by a high number of carboxyl and phenolic hydroxyl groups attached to aromatic rings (Fig. 2. 3) (Szyma ski et al., 2016). The presence of aromatic structures suggests that algae or microbes are involved in the humification process to create humic substances (Hatcher et al., 1981). Despite the complex structure of humic acids being heterogenous and their elemental composition varying greatly, it was found that there was no relationship between the humic acids and their original vegetation type when analysed with infrared spectroscopy and solid state nuclear magnetic resonance spectroscopy (Amalfitano et al., 1995). However, there is a difference in the C/N ratio of marine and soil humic acids, ranging from 6 – 9 for marine and 12 – 18 for soil (Gauthier et al., 1987). This suggests that the environment does play a role in

the heterogeneity of humic acids on a large scale, but differences on a more local scale are minimal.

2.5 Sorption Processes

Sorption is the term given to processes that remove metal ions from solution. This can occur through three main mechanisms: adsorption, incorporation, and precipitation.

2.5.1 Adsorption

Adsorption occurs when a solute is removed from solution and forms a surface complex on the mineral surface (Krauskopf and Bird, 1995). One of two types of complex can be formed: inner- or outer-sphere. Inner-sphere complexes form when hydroxyl groups on the sorbent surface create ionic or covalent bonds with ions in solution. When cations

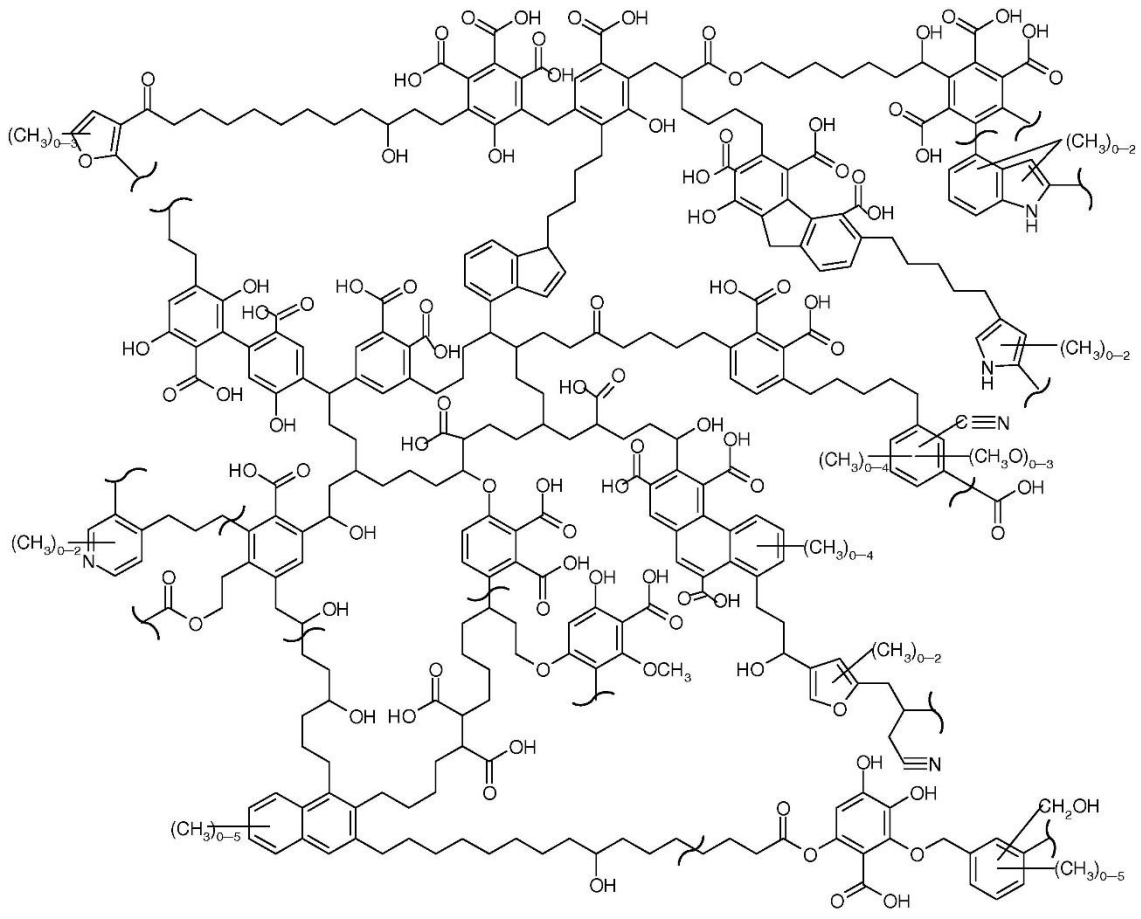

Figure 2.3: A model structure of humic acid. From (Szyma ski et al., 2016)

form inner-sphere complexes with an oxide surface, the process is known as a cation exchange reaction due to the cation replacing the H^+ of the hydroxyl group, for example:

$$S\text{-}OH+M^+ \leftrightarrow S\text{-}OM+H^+ \quad (2.4)$$

where S represents the mineral surface and M the cation. When anions bind to the sorbent surface, the process is a ligand exchange reaction and the anion replaces the hydroxyl group:

$$S\text{-}OH+L^- \leftrightarrow S\text{-}L+OH^- \quad (2.5)$$

where L represents the sorbing anion (Stumm, 1992). The adsorbing ion in an inner-sphere complex can either bind to one or two surface functional groups, and these are termed monodentate or bidentate respectively (Fig. 2.4) (Krauskopf and Bird, 1995).

With an increasing adsorbate concentration, it is also possible for clusters of ions to form on the surface, which are termed multinuclear complexes (Fig. 2.5) (Krauskopf and Bird, 1995).

Outer-sphere complexes (Fig. 2.4) are formed from long range electrostatic forces (Langmuir, 1997). These forces are weak and the ions keep their associated water molecules, but this also means that this type of complex is not as stable as inner-sphere complexes, and that they can't approach the sorbent closer than the radii of their

Figure 2.4: A schematic showing outer-sphere complexation (left) monodentate inner-sphere complexation (centre) and bidentate inner-sphere complexation (right). The horizontal line denotes the boundary between the mineral below and the solition. Small solid circles in the mineral represent metal ions and the large solid circles are oxygen atoms. M represents sorbate ions, and H denotes hydrogens in water molecules solvated about the surface complexes. Adapted from Krauskopf and Bird (1995)

hydration spheres (Harrison and de Mora, 1969; Krauskopf and Bird, 1995). Because of this, the inner- and outer-sphere complexes are often placed at different planes when modelling adsorption (e.g. the basic Stern model – see Chapter 3.6.1 for more detail).

Adsorption is dependent on a number of external factors, the most important of which is pH. This is because adsorption most commonly occurs between ions in solution and surface functional groups on the sorbent. The surface functional groups react with H^+ and OH^- ions in solution (equations 2.2 and 2.3) causing them to become more negatively charged with increasing pH and will attract ions of the opposite charge (Stumm, 1992). Due to this shift in surface charge, there is a pH at which the sorbent's net charge is 0, which is known as the point of zero charge (PZC) (Krauskopf and Bird, 1995).Therefore, at pH values below the PZC where the functional groups are positively

Figure 2.5: Schematic two-dimensional representation of a multinuclear surface complex of Pb bound by two inner-sphere surface complexes to goethite. From Krauskopf and Bird (1995).

charged more anions will be sorbed and in environments where the pH is above the PZC the functional groups are negatively charged and attract cations (Fig. 2.6).

The ionic strength of the system impacts the amount of adsorption that occurs due to ions competing for binding to the surface sites. As the ionic strength increases, more competing ions means that less of the desired ions are sorbed (Undabeytua et al., 2002). However, only outer-sphere complexation is affected by changes in ionic strength (Krauskopf and Bird, 1995).

Different sorbing ions have different pH ranges of the sorption edge, and this is particularly evident when multiple ions are in the system. The order of the sorption edges (from low to high pH for cations) is known as the selectivity sequence. Cations with sorption edges at low pH values are said to have a higher affinity to the sorbent and these

Figure 2.6: Adsorption of various oxyanions (a) and metal cations (b) each at a trace concentration of $5x10^{-7}$) by ferrihydrite as a function of pH at an ionic strength of 0.1 mol L-1. From Langmuir (1997).

will outcompete other cations for binding sites thereby shifting the sorption edge of the lower affinity cation to higher pH values (Bruemmer et al., 1988; Zhu et al., 2010).

2.5.2 Incorporation

Incorporation is a process that occurs when a foreign ion replaces one in a mineral lattice (Bradl, 2004). This takes place through either isomorphic substitution or coprecipitation. Isomorphic substitution occurs when ions that are adsorbed to the mineral surface diffuse into the mineral lattice and completely lose their hydration sphere in the process (Bradl, 2004; Schmidt et al., 2009). In order to be incorporated, the ions must diffuse beyond the interfacial region of the mineral, which is defined as the nanometer depth from the surface (Sposito, 1986). Coprecipitation often takes place by recrystallization, in which the primary solid dissolves and reprecipitates with the solution ions and this forms a more thermodynamically stable crystal (Curti, 1997).

The biggest control on which ions can be incorporated into a mineral is ionic radius, as ions with a similar ionic radius can substitute for each other, e.g. Mg^{2+} and Fe^{2+} with ionic radii of 0.72 Å and 0.78 Å, respectively (Krauskopf and Bird, 1995).

The ionic charge of an ion also influences whether it can be incorporated into a mineral structure or not. If the incorporating ion has the same charge as an ion in the mineral structure then there is the possibility of it replacing the structural ion (Regenspurg and Peiffer, 2005). While ions with differing ionic charges can replace structural ions, when the ionic charges are the same there is no change in the crystal structure (Shi et al., 2016). These changes are due to the mineral maintaining charge balance when an incorporating ion has a different charge to the structural ion. This change in charge must be compensated for by other substitutions in the mineral structure (Wood and Blundy, 2001).

The precipitation rate of the coprecipitate is also an important influence. With an increasing precipitation rate, the incorporation of Co, Mn, and Cd into calcite was found to decrease (Lorens, 1981). At slow growth rates it is possible for the ions near the mineral surface and those incorporated in it to reach equilibrium, but at faster growth rates this becomes increasingly difficult. In contrast, Sr incorporation increased with faster precipitation (Lorens, 1981). As Sr has a larger ionic radius than Ca^{2+} it is not preferentially incorporated into the coprecipitate, but at high precipitation rates all of the ions in the solution layer in contact with the mineral surface become indiscriminately trapped by the growing coprecipitate.

2.5.3 Precipitation

Precipitation is the formation of nuclei on a mineral surface by ions in a solution that then grow into a precipitate. Precipitation in this way can occur before the ions would precipitate in a solution without a surface (Sparks, 2005), this is because when precipitating a mineral from solution, stable nuclei are only formed once an activation barrier has been overcome – i.e. the solution must be supersaturated to a certain point (Stumm and Morgan, 1996). But, when a solid is already present in the solution, this reduces the activation energy necessary for stable nuclei to be formed (Stumm and Morgan, 1996).

In this way there is a continuum between surface complex formation and precipitation as ions sorbing onto a mineral surface lowers the energy required for the ions in solution to precipitate (Farley et al., 1985; Stumm, 1992). In this process, as ions form a layer of surface complexes on a mineral, a new hydroxide surface can be formed (Farley et al., 1985).

2.6 Cobalt Sorption

2.6.1 Cobalt sorption to iron oxides

Cobalt sorption to iron oxides has been studied extensively at the macroscopic level (e.g. Forbes et al., 1976; Schenck et al., 1983; Ainsworth et al., 1994; Landry et al., 2009) with sorption generally increasing from <10% to ~100% between pH 5.5 and 7.5. Small differences in the pH range of the sorption edge, such as a sorption edge between pH 5.5 and 7 (Landry et al., 2009) compared to 6.5 and 7.5(Schenck et al., 1983) are likely to be caused by different preparation methods (Nicholson and Eley, 1997). Differences in the preparation methods can affect sorption properties of the minerals, such as the PZC and surface area. Reported PZC values for ferrihydrite range from 6.8 (Ghoneimy et al., 1997) to 8.1 (Schultz et al., 1987) which will cause differences in the position of the sorption edge. This is because it affects the pH at which the mineral's surface charge changes. Ferrihydrite surface area values from the literature also show a range, from 175 $m^2 g^{-1}$ (Zhu et al., 2010) to 599 $m^2 g^{-1}$ (Rout et al., 2012). This affects the sorption edge as the surface area controls the concentration of binding sites and therefore the amount of ions that can sorb to the mineral surface (Wilkie and Hering, 1996).

The ionic strength of the background electrolyte has been found to have no effect on the sorption edge of Co sorbing to iron oxides. Increasing the ionic strength from 0.001 mol

L^{-1} to 0.1 mol L^{-1} had only a minor effect on the sorption edge by increasing the pH_{50} (the pH at which 50% of sorbing ions are sorbed) from 6.06 to 6.33 (Landry et al., 2009).

In environmental systems where other heavy metal cations are present, Co is outcompeted for binding sites on ferrihydrite, and this can shift the sorption edge to a higher pH range. In a system where Co, Cu, Cd, Ni, Pb, Mg, Sr, and Zn were present the selectivity sequence was: Pb > Cu > Zn > Ni > Cd > Co > Sr > Mg (Kinniburgh et al., 1976). Similar selectivity sequences have been found in other studies: Pb > Cd = Co (Ainsworth et al., 1994), Cu > Co > Mn (Bibak, 1994), and Cu > Pb > Zn > Co > Cd (Forbes et al., 1976). This suggests that in systems where there are multiple cations, the sorption edge of Co is likely to be shifted to a higher pH range due to other cations outcompeting it for binding sites.

Cobalt sorption to ferrihydrite has been modelled using a diffuse layer model (DLM) as described by Dzombak and Morel (1990). This is a 2-site model that assumes monodentate surface complexes according to:

$$\equiv Fe_{(s)}OH + Co^{2+}_{(aq)} = \equiv Fe_{(s)}OCo^{+} + H^{+}_{(aq)} \quad (2.6)$$

$$\equiv Fe_{(w)}OH + Co^{2+}_{(aq)} = \equiv Fe_{(w)}OCo^{+} + H^{+}_{(aq)} \quad (2.7)$$

where $\equiv Fe_{(s)}OH$ represents a strong adsorption site and $\equiv Fe_{(w)}OH$ a weak site. However, the parameters used by Dzombak and Morel (1990) do not describe data accurately at high pH vales where the $\equiv Fe_{(s)}OH$ sites reach saturation (Ainsworth et al., 1994). To resolve this issue Ainsworth et al. (1994) optimised the log K value for $\equiv Fe_{(w)}OH$. With the optimised log K, Co sorption was able to be reproduced across the full pH range of 3 – 10. Landry et al. (2009) also modelled Co sorption data to the DLM by Dzombak and Morel (1990), which they found produced a reasonable fit and matched their collected data in that there was no dependence on ionic strength.

Landry et al. (2009) also modelled their data with a single site DLM using protonation and deprotonation constants from Sverjensky and Sahai (1996) and fitting to the log K value of:

$$\equiv FeOH + Co^{2+}_{(aq)} = \equiv FeOCo^{+} + H^{+}_{(aq)} \quad (2.8)$$

This produced as statistically as good a fit as the two-site DLM by Dzombak and Morel (1990).

2.6.2 Cobalt sorption to kaolinite

Cobalt sorption to kaolinite as a function of pH has been found to occur in two stages: an initial stage at low to mid pH values where Co sorbs to permanently negatively charged surface sites, and a second stage at mid to high pH values that is associated with variable charge sites (e.g. Spark et al., 1995; Angove et al., 1998; Landry et al., 2009; Ikhsan et al.,

1999; Bhattacharyya and Sen Gupta, 2007). The initial sorption stage is dependent on ionic strength of the background electrolyte with the pH50 (the pH at which 50% of the cation is sorbed) increasing as the ionic strength increases, and with an ionic strength of 0.1 mol L^{-1} sorption is completely inhibited (Landry et al., 2009). This is caused by Co^{2+} competing with increasing amounts of the cation associated with the background electrolyte for binding sites on the kaolinite surface and implies that Co forms an outer-sphere complex with kaolinite at low pH (Spark et al., 1995). The second sorption stage is similar to sorption to pure silica and alumina oxides and is independent of ionic strength (Spark et al., 1995; Landry et al., 2009).

The type of background electrolyte used has also been found to affect the sorption edge at low to mid pH values (Spark et al., 1995). Using KNO_3 consistently inhibited sorption compared to NaCl, but how much by was dependent on the concentration of the electrolytes. At 10^{-1} mol L^{-1} sorption was minimal up to pH 6.5 and there was no visual difference. At 10^{-2} mol L^{-1} sorption reached 25% with NaCl at pH 6, but was 15% with KNO_3. At 10^{-3} mol L^{-1} the difference between percentage Co sorbed at pH 6 was ~6%. This was concluded to be because K+ competes more effectively with Co2+ than Na+ (Spark et al., 1995).

As with sorption to ferrihydrite, Co sorption to kaolinite is likely to be reduced in systems where multiple cations are present. The selectivity sequence has been found to be Cu > Zn > Co > Cd (Spark et al., 1995), and Pb ≈ Cu > Zn > Co > Mn (Ikhsan et al., 1999).

Extended X-ray absorption fine structure (EXAFS) spectroscopy has been used to discern the local environment of Co sorbed to kaolinite and to determine which surface complexes are formed (O'Day et al., 1994a; b). At low Co surface coverages and high pH, the Co data was fit with a small number of either Al or Si atoms (N = 0.6-1.5) and so it can be concluded that it forms bidentate inner-sphere mononuclear complexes (O'Day et al., 1994b). However, at pH values of ~8, Co was found to form multinuclear complexes on the kaolinite surface with a number (N = 2.1-5.7, depending on the Co surface coverage) of Co-Co neighbours present. Due to the high Co surface coverage the backscattering from the Co neighbours masked that from Al or Si and so it is not possible to determine the relationship between Co complexes and the kaolinite surface, though it can be assumed that it is also a bidentate inner-sphere complex, the same as at low surface coverage (O'Day et al., 1994a). Outer-sphere complexes cannot be determined by EXAFS due to the bonding of a hydrated ion to a Al/ Si atom resulting in distances over 5 Å (O'Day et al., 1994b). However, as the uptake of Co at low pH values is dependent on ionic strength and it is known that outer-sphere complexes are dependent on ionic

strength, then it can be implied that sorption of Co to kaolinite at low to mid pH is via outer-sphere complexation.

Angove et al. (1998) modelled Co sorption to kaolinite via bidentate complexes to two surface sites using a constant capacitance (CC) surface complexation model according to:

$$Co^{2+} + 2{\equiv}XK \leftrightarrow {\equiv}X_2Co + 2K^+ \quad (2.9)$$

$$Co^{2+} + 2{\equiv}SOH \leftrightarrow ({\equiv}SO)_2Co + 2H^+ \quad (2.10)$$

where ≡X- represents permanently negatively charged sites, ≡SOH represents variable charge Al or Si sites, and - in the absence of transition metal ions - K^+ from the background electrolyte is assumed to occupy the surface binding sites. This model fit the adsorption data well, only overpredicting sorption at the plateau between the two sorption stages. Ikhsan et al. (1999) used the same approach and found a good fit to their data. They also showed that the X_2Co complexes were responsible for the initial sorption stage at pH <7, and above this the majority of sorption was via $(SO)_2M$ complexes.

Landry et al. (2009) used a DLM to model their sorption data with a bidentate surface complex to permanent and variable charge sites according to:

$${\equiv}2X(Na) + Co^{2+}_{(aq)} \leftrightarrow {\equiv}X_2(Co) + 2Na^+_{(aq)} \quad (2.11)$$

$${\equiv}2SOH + Co^{2+}_{(aq)} \leftrightarrow ({\equiv}SO)_2Co + 2H^+_{(aq)} \quad (2.12)$$

respectively. This produced a good fit to the data at all Co concentrations (10^{-6} – 10^{-4}) and ionic strengths (10^{-3} – 10^{-1}), apart from at the lowest ionic strength where there was underprediction at low pH and overprediction at high pH.

All of the models discussed here are based on bidentate inner-sphere sorption complexes. However, spectroscopic methods (O'Day, et al., 1994a;b; Thompson et al., 2000) show that Co-Co multinuclear complexes occur under many circumstances, including a range of Co surface densities and pH. Therefore, despite the empirical utility of existing sorption models this aspect of Co behaviour is not well understood at the molecular level.

2.7 Removal of cobalt from soils

The period of time left for Co to remain in contact with soil materials (e.g. kaolinite and ferrihydrite) does not appear to impact the uptake of Co onto the solid surfaces past the initial few minutes (Ainsworth et al., 1994; Backes et al., 1995; McLaren et al., 1998). Although, in the case of Fe oxides, an increase in sorption with time could be masked by

a decrease in pH as protons are known to be released when trace metals are sorbed to the surface (Backes et al., 1995). However, the ageing period of Co in soils and with individual soil components does affect its ability to be removed.

Co sorption to ferrihydrite was completely reversible within 16 hours by decreasing the pH with no hysteresis between the sorption and desorption curves (Ainsworth et al., 1994). However, at 2, 9 and 16 weeks, the amount of Co removed decreased compared to the previous ageing period, with 20% Co remained sorbed to the ferrihydrite after 16 weeks. The amount of time left for Co to desorb from ferrihydrite (and goethite) did not significantly affect the amount of Co that was released (Backes et al., 1995).

As with ferrihydrite, the release of Co from kaolinite decreased with an increased ageing period, though after no ageing period is there completely reversible sorption (Thompson et al., 2000). Desorption was carried out by reducing the pH to7. This confirms that the sorbed phase increases in stability with sorption time. However, the amount of Co released increased the longer it was allowed to desorb, up to 10,000 hours.

The extraction of Co from 13 soils with a range of international origins (4 from Australia, 3 from Belgium, 2 from Greece, and 1 each from Italy, UK, USA and France) over periods ranging from 2 hours to a year was studied (Wendling et al., 2009a). In general, the amount of Co extractable by $CaCl_2$ decreased with ageing, with soils that were measured to be more acidic showing the greatest amount of extractable Co. For example, after 15 days the soil from Athens, Greece (pH 4.5) ~35% of Co was extracted, but after the same length of time only <5% Co was released from the Woburn, UK soil (pH 6.2). After 365 days of ageing, the same soils had ~10% and <1% extractable Co, respectively.

The decrease in the amount of Co released with an increase in ageing period is thought to be because of a number of processes: surface precipitation, surface oxidation, diffusion into micropores, or incorporation into crystal lattices (Wendling, et al., 2009). In the case of ageing the metal ions with ferrihydrite over a period of several weeks it is possible that the metal becomes incorporated through isomorphic substitution into the mineral as it recrystallizes into a more stable form (Ainsworth et al., 1994). An EXAFS study of Co sorbed to kaolinite after ageing periods of up to 300 days showed that Co formed a hydrotalcite-like precipitate on the surface of the kaolinite (e.g. $Co_xAl(OH)_{2x+2}(A^{n-})_{1/n,}$ where x is a number between 2 and 4 and A^{n-} is a nitrate or silicate anion). (Thompson et al., 2000). This structure formed at all Co sorption densities (0.25 – 1.1 μmol m^{-2}), though was only present at the lowest sorption density after 184 days. Both of these are likely to be the cause of Co not being released back into solution.

The reduction in labile Co with ageing has been modelled with a semi-mechanistic model that assumed the processes involved were precipitation of Co on the solid surface and diffusion into the mineral surface (Wendling et al., 2009b). This produced a good fit to the data at an ageing period of 2 hours, however at longer ageing periods there was overprediction of the amount of Co released, which suggests that either the model was not properly constrained or there was a process that was not included in the model.

2.7.1 Current decontamination methods

There are many current decontamination techniques, and the development of commercially viable and efficient methods is an ongoing research priority (Tadesse et al., 1994). Remediation techniques can be categorised as either in-situ, prepared bed, or in-tank reactors. In-situ methods treat the contaminant where it is located without excavation of the soil. Prepared bed techniques either move the contaminated soil to an area on the site that has been designed to enhance treatment or prevent the transport of pollutants, or the soil is relocated to a storage area while the original location is prepared for use, and once the contaminated soil is returned the treatment is provided. In-tank treatments are used for the treatment of contaminated soil where it is relocated and placed in an enclosed reactor where the treatment will take place (Sims, 1990). Each of these methods can then be used with chemical, physical, or biological techniques in order to remove the pollutant from the soil (Tadesse et al., 1994). This review will focus on the most commonly used decontamination methods.

2.7.1.1 Soil washing and flushing

These techniques involve flushing the contaminated soil with a solution designed to remove the particular pollutant. This could be an acidic or basic aqueous solution, an oxidising agent (such as hydrogen peroxide) that can chemically change the contaminant, or a chelating agent that can bind the contaminant to two or more of its functional sites to create a ring that prevents the contaminant from bonding to the soil constituents (Raghavan et al., 1991). The difference between the two methods is that washing is an in-tank method that requires the transport of the soil to a suitable container, whereas flushing is an in-situ method. These techniques are used for the removal of organic and inorganic contaminants, but is most suitable for the removal of heavy metals, and non-volatile hydrophobic and hydrophilic organic compounds. Once the soil has been adequately flushed of the contaminant, the washing fluid then needs to be treated and the problem somewhat repeats itself (Tadesse et al., 1994).

This method can vary in its effectiveness. An alluvial sediment that had been exposed to ^{137}Cs and ^{60}Co was washed and while 84% of Co was removed from the sediment, only

18% of Cs was (Gombert, 1994). This implies that the washing solution needs to be researched to ensure it is suitable for the contaminant.

2.7.1.2. Permeable Reactive Barrier (PRB)

A PRB is an in-situ technique that uses a permanent, semi-permanent, or replaceable reactive material placed in the subsurface across the flow of groundwater or the contaminated plume (Fig. 2.7). The contaminants must then pass through the barrier as it flows, and as it does so a reaction will occur that will transform the contaminant into a less toxic or immobile species (Mulligan et al., 2001; Thiruvenkatachari et al., 2008).

The barrier can be made of a variety of materials, depending on the reactions desired. The materials chosen will have one or more favourable qualities, such as inducing changes in pH, causing precipitation of aqueous ions, or having a high sorption capacity (Thiruvenkatachari et al., 2008). For example, sulfate-reducing bacteria have been used to promote precipitation of the heavy metals as insoluble metal sulphides. This resulted in the reduction of Co from 5.3 μg L^{-1} in the influent to 1.1 μg L^{-1} in the barrier (Ludwig et al., 2002). Limestone and red mud barriers have also been tested as potential PRB materials (Komnitsas et al., 2004). Limestone is used to raise the pH of the aqueous system in order to encourage precipitation and remove heavy metals from aqueous solutions. Red mud has a high surface reactivity and has a higher inherent alkalinity than limestone so can also increase the pH of the system. Both materials removed Co^{2+} from solution by sorption to the solid surface, however their effectiveness decreased over time with more Co being present in solution after passing through the materials after 12 weeks

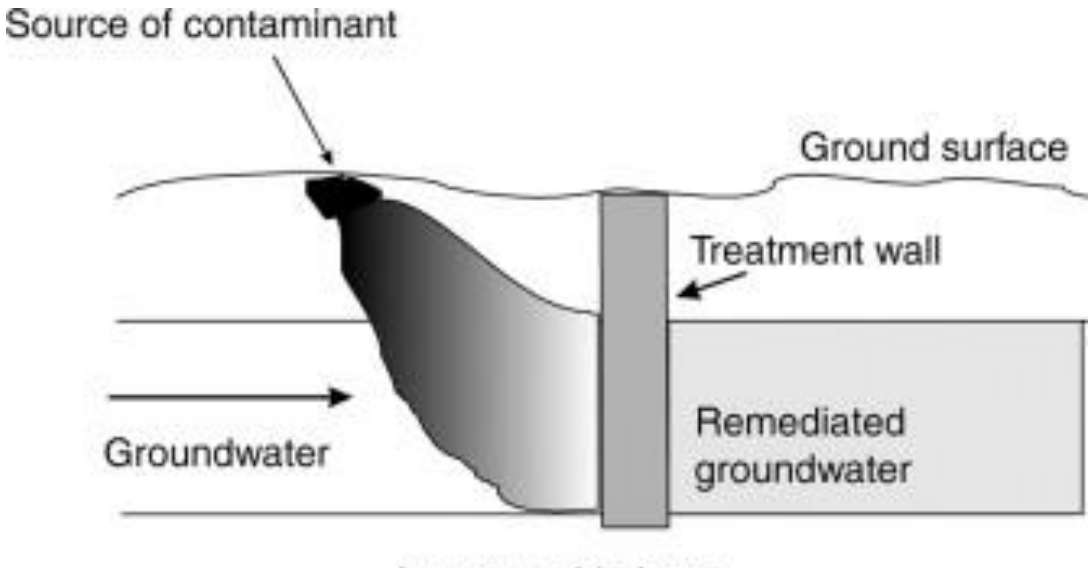

Figure 2.7: Permeable reactive treatment barrier placed in the groundwater to remove metal contaminants. From Mulligan et al. (2001).

(4 mg L^{-1}, as opposed to negligible amounts at the beginning of the experiment) (Komnitsas et al., 2004). This suggests that the materials would have to be replaced after several weeks in order to maintain levels of removal.

2.7.1.3 Phytoremediation

Phytoremediation is a biological technique for the removal of contaminants from soils and involves using non-food crops to absorb metals from the soil. The metals are then stored in the leaf and stalk until the plants are harvested – though it has been found that up to 69.3% of the Co in the plant is found in the roots (Lotfy and Mostafa, 2014). They are then burnt and the ash that remains contains a high concentration of the stored metal (Robinson et al., 1999). Because this technique relies on plant roots absorbing the toxic metals, it is limited to low levels of contamination that occurs in the upper layers of the soil (Mulligan et al., 2001). There are 26 known plants that are hyperaccumulators of Co – they have an unusually high uptake of metals from the soil (90% uptake (Saleh, 2012)). Hyperaccumulators are often metal specific and can contain up to 2 orders of magnitude more of a contaminant than regular plants (Jacobs and Walter, 2005).

Compounds can be added to the soil to increase metal solubility and therefore potentially increase the metal uptake by the chosen plant. Common additions to the soil are EDTA, citric acid, nitrogen fertiliser and DTPA (Sheoran et al., 2009). However a downfall of this technique is that the compound added could then pose a risk to the environment (Robinson et al., 1999).

One of these Co hyperassumulator plants – *Berkheya coddii* – has a high biomass production, making it a good candidate for phytoremediation because as it grows larger it will be able to store more Co (Robinson et al., 1999). When compounds were added that increased the pH of the soil (e.g. Mg/ Ca carbonate) the Co uptake decreased, whereas when sulphur and acid mine tailings were added to the soil the amount of Co absorbed by the plant increased, most likely because of the decrease in pH. This is supported by other studies showing that a low pH environment (~4.9) resulted in the highest uptake of metal ions in the plant (Bagga and Peterson, 2001; Saleh, 2012).

2.8 References

Ainsworth C. C., Pilon J. L., Gassman P. L., Van W. G. and Sluys D. (1994) Cobalt, Cadmium, and Lead Sorption to Hydrous Iron Oxide: Residence Time Effect. *Soil Sci. Soc. Am. J.* **58**, 1615–1623.

Amalfitano C., Quezada R. A., Wilson M. A. and Hanna J. V. (1995) Chemical composition of humic acids: A comparison with precurosor “light fraction” litter from different vegetations using spectroscopic techniques. *Soil Sci.* **159**.

Andres E., Loukili N. H., Noel E., Kaltenbach G., Abdelgheni M. B., Perrin A. E., Noblet-Dick M., Maloisel F., Schlienger J. and Blicklé J. (2004) Vitamin B12 (cobalamin) deficiency in elderly patients. *Can. Med. Assoc. J.* **171**, 251–259.

Angelico R., Ceglie A., Ji-Zheng H., Yu-Rong L., Palumbo G. and Colombo C. (2014) Particle size, charge and colloidal stability of humic acids coprecipitated with Ferrihydrite. *Chemosphere* **99**, 239–247.

Angove M. J., Johnson B. B. and Wells J. D. (1998) The Influence of Temperature on the Adsorption of Cadmium(II) and Cobalt(II) on Kaolinite. *J. Colloid Interface Sci.* **204**, 93–103.

Anno G. H., Baum S. J., Withers H. R. and Young R. W. (1989) Symptomatology of Acute Radiation Effects in Humans After Exposure to Doses of 0.5-30 Gy. *Health Phys.* **56**, 821–838.

Aubert H. and Pinta M. (1977) *Trace Elements in Soils*., Elsevier Scientific Publishing Company, Oxford.

Aylmore L. A. G., Sills I. D. and Quirk J. P. (1970) Surface area of homoionic illite and montmorillonite clay minerals as measured by the sorption of nitrogen and carbon dioxide. *Clays Clay Miner.* **18**.

Backes C. A., McLaren R. G., Rate A. W. and Swift R. S. (1995) Kinetics of cadmium and cobalt desorption from iron and manganese oxides. *Soil Sci. Soc. Am. J.* **59**, 778–785.

Baes C. F. J. and Mesmer R. E. (1976) *The Hydrolysis of Cations*., John Wiley & Sons Inc, New york.

Bagga D. K. and Peterson S. (2001) Phytoremediation of arsenic-contaminated soil as affected by the chelating agent CDTA and different levels of soil pH. *Remediat. J.* **12**, 77–85.

Baize D. (1997) Total Contents of Metallic Trace Elements in Soils. *INRA, Pairs*.

Bangash M. A., Hanif J. and Khan M. A. (1992) Sorption behaviour of cobalt on illitic soil. *WASTE Manag.* **12**, 29–38.

Barani K. and Kalantari M. (2017) Recovery of kaolinite from tailings of Zonouz kaolin-washing

plant by flotation-flocculation method. *Integr. Med. Res.*

Barshad I. (1964) Chemistry of Soil Development. In *Chemistry of the Soil* (ed. F. E. Bear). Van Nostrand Reinhold Company, London.

Beckett R., Jue Z. and Giddings J. C. (1987) Determination of Molecular Weight Distributions of Fulvic and Humic Acids Using Flow Field-Flow Fractionation. *Environ. Sci. Technol* **2**, 289–295.

Bhattacharyya K. G. and Sen Gupta S. (2007) Adsorption of Co(II) from Aqueous Medium on Natural and Acid Activated Kaolinite and Montmorillonite. *Sep. Sci. Technol.* **4215**, 3391–3418.

Bibak A. (1994) Cobalt, Copper, and manganese adsorption by aluminum and iron oxides and humic acid. *Commun. Soil Sci. Plant Anal.* **25**, 3229–3239.

Bradl H. B. (2004) Adsorption of heavy metal ions on soils and soils constituents. *J. Colloid Interface Sci.* **277**, 1–18.

Brady P. V., Cygan R. T. and Nagy K. L. (1996) Molecular Controls on Kaolinite Surface Charge. *J. Colloid Interface Sci.* **183**, 356–364.

Brookins D. G. (1988) *Eh-pH Diagrams for Geochemistry*., Springer-Verlag, London.

Bruemmer G. W., Gerth J. and Tiller K. G. (1988) Reaction Kinetics of the Adsorption and Desorption of Nickel, Zinc and Cadmium by Goethite. I. Adsorption and Diffusion of Metals. *J. Soil Sci.* **39**, 37–52.

Bruland K. (1983) Trace Elements in Sea-Water. In *Chemical Oceanography Volume 8* (eds. J. Riley and R. Chester). Academic Press, London.

Calace N., Petronio B. M., Persia S., Pietroletti M. and Pacioni D. (2007) A new analytical approach for humin determination in sediments and soils. *Talanta* **71**, 1444–1448.

Carr M. H. and Turekian K. K. (1961) The Geochemistry of Cobalt. *Geochim. Cosmochim. Acta* **23**.

Chen C., Habert G., Bouzidi Y. and Jullien A. (2010) Environmental impact of cement production: detail of the different processes and cement plant variability evaluation. *J. Clean. Prod.* **18**, 478–485.

Christl I. and Kretzschmar R. (2001) Interaction of copper and fulvic acid at the hematite-water interface. *Geochim. Cosmochim. Acta* **65**, 3435–3442.

Coles D. G., Ragaini R. C., Ondov J. M., Fisher G. L., Silberman D. and Prentice B. A. (1979) Chemical Studies of Stack Fly Ash from a Coal-Fired Power Plant. *J. Am. Chem. Soc.* **13**.

Collins R. N. and Kinsela A. S. (2010) The aqueous phase speciation and chemistry of cobalt in terrestrial environments. *Chemosphere* **79**, 763–771.

Curti E. (1997) *Coprecipitation of radionuclides: basic concepts, literature review and first applications*.,

Dilworth M. J., Robson A. D. and Chatel D. L. (1979) Cobalt and Nitrogen Fixation in Lupinus Angustifolius L. II. Nodule Formation and Function. *New Phytol.* **83**, 63–79.

Dunitz J. D. (1957) The Crystal Structures of Copper Dipyridine Dichloride and the Violet Form of Cobalt Dipyridine Dichloride. *Acta Cryst* **10**.

Dzombak D. A. and Morel F. (1990) *Surface Complexation Modeling: Hydrous Ferric Oxide*., John Wiley & Sons Inc, New York.

Enghag P. (2004) *Encyclopedia of the Elements: Techical data, history, processing, applications*., Wiley-VCH.

Farley N. J., Dzombak D. A. and O F. M. M. M. (1985) A Surface Precipitation Model for the Sorption of Cations on Metal Oxides. *J. Colloid Interface Sci.* **106**.

Forbes E. A., Posner A. M. and Quirk J. P. (1976) The Specific Adsorption of Divalent Cd, Co, Cu, Pb, and Zn on Goethite. *J. Soil Sci.* **27**, 154–166.

Gál J., Hursthouse A., Tatner P., Stewart F. and Welton R. (2008) Cobalt and secondary poisoning in the terrestrial food chain: Data review and research gaps to support risk assessment. *Environ. Int.* **34**, 821–838.

Gauthier T. D., Seitz W. R. and Grant C. L. (1987) Effects of structural and compositional variations of dissolved humic materials on pyrene Koc values. *Environ. Sci. Technol.* **21**, 243–8.

Ghoneimy H. F., Morcos T. N. and Misak N. Z. (1997) Adsorption of Co 2+ and Zn 2+ ions on hydrous Fe(III), Sn(IV) and mixed Fe(III)/Sn(IV) oxides Part I. Characteristics of the hydrous oxides, apparent capacity and some equilibria measurements. *Colloids Surfaces A Physicochem. Eng. Asp.* **122**, 13–26.

Gombert D. (1994) Treatability Testing to Evaluate What Can Work. *Nucl. Technol.* **108**, 90–99.

Grim R. E. (1968) *Clay Mineralogy*., McGraw-Hill, New York.

Harrison R. M. and de Mora S. . (1969) *Introductory Chemistry for the Environmental Sciences*., Cambridge University Press, Cambridge.

Hatcher P. G., Maciel G. E. and De~qls L. W. (1981) Aliphatic structure of humic acids; a clue to their origin. *Orqamc Geochemistry* **3**.

Heggle D. and Lewis T. (1984) Cobalt in pore waters of marine sediments. *Nature* **311**.

Helal A. A., Murad G. A. and Helal A. A. (2011) Characterization of different humic materials by various analytical techniques.

Helios Rybicka E., Calmano W. and Breeger A. (1995) Heavy metals sorption/desorption on competing clay minerals; an experimental study. *Appl. Clay Sci.* **9**, 369–381.

Huertas F. J., Chou L. and Wollast R. (1998) Mechanism of kaolinite dissolution at room temperature and pressure: Part 1. Surface speciation. *Geochim. Cosmochim. Acta* **62**.

Ikhsan J., Johnson B. B. and Wells J. D. (1999) A Comparative Study of the Adsorption of Transition Metals on Kaolinite. *J. Colloid Interface Sci.* **217**.

Jackson M. L. (1969) Chemical Compopsition of Soils. In *Chemistry of the Soil* (ed. F. E. Bear). American Chemical Society, London.

Jacobs J. S. and Walter L. (2005) Groundwater and Cobalt: Chemical behaviour and treatment. In *Water Encyclopedia Vol. 5* (eds. J. Lehr, J. Keeley, J. Lehr, and T. B. Kingery III). John Wiley & Sons, Hoboken, NJ.

Jandová J., Vu H. and Dvořák P. (2005) Treatment of sulphate leach liquors to recover cobalt from waste dusts generated by the glass industry. *Hydrometallurgy* **77**.

Jenny H. (1941) *Factors of Soil Formation*., McGraw-Hill Book Company, London.

Johansson C., Norman M. and Burman L. (2009) Road traffic emission factors for heavy metals. *Atmos. Environ.* **43**, 4681–4688.

Kabata-Pendias A. (2011) *Trace Elements in Soils and Plants*., CRC Press, London.

Keen B. A. and Raczkowski H. (1921) THE RELATION BETWEEN THE CLAY CONTENT AND CERTAIN PHYSICAL PROPERTIES OF A SOIL. *J. Agric. Sci.* **11**.

King R. B. (1994) *Encyclopedia of Inorganic Chemistry*., John Wiley & Sons, Chichester.

Kinniburgh D. G., Jackson M. L. and Syers J. K. (1976) Adsorption of Alkaline Earth, Transition, and Heavy Metal Cations by Hydrous Oxide Gels of Iron and Aluminum. *Soil Sci. Soc. Am. Journal* **40**.

Kliewer M. and Evans H. J. (1963) Cobamide Coenzyme Contents of Soybean Nodules & Nitrogen Fixing Bacteria in Relation to Physiological Conditions. *Plant Physiol.* **36**, 197–201.

Komnitsas K., Bartzas G. and Paspaliaris I. (2004) Efficiency of limestone and red mud barriers: laboratory column studies. *Miner. Eng.* **17**, 183–194.

Kononova M. M. (1966) *Soil Organic Matter*., Pergamon Press, New York.

Krauskopf K. . and Bird D. . (1995) *Introduction to Geochemistry*. 3rd ed., McGraw-Hill, New York.

Krupka K. M. and Serne R. J. (2002) *Geochemical Factors Affecting the Behaviour of Antimony, Cobalt, Europium, Technetium, and Uranium in Vadose Sediments*.,

Kurata A. (1974) Cobalt Content in the Shallow Sea Sediments ~. *J. Oceanogr. Soc. Japan* **30**, 199–202.

Landry C. J., Koretsky C. M., Lund T. J., Schaller M. and Das S. (2009) Surface complexation modeling of Co(II) adsorption on mixtures of hydrous ferric oxide, quartz and kaolinite. *Geochim. Cosmochim. Acta* **73**, 3723–3737.

Langmuir D. (1997) *Aqueous Environmental Geochemistry*., Prentice Hall, London.

Lee Abdullah T., Endan J. and Mohd Nazir B. (2009) Changes in Flower Development, Chlorophyll Mutation and Alteration in Plant Morphology of Curcuma alismatifolia by Gamma Irradiation. *Am. J. Appl. Sci.* **6**, 1436–1439.

Liu C., Zhu Z., Li F., Liu T., Liao C., Lee J.-J., Shih K., Tao L. and Wu Y. (2016) Fe(II)-induced phase transformation of ferrihydrite: The inhibition effects and stabilization of divalent metal cations.

Liu X., Lu X., Sprik M., Cheng J., Meijer E. J. and Wang R. (2013) Acidity of edge surface sites of montmorillonite and kaolinite.

Lorens R. B. (1981) Sr, Cd, Mn and Co distribution coefficients in calcite as a function of calcite precipitation rate. *Geochim. Cosmochim. Acta* **45**, 81–553.

Lotfy S. M. and Mostafa A. Z. (2014) Phytoremediation of contaminated soil with cobalt and chromium. *J. Geochemical Explor.* **144**, 367–373.

Ludwig R. D., McGregor R. G., Blowes D. W., Benner S. G. and Mountjoy K. (2002) A Permeable Reactive Barrier for Treatment of Heavy Metals. *Ground Water* **40**, 59–66.

Ma Y. and Hooda P. S. (2010) Chromium, Nickel and Cobalt. In *Trace Elements in Soils* (ed. P. S. Hooda). John Wiley & Sons, London. pp. 461–480.

Maxie E. C., Sommer N. F., Muller C. J. and Rae H. L. (1966) Effect of gamma radiation on the ripening of bartlett pears. *Plant Physiol.* **41**, 437–42.

McLaren R. G., Backes C. a., Rate A. W. and Swift R. S. (1998) Cadmium and Cobalt Desorption Kinetics from Soil Clays: Effect of Sorption Period. *Soil Sci. Soc. Am. J.* **62**, 332–337.

Melki M. and Marouani A. (2010) Effects of gamma rays irradiation on seed germination and growth of hard wheat. *Environ. Chem. Lett.* **8**, 307–310.

Melki M. and Sallami D. (2008) Studies the effects of low dose of gamma rays on the behaviour of chickpea under various conditions. *Pakistan J. Biol. Sci. PJBS* **11**, 2326–30.

Mengel K. and Kirkby E. . (1978) *Principles of Plant Nutrition*., International Potash Institute, Berne.

Mettler F. A. and Voelz G. L. (2002) Major Radiation Exposure — What to Expect and How to Respond. *N. Engl. J. Med.* **346**, 1554–1561.

Mitchell R. (1967) Trace Elements in Soils. In *Chemistry of the Soil1* (ed. F. Bear). Reinhold Publishing Company, London.

Motojima K., Tachikawa E. and Kamiyama H. (1978) REMOVAL OF RADIOCOBALT IN WASTE WATER BY ACTIVATED CHARCOAL USING OXINE AS A CHELATING AGENT. *Ann. Nucletlr Energy* **5**.

Mudd G. M., Weng Z., Jowitt S. M., Turnbull I. D. and Graedel T. E. (2013) Quantifying the recoverable resources of by-product metals: The case of cobalt. *Ore Geol. Rev.* **55**, 87–98.

Mulligan C. N., Yong R. N. and Gibbs B. F. (2001) Remediation technologies for metal-contaminated soils and groundwater: an evaluation. *Eng. Geol.* **60**, 193–207.

Nicholson K. and Eley M. (1997) Geochemistry of Manganese Oxides: Metal Adsorption in Freshwater and Marine Environments. *Geol. Soc. Spec. Publ.* **119**, 309–326.

Nockolds S. R. and Allen R. (1954) The geochemistry of some igneous rock series - I. *Geochim. Cosmochim.* **5**.

Nockolds S. R. and Allen R. (1953) The geochemistry of some igneous rocks. *Geochim. Cosmochim.* **4**.

Nockolds S. R. and Mitchell R. L. (1948) The geochemistry of some Caledonian plutonic rocks: a study in the relationship between the major and trace elements of igneous rocks and their minerals. *Trans. R. Soc. Edinburgh* **61**.

O'Day P. A., Brown JR G. E. and Parks G. A. (1994a) X-Ray Absorption Spectroscopy of Cobalt(II) Multinuclear Surface Complexes and Surface Precipitates on Kaolinite. *J. Colloid Interface Sci.* **165**, 269–289.

O'Day P. A., Parks G. A. and Brown Jr G. E. (1994b) Molecular Structure and Binding Sites of Cobalt(II) Surface Complexes on Kaolinte from X-Ray Absorption Spectroscopy. *Clays Clay Miner.* **42**, 337–355.

van Olphen H. (1977) *Introduction to Clay Colloid Chemistry*. 2nd ed., Wiley-Interscience, New York.

Ona-Nguema G., Morin, Guillaume, Juillot F., Calas G. and Brown Jr G. E. (2005) EXAFS Analysis of Arsenite Adsorption onto Two-Line Ferrihydrite, Hematite, Goethite, and Lepidocrocite. *Environ. Sci. Technol.* **39**.

Palit S., Sharma A. and Talukder G. (1994) Effects of Cobalt on Plants. *Bot. Rev.* **60**.

Peacock C. L. and Sherman D. M. (2005) Surface complexation model for multisite adsorption of copper(II) onto kaolinite. *Geochim. Cosmochim. Acta*.

Pettit R. E. (2004) *Organic Matter, humus, humate, humic acid, fulvic acid and humin: Their importance in soil fertility and plant health*.,

Raask E. (1985) The Mode of Occurrence and Concentration of Trace Elements in Coal. *Prog. Energy Combust. Sci.* **11**.

Raghavan R., Coles E. and Dietz D. (1991) Cleaning Excavated Soil Using Extraction Agents: A State-of-the-Art Review. *J. Hazard. Mater.* **26**, 81–87.

Reddy M. S., Basha S., Joshi H. V and Jha B. (2005) Evaluation of the emission characteristics of trace metals from coal and fuel oil fired power plants and their fate during combustion. *J. Hazard. Mater.* **123**, 242–249.

Regenspurg S. and Peiffer S. (2005) Arsenate and chromate incorporation in schwertmannite. *Appl. Geochemistry* **20**, 1226–1239.

Robinson B. H., Brooks R. R. and Clothier B. E. (1999) Soil Amendments Affecting Nickel and Cobalt Uptake by Berkheya coddii : Potential Use for Phytomining and Phytoremediation. *Ann. Bot.* **84**, 689–694.

Rout K., Mohapatra M. and Anand S. (2012) 2-Line Ferrihydrite: Synthesis, Characterization and its Adsorption Behaviour for Removal of Pb(II), Cd(II), Cu(II) and Zn(II) from Aqueous Solutions. *Dalt. Trans.* **41**, 3302–3312.

Sacconi B. L., Maggio F. and Cavasino F. P. (1962) Studies in Coordination Chemistry. IX.' Investigation of the Stereochemistry of Some Complex Compounds of Cobalt (11) with N-Substituted Salicylaldimines. **84**.

Saleh H. M. (2012) Water hyacinth for phytoremediation of radioactive waste simulate contaminated with cesium and cobalt radionuclides. *Nucl. Eng. Des.* **242**, 425–432.

Schenck C. V, Dillard J. G. and Murray J. W. (1983) Surface Analysis and the Adsorption of Co(ll) on Goethite. *J. Colloid Interface Sci.* **95**, 398–409.

Schmidt M., Stumpf T., Walther C., Geckeis H. and Fanghänel T. (2009) Incorporation versus adsorption: substitution of Ca 2+ by Eu 3+ and Cm 3+ in aragonite and gypsum.

Schultz M. F., Benjamin M. M. and Ferguson J. F. (1987) Adsorption and Desorption of Metals on Ferrihydrite: Reversibility of the Reaction and Sorption Properties of the Regenerated Solid. *Environ. Sci. Technol.* **21**, 863–869.

Schwertmann U. and Cornell R. M. (2003) *Iron oxides: Structure, Properties, Reactions, Occurrences and Uses.*, Wiley-VCH.

Schwertmann U. and Cornell R. M. (1991) *Iron Oxides in the Laboratory: Preparation and Characteristics.*, VCH, Weinheim.

Sheoran V., Sheoran A. S. and Poonia P. (2009) Phytomining: A review. *Miner. Eng.* **22**, 1007–1019.

Sherman D. M., Peacock C. L. and Hubbard C. G. (2008) Surface complexation of U(VI) on

goethite (α-FeOOH). *Geochim. Cosmochim. Acta* **72**, 298–310.

Shi H., He F. and Ye J. (2016) Synthesis and structure of iron- and strontium-substituted octacalcium phosphate: Effects of ionic charge and radius. *J. Mater. Chem. B* **4**, 1712–1719.

Sidrak G. H. and Suess A. (1973) Effects of low doses of gamma radiation on the growth and yield of two varieties of tomato. *Radiat. Bot.* **13**, 309–314.

Silva F. L. F., Matos W. O. and Lopes G. S. (2015) Determination of cadmium, cobalt, copper, lead, nickel and zinc contents in saline produced water from the petroleum industry by ICP OES after cloud point extraction. *Anal. Methods* **7**, 9844–9849.

Sims R. C. (1990) Soil Remediation Techniques at Uncontrolled Hazardous Waste Sites A Critical Review. *J. Air Waste Manag. Assoc.* **40**.

Smith K. and Paterson J. (1995) Manganese and Cobalt. In *Heavy Metals in Soils* (ed. B. Alloway). Springer, Dordrecht.

Spark K. M., Wells J. D. and Johnson B. B. (1995) Characterizing trace metal adsorption on kaolinite. *Eur. J. Soil Sci.* **46**, 633–640.

Sparks D. L. (1995) *Environmental Soil Chemistry*., Academic Press, London.

Sparks D. L. (2005) Metal and oxyanion sorption on naturally occurring oxide and clay mineral surfaces. In *Environmental Catalysis* (ed. V. Grassion). Taylor and Francis.

Sposito G. (1986) Distinguishing adsorption from surface precipitation. In *Geochemical Processes at Mineral Surfaces* (eds. J. Davis and K. Hayes). American Chemical Society, Washington, DC.

Sposito G. (1984) *The Surface Chemistry of Soils*., Oxford University Press, New York.

Stevenson F. J. (1994) *Humus chemistry: Genesis, Composition, Reactions*. 2nd ed., John Wiley & Sons Inc, New York.

Stumm W. (1992) *Chemistry of the Solid-Water Interface: Processes at the Mineral-Water and Particle-Water Interface in Natural Systems*., John Wiley & Sons Inc, New York.

Stumm W. and Morgan J. J. (1996) *Aqueous Chemistry: Chemical Equilibria and Rates in Natural Waters*., John Wiley & Sons Inc, New York.

Sverjensky D. A. and Sahai N. (1996) Theoretical prediction of single-site surface-protonation equilibrium constants for oxides and silicates in water. *Geochim. Cosmochim. Acta* **60**, 3773–3797.

Swanner E. D., Planavsky N. J., Lalonde S. V, Robbins L. J., Bekker A., Rouxel O. J., Saito M. A., Kappler A., Mojzsis S. J. and Konhauser K. O. (2014) Cobalt and marine redox evolution. *Earth Planet. Sci. Lett.* **390**, 253–263.

Szyma ski K., Morawski A. W. and Mozia S. (2016) Humic acids removal in a photocatalytic membrane reactor with a ceramic UF membrane. *Chem. Eng. J.* **305**, 19–27.

Tadesse B., Donaldson J. D. and Grimes S. M. (1994) Contaminated and polluted land: A general review of decontamination management and control. *Chem. Technol. Biotechnol.* **60**, 227–240.

Tatsumoto M. (1957) Chemical investigations of deep-sea deposits - XXII. Cobalt and nickel in sea deposits. *Chem. Soc. Japan Pure Chem. Sect.* **78**.

Thiruvenkatachari R., Vigneswaran S. and Naidu R. (2008) Permeable reactive barrier for groundwater remediation. *J. Ind. Eng. Chem.* **14**.

Thompson H. A., Parks G. A. and Brown G. E. (2000) Formation and Release of Cobalt(II) Sorption and Precipitation Products in Aging Kaolinite–Water Slurries. *J. Colloid Interface Sci.* **222**, 241–253.

Tipping E. (2002) *Cation binding by humic substances*., Cambridge University Press, Cambridge.

Tokaz E. J., Boyd W. A., Freedman J. H. and Waalkers M. P. (2013) Toxic Effects of Metals. In *Casarett & Doull's Toxicology: The Basic Science of Poisons* (ed. C. D. Klaassen). McGraw-Hill, Hightstown, NJ.

Towe K. M. and Bradley W. F. (1967) Mineralogical constitution of colloidal "hydrous ferric oxides." *J. Colloid Interface Sci.* **24**.

Tunega D., Benco L., Haberhauer G., Gerzabek M. H. and Lischka H. (2002) Ab Initio Molecular Dynamics Study of Adsorption Sites on the (001) Surfaces of 1:1 Dioctahedral Clay Minerals. *J. Phys. Chem. B* **106**.

Undabeytua T., Nir N., Rytwo G., Serban C., Morillo E. and Maqueda C. (2002) Modeling Adsorption-Desorption Processes of Cu on Edge and Planar Sites of Montmorillonite. *Environ. Sci. T* **36**.

Ward Whicker F. and Schultz V. (1982) *Radioecology: Nuclear Energy and the Environment Volume One*., CRC Press, Boca Raton.

Wasserman M. A., Bartoly F., Poquet I. and Perez D. V. (2001) Assessment of the mobility and bioavailability of 60 Co and 137 Cs in contaminated soils. In *roceedings of the 5 Regional congress on radiation protection and safety; 2 Iberian and Latin American Congress on Radiological Protection; Regional IRPA Congress Societies* Brazil.

Wendling L. A., Kirby J. K. and McLaughlin M. J. (2009a) AGING EFFECTS ON COBALT AVAILABILITY IN SOILS. *Environ. Toxicol. Chem.* **28**, 1609.

Wendling L. A., Ma Y., Kirby J. K. and McLaughlin M. J. (2009b) A Predictive Model of the Effects of Aging on Cobalt Fate and Behavior in Soil. *Environ. Sci. Technol* **43**, 135–141.

Wilkie J. A. and Hering J. G. (1996) Adsorption of arsenic onto hydrous ferric oxide: Effects of adsorbate/adsorbent ratios and co-occurring solutes. In *Colloids and Surfaces A: Physicochemical and Engineering Aspects*

Wood B. J. and Blundy J. D. (2001) The effect of cation charge on crystal–melt partitioning of trace elements. *Earth Planet. Sci. Lett.* **188**, 59–71.

Young R. S. (1957) The geochemistry of cobalt. *Geochim. Cosmochim. Acta* **13**.

Yuwono V. M., Burrows N. D., Soltis J. A., Do T. A. and Penn R. L. (2012) Aggregation of ferrihydrite nanoparticles in aqueous systems. *Faraday Discuss.* **159**.

Zhu J., Pigna M., Cozzolino V., Caporale A. G. and Violante A. (2010) Competitive sorption of copper(II), chromium(III) and lead(II) on ferrihydrite and two organomineral complexes. *Geoderma* **159**, 409–416.

Chapter 3: Methodologies

3.1 Batch Sorption Experiments

Batch sorption experiments were performed to investigate Co uptake to a number of materials. These were conducted in 50 mL plastic centrifuge tubes at room temperature and in aerobic conditions. In these experiments a known amount of solid was mixed with a known amount of Co and background electrolyte. The amount and concentration of these varied for the individual experiments and specific information can be found in the methods section of the experimental chapters (Chapters 4, 5 and 6). The pH was then set to a desired value through dropwise (10 µL aliquots) addition of either 0.01, 0.1, or 0.5 mol L^{-1} HCl or NaOH. pH was recorded when there was less than 0.01 pH unit change in 15 seconds. This was repeated twice a day for 4 days in order to overcome the sorbent's buffering capacity and reduce pH drift during the equilibration period. The samples were shaken continuously while the pH was monitored and set back to within ±0.15 of the desired pH. The samples then continued to be shaken once the pH had been set for the final time and the equilibration period started.

After the equilibration period, the pH of each sample was measured again and recorded as the final pH.

To produce a sorption edge, the pH was varied across the range 3.5 – 8.5, while keeping the amount of solid, background electrolyte concentration, and Co concentration the same. The pH was measured using a Thermo Scientific Orion 9102BNWP bench top pH meter and glass bulb electrode calibrated to pH 4 and 7 using standard buffer solutions.

3.2 Desorption experiments

Desorption experiments were carried out by aging the sorbed samples for a period of time (either 1, 7, 28, or 84 days). The samples were centrifuged and prepared for ICP-OES as described in Section 3.1. The supernatant was then discarded and replaced by 30 ml of either DIW, 0.01 mol L^{-1} EDTA, 0.01 mol L^{-1} citric acid, or 0.01 mol L^{-1} hydrochloric acid. After equilibrating for 24 hours on a shaker table, the samples were centrifuged and prepared for ICP-OES analysis.

3.3 Solution analysis by ICP-OES

Cobalt sorption was determined by measurement on an inductively coupled plasma atomic emission spectrometer (ICP-OES). This process works based on the ability of metals to release electromagnetic radiation when they are raised to higher energy states and return to their ground state. Each metal produces radiation at a unique wavelength and so metals can be identified by the spectrum of radiation that they produce. The intensity of radiation released is proportional to the number of atoms excited, and therefore by comparing the sample spectra to known standards the concentration of atoms in the sample can be determined (Mendham et al., 2000).

In ICP-OES this excitation of atoms occurs in a plasma (usually ionised argon gas) that is heated to between 7000 and 15000 K. The sample solution is first nebulised into a fine aerosol and then carried into the burning plasma by a stream of argon gas. In an inductively coupled plasma source the argon stream flows through the central of three concentric tubes and the sample is excited by several turns of a metal induction tube that has a radiofrequency current flowing through it. A second stream of argon flows in a helical pattern in the outermost tube and maintains the plasma. The plasma is initially ignited by a spark and then continues to be self-sustaining. Once the excited sample ions reach the flame they emit radiation. The radiation is captured by a photomultiplier tube which converts it into an electrical current, and the resulting voltage is proportional to the concentration of the element in the sample (Mendham et al., 2000).

Sorption samples were prepared for ICP-OES by centrifuging for 10 minutes at 4000 RPM. A 5 mL sample of the supernatant was then filtered through a 0.22 μm syringe filter and added to 5 mL of 2% HNO_3 ready for ICP analysis of the Co concentration. In the case of samples with a high humic acid content, once filtered through the syringe filter, they were filtered at 10k Dalton in centrifuge filters, after which 5 mL was added to 5 mL of 2% HNO_3. The samples were analysed on a Thermo iCAP 7400 radial ion-coupled plasma optical emission spectrometer (ICP-OES; ThermoFisher Scientific, USA). Percentage sorption was then calculated by subtracting the measured Co concentration from the amount of Co that was initially added and multiplying by 100.

3.4 X-ray powder diffraction (XRD)

The fundamental principle of XRD is that typical electromagnetic waves are described by a sine wave, and if two identical waves do not coincide they have a phase shift (δφ) (Fig. 3.1). When x-rays are scattered off atoms at different angles they arrive at a detector with

a phase shift. The detector measures the intensity of each of the waves and so phase shifts can give information about relative atomic positions of a crystalline structure (Dinnebier and Billinge, 2008).

However, diffracted rays will only produce constructive interference, and thereby intensify the beam, when the difference in length between the two rays is equal to the wavelength, or a multiple of it. The angle at which constructive interference occurs is determined according to Bragg's Equation:

$$2d \sin\theta = n\lambda \qquad (3.1)$$

where d is the distance between planes in the crystal, n is a positive integer called the order of reflection, θ is the scattering angle of the diffracted x-ray, and λ is the wavelength (Fig 3.2) (Whiston, 1996). By powdering a crystal, the number of planes increases and they all face different directions; this increases the likelihood that some of the planes will satisfy the Bragg Equation (Whiston, 1996).

By using a monochromatic x-ray beam and rotating the sample through a range of 2θ values, the detector can measure all possible angles that fulfil the Bragg Equation and

Figure 3.1: Graphical illustration of the phase shift between two sine waves of equal amplitude. From Dinnebier and Billinge (2008).

thus produce all the diffraction peaks associated with the sample (Cockcroft and Fitch, 2008) .

Samples were ground into a powder using a mortar and pestle, and then loaded into Si sample holders of Ø 5mm x 1mm depth and levelled using a glass slide. Samples were analysed on a Philips PW1050 X-ray diffractor configured in vertical θ/2θ Bragg-Brentano using Cu Kα radiation with a Ni filter graphite secondary (the monochromator is positioned after the sample) monochromator and scanning between 5-70° 2θ. Diffraction peaks from unknown samples were matched to known standard reference patterns using Diffrac.Suite Eva v3.0 software using the International Centre for Diffraction Data (ICDD) PDF2 database.

3.5 X-ray Absorption Spectroscopy (XAS)

The basis of collecting XAS data is to bombard a sample with x-rays of known energy. At element specific threshold energies, atoms in the sample will absorb some of the x-rays, causing the excitation or ejection of an electron from a *K*, *L* or *M* electron shell and creating a core-hole. The amount of x-rays absorbed can be quantified by comparing the energy of the x-rays before absorption with the energy after. The intensity of an x-ray passing through a sample of a given thickness is described by the absorption coefficient, μ:

$$I = I_0 e^{-\mu t} \qquad (3.2)$$

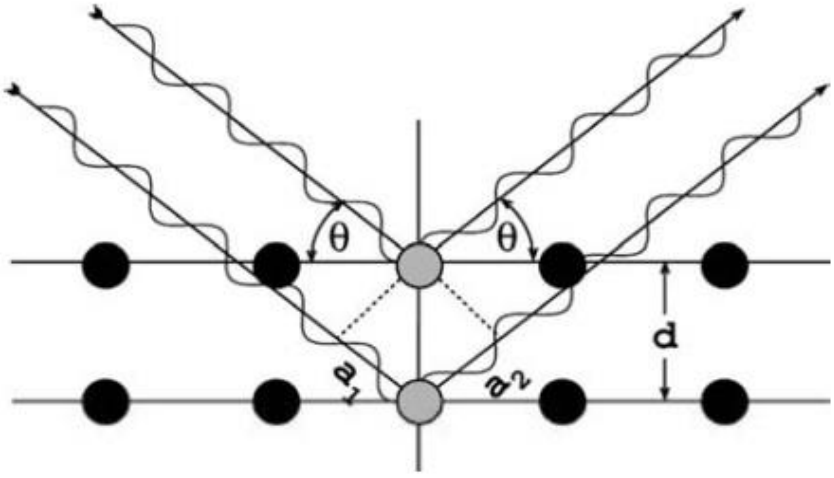

Figure 3.2: Geometric derivation of Bragg's law: Constructive interference occures when the delay between waves scattered from adjacent lattice planes given by *a1* + *a2* is an integer multiple of the wavelength λ. From Stanjek and Häusler (2004).

Where I is the intensity of the beam transmitted through the sample, I_0 is the initial x-ray intensity, and t is the thickness of the sample. The absorption coefficient is dependent on x-ray energy, atomic number, atomic mass, and density of the sample. Because the absorption coefficient is dependent on the atomic number and atomic mass, this makes it possible to determine the elements present in a sample (Newville, 2004).

The energy after absorption can either be measured by transmission or fluorescence. In transmission measurements, the amount of x-rays absorbed is calculated from the difference in initial x-ray intensity and that measured once the x-rays have passed through the sample, as in Equation 3.2 (Newville, 2004). However, this approach is limited to samples containing a concentration of the absorbing atom of >500 ppm (Penner-Hahn, 2003). Measurements in fluorescence involve detecting the refilling of the core hole and can be used for more dilute samples (Penner-Hahn, 2003; Newville, 2004). This is either by measuring the fluorescence x-rays produced by the excited atom as an electron drops down a shell to fill the core hole, or by measuring the kinetic energy of ejected electrons as the core hole is filled. The latter is known as the “Auger process”, which occurs when an electron at a higher shell drops to fill the core hole and simultaneously ejects another electron from the same higher shell (Bunker, 2010). When fluorescence measurements are being taken the formula to measure the absorption coefficient becomes:

$$\mu(E) \propto I_f/I_0 \qquad (3.3)$$

where I_f is the emitted fluorescent x-rays or electron emission (Newville, 2004)

The initial ejection of the electron from an atom creates a photoelectron that scatters off nearby atoms and back to the absorbing atom, causing constructive or destructive interference. The photoelectron can also scatter from one neighbouring atom to another before returning to the absorbing atom; this is known as multiple scattering (Calvin, 2013).

By measuring the absorption over a range of x-ray energies a spectrum is produced (e.g. Fig. 3.3).

3.5.1. Synchrotrons

Despite synchrotron radiation working in the same way as radiation from x-ray tubes, synchrotrons are necessary to study XAS as they produce spectral brightness of more than 10 orders of magnitude greater than that from x-ray tubes, which allows the beam to be focussed onto small samples while maintaining the intensity of the x-rays (Penner-Hahn, 2003; Balerna and Mobilio, 2015).

Synchrotron light sources work by injecting electrons that are travelling at velocities near the speed of light into a storage ring to produce broad-spectrum radiation, that extends through the visible light to X-rays (Kunz, 1979; Calvin, 2013). To prevent the electron beam from decaying through interactions with other particles, the electrons travel around the storage in a vacuum chamber that is kept under ultrahigh vacuum conditions (Margaritondo, 1987). However, residual gas particles often remain which gradually causes decay over several hours, requiring the electron beam to be "topped up". This can either be through the continuous addition of electrons throughout the day (such as every 10 minutes as occurs at Diamond Light Source) or by injecting a large amount of electrons twice a day. Continuously adding electrons makes the beamlines more stable and the electron beam is able to remain at maximum intensity at all times (Diamond Light Source, 2018)

The storage ring consists of straight sections alternating with bending magnets that cause the electrons to bend their trajectory around the ring. Insertion devices, such as "wigglers" and "undulators", are also present in modern synchrotrons in order to produce more intense light (Bunker, 2010; Diamond Light Source, 2018). These consist of pairs of magnets of alternating orientation in a row so that passing electrons feel a magnetic field of alternating polarity. This causes the electron path to oscillate back and forth, which produces radiation at each bend (Bunker, 2010).

Figure 3.3 Schematic illustration of an X-ray absorption spectrum, showing the structured absorption that is seen both within ca. 50eV of the edge (the XANES) and for several hundred to >1000eV above the edge (the EXAFS). From Penner-Hahn (2003).

As the electrons are bent by the bending magnets or insertion devices they lose energy in the form of electromagnetic radiation, and these are then channelled into the beamlines where the experimental stations are located (Calvin, 2013; Diamond Light Source, 2018). In the beamlines, the radiation is first focussed and filtered through the use of mirrors and monochromators before being introduced to the sample. The mirrors are used to preserve the high optical quality of the photon beam by focussing the radiation along the beamline, while the monochromator eliminates photons that have energies outside of the desired range (Margaritondo, 1987).

3.5.2 EXAFS sample preparation

EXAFS spectra were collected at the Co K-edge (7722 eV) at Beamline B18 at Diamond Light Source Ltd, UK, operating at 3 GeV with a typical current of 300 mA. The X-rays at B18 are generated from a bending magnet source. The beam is vertically collimated by a Si mirror before passing through a double crystal Si monochromator. It was then focused onto the sample to give a spot size of 200x250 μm at the sample. Air dried (40 °C) sorption samples were presented to the beam as 8 mm pressed pellets using cellulose as a dilutant to reduce chemical thickness. The sample pellets were held in KaptonTM tape for analysis, and a separate 1000 mg L^{-1} $Co(NO_3)$ solution was also prepared and held in a polythene bag for analysis. Spectra were collected for the samples containing Ka and HA in fluorescence mode at room temperature (~295°K) using a 32 element solid state Ge detector, and for the samples containing Fh in transmission mode at room temperature. An aqueous Co^{2+} standard was also analysed and held up to the beamline in a zip-lock plastic bag. More detailed information on EXAFS sample preparation can be found in Chapter 4.2.3.

3.5.3. Extended X-ray Absorption Fine Structure (EXAFS) Spectroscopy

The features of the XAS spectrum are analysed to gain an understanding of the sample. In EXAFS spectroscopy, the features of interest are the oscillations at energies of roughly 40 to 800 eV above the absorption edge, which is a sharp rise in absorption caused by the excitation of the atom (Bianconi, 1980). The absorption edge is unique to each element, making it possible to analyse certain elements of interest in a sample. There are also multiple edges for each element, which are named according to the principle quantum number of the electron that has been excited (K for n = 1, L for n = 2, M for n = 3 etc.) (Penner-Hahn, 2003)

Once analysed, these oscillations provide information on the local environment (up to ~5 Å) of a particular element in the sample, such as the bond length and coordination

number between the absorbing atom and its neighbours (Penner-Hahn, 2003). This information, however, is an average of the local environments of each atom of that element in the sample, and therefore the technique is best used with homogenous samples (Bianconi, 1980; Calvin, 2013).

In order to analyse raw EXAFS data, it is necessary to first remove the background. Errors propagated during background subtraction will not affect the measured interatomic distance, but will affect the coordination number determined from the data (Bianconi, 1980).

Because EXAFS is interested in the oscillations in the absorption coefficient, the atomic background is removed and the EXAFS is defined as:

$$X(E) = \frac{\mu(E) - \mu_0(E)}{\Delta\mu_0(E_0)} \qquad (3.4)$$

Where $\mu_0(E)$ represents the bare atom background, and $\Delta\,\mu_0(E)$ is the edge step. This gives the oscillations normalised to one absorption event (Bianconi, 1980; Newville, 2004).

X(E) is then converted to X(k) using the formula:

$$k = \sqrt{\frac{2m_e(E-E_0)}{\hbar^2}} \qquad (3.5)$$

where m_e is the electron mass, E_0 is the binding energy of the photoelectron and $\hbar$ is Planck's constant. This step is important because as XAFS is an interference effect that is dependent on the nature of the photoelectron being like a wave, it is convenient for the EXAFS to be in terms of the photoelectron wavenumber. The X(k) is then often weighted by k^2 or K^3 in order to amplify oscillations at high k values (Penner-Hahn, 2003; Newville, 2004).

A Fourier transform of the k-space data is taken to decompose the signal into its different constituent frequencies. This makes it possible to identify each coordination shell as they produce distinct peaks.

EXAFS data analysis of the Co K-edge was undertaken using the Demeter software package v0.9.24 (Ravel and Newville, 2005). Spectra were averaged, background subtracted and normalised using the Athena application. The processed spectra were then fit *ab initio* to model spectra in Artemis to determine the atomic coordination surrounding the central Co atom.

3.6 Scanning transmission electron microscopy (STEM)

The STEM is a highly versatile microscope that is capable of atomic resolution imaging and nanoscale analysis.

A STEM works by accelerating electrons to a typical energy of 100 – 300 keV from an electron gun that are focused at a sample. In contrast to a conventional TEM where lenses are placed between the sample and the detector to magnify the exit wave, the STEM has a series of lenses between the electron gun and the sample to focus the electrons before they reach the sample. This creates a small electron probe (0.2 – 5 nm) that can scan the sample, rather than illuminate the entire sample at once (Reimer and Kohl, 2010). The electron beam also has to pass through a monochromator to ensure the electrons have a narrow energy distribution. The electrons are scattered by the sample, and these are detected and their intensity measured as a function of the probe position to form an image. Most commonly, the detectors measure the transmitted electrons and so are placed after the sample. Because of this samples are required to be electron transparent (typically <50 nm) (Nellist, 2008).

Commonly used STEM detectors are bright-field (BF) and annular dark-field (ADF) detectors. Both of these detectors sum the electron intensity to produce an image, however BF detector measures electron intensity over a disc along the optic axis of the microscope while the ADF detector measures electrons over a ring around the optic axis where only scattered electrons can be detected. ADF imaging is important to STEM because it is capable of differentiating different elements in a sample as it is sensitive to atomic number (Nellist, 2008).

Separate Fh, Ka and HA samples with Co surface loadings of approximately 1 wt% were prepared for STEM analysis in the same way as the sorption experiments. Briefly 0.03 dry g equivalent of sorbent was suspended in 29.5 mL of 10^{-3} mol L^{-1} $NaNO_3$ and 0.6 mL 0.01 mol L^{-1} Co^{2+}. After 16 hrs the final pH was 7.5 ±0.5; consistent with > 90% aqueous Co removal in previous batch sorption experiments. Samples were then dispersed in methanol (or DI water in the case of HA) and a drop was pipetted onto a lacy / holey thin-film across a copper grid using a glass Pasteur pipette. As DI water was used to disperse the HA sample, the carbon film and grid underwent plasma treatment in a Fischione 1020 plasma cleaner for 10 seconds to make the film hydrophilic and ensure the sample was evenly distributed. (S)TEM images, energy dispersive X-ray (EDX) microanalysis elemental maps and electron energy loss spectra (EELS) were collected on an FEI Titan3 Themis 300: X-FEG 300 kV S/TEM. This was fitted with S-TWIN objective lens, monochromator (energy spread 1.1 eV when the monochromator is de-

excited), multiple high-angle annular dark-field (HAADF), annular dark-field (ADF), bright-field (BF) STEM detectors, FEI Super-X 4-detector EDX system, Gatan Quantum ER 965 energy filter for EELS and energy filtered TEM and Gatan OneView 4K CMOS digital camera. To minimise potential sample damage (which was most important for kaolinite samples) a low beam current of 0.3 nA was used throughout data acquisition and limited magnification (280k x) BF TEM imaging with short acquisition times (< 1 s) was performed before commencement of HAADF STEM imaging and EDX elemental mapping (using a ~80 pA probe current).

3.6.1. Electron Energy Loss Spectroscopy (EELS)

EELS uses the signals of the inelastically scattered electrons (those that interact electrostatically with the orbiting electrons of an atom which results in the loss of energy (Egerton, 1986)) from the sample to give analytical information about the sample, such as the chemistry and electronic structure (Nellist, 2008).

The experimental set up is the same as that for STEM and also requires a monochromator to limit the energy of the electrons (section 3.5, above). The electrons that were transmitted through the sample pass through a spectrometer that deflects all the electrons through 90 degrees. Electrons with more energy will be deflected less thus dispersing the beam into a spectrum of energies. The spectrum is then detected by either a serial spectrometer where the spectrum is scanned across a slit by varying the strength of the magnetic field, or by a parallel spectrometer where the entire spectrum is collected at once (Ibach and Mills, 1982; Goodhew et al., 2001).

In an EELS spectrum, inelastic scattering is visible as an edge. These occur at the ionization threshold of an atom, where the energy lost by the electron is approximately equal to the ionisation energy of the corresponding atomic shell. Since binding energies are dependent on the atomic number of the scattering atom, this technique is capable of determining which elements are present in the sample (Egerton, 1986).

3.6.2. Energy Dispersive X-ray (EDX) microanalysis

EDX is the principle method for analysing the chemical composition of a sample in a TEM (Titchmarsh, 1993).

In a similar way to that of STEM and EELS, an electron beam is focused at the sample and the electrons interact with the atoms in the sample. As the electrons pass through the sample, they can cause the ionization of an atom's inner-shell which results in the emission of x-rays characteristic to that element. The x-rays are then measured by a detector, and because the x-rays have unique energies depending on the atom that the

electron was scattered by they give information on the chemical composition of the sample (Reimer and Kohl, 2010).

The detector is a piece of semiconducting Si or Ge that is in line of sight of the sample, as X-rays cannot be deflected. Each x-ray that reaches the detector excites electrons in the conduction band of the Si (or Ge), which results in identical number of positively charged holes in the outer electron shells. As the energy required to excite each electron is known to be 3.8 eV the number of electron hole pairs generated is proportional to the energy of the detected x-ray. If a voltage is applied across the Si semiconductor, a current will flow when an x-ray is absorbed and the magnitude of the current will be proportional to the energy of the x-ray. (Goodhew et al., 2001).

3.7 Thermodynamic Modelling of the mineral-water interface

The sorption behaviour of Co on end-member Fh, Ka and HA and the organo-mineral composites was fit to a thermodynamic surface complexation model using the program EQLFOR (Sherman et al., 2008; Sherman, 2009). The Fh and Ka models were then combined with the HA model using a linear component additivity approach to explore Co sorption behaviour on the Fh and Ka organo-mineral composites. The surface electrostatics in all the models were accounted for by adopting the basic Stern model (BSM). The Davies equation was used for activity corrections to the stability constants for aqueous species:

$$\log\gamma_i = Az_i^2\left(\frac{\sqrt{\mu}}{1+\sqrt{\mu}} - 0.3\mu\right) \qquad (3.6)$$

where γ is the activity coefficient, i represents the chemical species, z_i is the ionic charge of aqueous species, μ is the ionic strength of the solution and A and B are temperature dependent constants.

Detailed discussion on the development of the end-member Fh, Ka, HA, and organo-mineral composite models is available in Chapter 4.3.

3.7.1. Basic Stern Model

The BSM is a thermodynamic surface complexation model that employs the electrical double layer (EDL) theory. This theory states that the surface charge of a sorbent in solution creates an electrostatic potential that reduces with distance away from the surface. Because of this, EDL theory assumes that close to the surface there will be an excess of counterions (ions of the opposite charge to the surface charge) and as distance

from the surface increases the amount of coions (ions with the same charge as the surface) increases (Langmuir, 1997) (Fig. 3.4).

Because of the difference in electric potential close to the surface and further away, the activity of ions differs depending on their distance from the surface (Allison et al., 1991). This change in activity is described by an exponential Boltzmann expression:

$$(X_s^z)=(X^z)[e^{-\psi F/RT}]^z \quad (3.7)$$

Where z is the charge of ion X, (X_s^z) is the activity of ion X of charge z near the surface, (X^z) is the activity of X in the bulk solution unaffected by the surface, and $e^{-\psi F/RT}$ is the Boltzmann factor, wherein ψ is the potential in volts at the adsorption plane, F is the Faraday constant, R is the ideal gas constant, and T is the temperature (Langmuir, 1997).

The BSM expands on the EDL theory and explains the solid/ solution interface as having two regions: one, the Stern layer where counterions in contact with the solid are located, and two, a Gouy layer which is a diffuse layer further away from the solid (Fig 3.5). The Stern layer is split into two planes, the inner Helmholtz plane (IHP) and the outer

Figure 3.4: Depiction of the EDL theory. (a) shows the location of the co- and counter-ions in the mineral-water interface. At the surface there are only counter-ions, but the further away from the surface the more co-ions there are. (b) shows the charge distribution across the interface. Adapted from Harrison and de Mora (1969).

Helmholtz plane (OHP). The IHP is where counterions that are specifically adsorbed to the solid surface are located, including H^+ and OH^-. Counterions that are outer-spherically sorbed to the surface are located in the OHP because they are fully solvated and cannot approach as close to the solid surface. The Gouy layer uses the concept of the EDL as it contains mostly counterions but some coions are present (Harrison and de Mora, 1969; Stumm and Morgan, 1996).

Traditionally, the uptake and release of protons to/ from the mineral surface was described as:

$$SOH + H^+ \leftrightarrow SOH_2^+ \quad (3.8)$$

$$SOH \leftrightarrow SO^- + H^+ \quad (3.9)$$

where SO^- represents the surface site and H^+ is the proton. This is termed the 2-p*K* approach as it requires 2 stability constants (Lützenkirchen, 1998). However, more recently a 1-p*K* model is used:

$$\equiv SOH^{-0.5} + H^+ \leftrightarrow \equiv SOH_2^{+0.5} \quad (3.10)$$

This formalism is preferred as the stability constant *K* can be obtained experimentally through titrations to determine the point of zero charge (Lützenkirchen, 1998). This is also preferred due to its consistency with the Pauling Bond Valence Theory, which states that the total strength of the valency bonds that reach an anion from all neighbouring

Figure 3.5: Schematic arrangement of sorbates at a charged sorbent interface, as described by the BSM. From Thompson and Goyne (2012).

cations is equal to the charge of the anion (Boily et al., 2001). For a trivalent cation (e.g. Fe^{3+}) that has a coordination number of 6, this results in a net charge of -0.5 i.e. $\equiv SOH^{-0.5}$

Cation sorption to a solid surface is written as:

$$\equiv SO^- + M^{2+} \leftrightarrow \equiv SOM^+ \quad (3.11)$$

Where SO^- is the surface site and M^{2+} represents the cation. Assuming that M^{2+} is sorbed to the 0-plane, the amount of M^{2+} at the solid surface cannot be directly measured. Therefore, it is assumed to be related to the bulk M^{2+} activity through the Boltzmann expression in Eqn. 3.7, where X^z is replaced by M^{2+}. The mass-action expression and its intrinsic constant can thus be written:

$$K^{int}_{M^{2+}} = \frac{(SOM^+)}{(SO^-)(M^{2+})\exp(-\psi_0 F/RT)} \quad (3.12)$$

However, Eqn. 3.11 assumes a 2-p*K* formalism and is thus a rather crude representation of the reactions at the mineral-water interface. This is because (as explained above) $\equiv SO^-$ is not possible in reality.

The use of models on their own to determine the processes at the mineral-water interface is limited. This is because the simplest complex will often produce the best fit. For example, previous studies have reported models that show good fits with monodentate complexes between cations and common mineral surfaces (e.g. iron oxides and clays) (e.g. Dzombak and Morel, 1990; Ainsworth et al., 1994; Landry et al., 2009). Recent spectroscopic studies have shown that monodentate complexes do not form at the mineral-water surface, but rather bidentate and polynuclear complexes do (e.g. O'Day, et al., 1994a;b; Moon and Peacock, 2012). Therefore, models require constraining with molecular level information in order for them to be useful, which is what I present in Chapters 4 and 5.

3.7.2. Model Framework and input parameters

Surface complexation models were developed for the sorption of Co onto end-member Fh, Ka and HA that are consistent with the EXAFS data. The model framework for Co sorption to Fh is based on the model for copper sorption to Fh by Moon and Peacock (2013) and Otero Fariña et al. (2017b), the framework for Co sorption to Ka is adapted from the model for Co sorption to Ka by Heidmann et al. (2005b), and the framework for Co sorption to HA is based on the model for copper sorption to HA by Otero Fariña et al., (2017b). The model input parameters were obtained either through fitting potentiometric titration data for the sorbent acid-base behaviour, or from direct measurement of the

sorbent physiochemical characteristics, and are detailed in Moon and Peacock (2013) for Fh, Heidmann et al. (2005b) for Ka and López et al. (2012) for HA.

The basic stern model (BSM) is used to model surface electrostatics in the Fh, Ka and HA sorption systems. For Fh, a 3-site 1 pK formalism is assumed for the protonation of the Fh surface, involving two types of singly-coordinated surface oxygens (sorbing cations in edge-sharing ($\equiv FeOH^{-0.5}(e)$) and corner-sharing ($\equiv FeOH^{-0.5}(c)$) configuration), and the triply coordinated oxygens ($\equiv Fe3O^{-0.5}$) (e.g., Hiemstra et al., 1989; Hiemstra and van Riemsdijk, 2009; Moon and Peacock, 2013; Otero Fariña et al., 2017b). A 2-site, 1pK formalism is used for the protonation of the Ka surface. This involves a singly-coordinated surface oxygen ($\equiv AlOH^{-0.5}$) representing the pH-dependent charge, and negatively charged sites ($\equiv X^-$) to represent the permanent negative charge (e.g., Heidmann et al. (2005b). For the HA, a 1-site 1 pK formalism is used, involving $\equiv RCOO^-$ sites where the stability constants for the protonation of these sites and the site densities are constrained using the NICA-Donnan model (Kinniburgh et al., 1999), calibrated on multiple data sets (López et al. 2012).

The sorption data are fit by iterating the log K for the surface complexation reaction that represents the formation of the Co-Fh, -Ka or -HA complexes that were identified by EXAFS analysis. The three Fh systems that contained 10^{-2} mol L^{-1} ionic strength (5.8, 0.58 and 0.058 wt% Co) and two of the Ka systems that contained 10^{-2} mol L^{-1} ionic strength (0.058 and 0.0058 wt% Co) are fit simultaneously. Due to the limitations of EQLFOR, systems with different ionic strengths are fit separately.

3.7.3. Sensitivity Analysis of the Co-Ferrihydrite, -Kaolinite, and Humic Acid Surface Complexation Models

A sensitivity analysis was performed to evaluate the sensitivity of the end-member models to the input parameters. For each model, the input parameters (C_{stern}, electrolyte binding constants, surface site densities, and surface area) were systematically varied while monitoring the log *K* values for the Co adsorption complexes. The analyses are based on the protocols of Moon and Peacock (2013). The C_{stern} was varied by ±50%, the log K electrolyte binding constants between -1.5 and 0.5, and the surface site densities and the surface areas were varied by a factor of ±3. These were determined to be plausible ranges in the input parameters and therefore the resulting log *K* values would represent a sensible range wherein the model fit would still be good.

3.8 References

Ainsworth C. C., Pilon J. L., Gassman P. L., Van W. G. and Sluys D. (1994) Cobalt, Cadmium, and Lead Sorption to Hydrous Iron Oxide: Residence Time Effect. *Soil Sci. Soc. Am. J.* **58**, 1615–1623.

Allison J. D., Brown D. S. and Novo-Gradac K. J. (1991) MINTEQ2, A geochemical assessment data base and test cases for environmental systems. *Rep. EPA/600/3-91/-21*.

Balerna A. and Mobilio S. (2015) Introduction to Synchrotron Radiation. In *Synchrotron Radiation: Basics, Methods and Applications* (eds. S. Mobilio, F. Boscherini, and C. Meneghini). Springer, London.

Bianconi A. (1980) Surface X-ray absorption spectroscopy: Surface EXAFS and Surface XANES. *Appl. Surf. Sci.* **6**.

Boily J.-F., Lü Tzenkirchen J., Balmès O., Beattie J., Sjö Berg S. and Boily J.-F. (2001) Modeling proton binding at the goethite (a-FeOOH)–water interface. *Colloids Surfaces A Physicochem. Eng. Asp.* **179**, 11–27.

Bunker G. (2010) *Introduction to EXAFS*., Cambridge University Press, Cambridge.

Calvin S. (2013) *XAFS for Everyone*., CRC Press, London.

Cockcroft J. K. and Fitch A. N. (2008) Experimental Setups. In *Powder Diffraction: Theory and Practice* (eds. R. E. Dinnebier and S. J. L. Billlinge). The Royal Society of Chemistry, Cambridge.

Diamond Light Source (2018) How Diamond Works. Available at: http://www.diamond.ac.uk/Home/About/How-Diamond-Works.html [Accessed February 7, 2018].

Dinnebier R. E. and Billinge S. J. L. (2008) Principles of Powder Diffraction. In *Powder Diffraction: Theory and Practice* (eds. R. E. Dinnebier and S. J. L. Billlinge). The Royal Society of Chemistry, Cambridge.

Dzombak D. A. and Morel F. (1990) *Surface Complexation Modeling: Hydrous Ferric Oxide*., John Wiley & Sons Inc, New York.

Egerton R. F. (1986) *Electron Energy-Loss Spectroscopy in the Electron Microscope*., Springer, London.

Goodhew P. J., Humphreys J. and Beanland R. (2001) *Electron Microscopy and Analysis*., Taylor and Francis, London.

Harrison R. M. and de Mora S. . (1969) *Introductory Chemistry for the Environmental Sciences*., Cambridge University Press, Cambridge.

Heidmann I., Christl I., Leu C. and Kretzschmar R. (2005) Competitive sorption of protons and metal cations onto kaolinite: experiments and modeling. *J. Colloid Interface Sci.* **282**, 270–282.

Ibach H. and Mills D. L. (1982) *Electron Energy Loss Spectroscopy and Surface Vibrations*., Academic Press, London.

Kunz C. (1979) Introduction - Properties of Synchrotron Radiation. In *Synchrotron Radiation: Techniques and Applications* (ed. C. Kunz). Springer-Verlag, New York.

Landry C. J., Koretsky C. M., Lund T. J., Schaller M. and Das S. (2009) Surface complexation modeling of Co(II) adsorption on mixtures of hydrous ferric oxide, quartz and kaolinite. *Geochim. Cosmochim. Acta* **73**, 3723–3737.

Langmuir D. (1997) *Aqueous Environmental Geochemistry*., Prentice Hall, London.

López R., Gondar D., Antelo J., Fiol S. and Arce F. (2012) Study of the acid-base properties of a peat soil and its humin and humic acid fractions. *Eur. J. Soil Sci.* **63**, 487–494.

Lützenkirchen J. (1998) Comparison of 1-pK and 2-pK versions of surface complexation theory by the goodness of fit in describing surface charge data of (hydr)oxides. *Environ. Sci. Technol.* **32**, 3149–3154.

Margaritondo G. (1987) *Introduction to Synchrotron Radiation*., Oxford University Press, Oxford.

Mendham J., Denney R. . ., Barnes J. D. and Thomas M. (2000) *Vogel's Textbook of Quantitative Chemical Analysis*. 6th ed., Prentice Hall, London.

Moon E. M. and Peacock C. L. (2012) Adsorption of Cu(II) to ferrihydrite and ferrihydrite-bacteria composites: Importance of the carboxyl group for Cu mobility in natural environments. *Geochim. Cosmochim. Acta* **92**, 203–219.

Moon E. M. and Peacock C. L. (2013) Modelling Cu(II) adsorption to ferrihydrite and ferrihydrite-bacteria composites: Deviation from additive adsorption in the composite sorption system. *Geochim. Cosmochim. Acta* **104**, 148–164.

Nellist P. D. (2008) Scanning Transmission Electron Microscopy. In *Science of Microscopy2* (eds. P. W. Hawkes and J. C. H. Spence). Springer, London.

Newville M. (2004) Fundamentals of X-ray Absorption Fine Structure. In *Consortium for Advanced Radiation Sources* University of Chicago (USA).

O'Day P. A., Brown JR G. E. and Parks G. A. (1994) X-Ray Absorption Spectroscopy of Cobalt(II) Multinuclear Surface Complexes and Surface Precipitates on Kaolinite. *J. Colloid Interface Sci.* **165**, 269–289.

O'Day P. A., Parks G. A. and Brown Jr G. E. (1994) Molecular Structure and Binding Sites of

Cobalt(II) Surface Complexes on Kaolinte from X-Ray Absorption Spectroscopy. *Clays Clay Miner.* **42**, 337–355.

Otero-Fariña A., Peacock C. L., Fiol S., Antelo J. and Carvin B. (2018) A universal adsorption behaviour for Cu uptake by iron (hydr)oxide organo-mineral composites. *Chem. Geol.*

Penner-Hahn J. E. (2003) 2.13 X-ray Absorption Spectroscopy. In *Comprehensive Coordination Chemistry II V2* (eds. J. A. McCleverty and T. J. Meye). Pergamon, Oxford. pp. 159–186.

Ravel B. and Newville M. (2005) ATHENA, ARTEMIS, HEPHAESTUS: data analysis for X-ray absorption spectroscopy using IFEFFIT. *J. Synchrotron Rad* **12**, 537–541.

Reimer L. and Kohl H. (2010) *Transmission Electron Microscopy: Physics of Image Formation*. 5th ed., Springer, London.

Sherman D. M. (2009) Surface Complexation Modeling: Mineral Fluid Equilbria at the Molecular Scale. *Rev. Mineral. Geochemistry* **70**, 181–205.

Sherman D. M., Peacock C. L. and Hubbard C. G. (2008) Surface complexation of U(VI) on goethite (α-FeOOH). *Geochim. Cosmochim. Acta* **72**, 298–310.

Stanjek H. and Häusler W. (2004) Basics of X-ray Diffraction. *Hyperfine Interact.* **154**, 107–119.

Stumm W. and Morgan J. J. (1996) *Aqueous Chemistry: Chemical Equilibria and Rates in Natural Waters.*, John Wiley & Sons Inc, New York.

Thompson A. and Goyne K. W. (2012) Introduction to the Sorption of Chemical Constituents in Soils. *Nat. Educ. Knowl.* **4**.

Titchmarsh J. M. (1993) Energy Dsipersive X-Ray Analysis (EDX) in the TEM/STEM. In *Quantitative Microbeam Analysis* (eds. A. G. Fitzgerald, B. E. Storey, and D. Fabian). SUSSP Publications, Edinburgh.

Whiston C. (1996) *X-Ray Methods.*, John Wiley & Sons, Chichester.

Chapter 4 : A universal uptake mechanism for cobalt(II) on soil constituents: ferrihydrite, kaolinite, humic acid, and organo-mineral composites

This first experimental chapter presents results of an investigation into Co sorption onto ferrihydrite, kaolinite, humic acid and organo-mineral composites. This chapter is based on a paper under revision for *Geochimica et Cosmochimica Acta*.

4. 1. Introduction

Cobalt is a heavy metal that is released into the environment by a variety of industrial sources including, for example, coal power plants, vehicle emissions, and through metal production (Gál et al., 2008). Cobalt can also be present as a radionuclide, most commonly as ^{60}Co, which decays through ionising gamma radiation and has a half-life of ~5 years. ^{60}Co can be present in the cooling water of nuclear reactors, or in radioactive waste, meaning that it is possible for it to be released into the wider environment (CEFAS, 2005). Cobalt most commonly occurs as the Co^{2+} ion, which is highly soluble in water and, therefore, potentially very mobile in the environment. While it is a bioessential nutrient at low concentrations, Co contamination has negative impacts on plants as too high an uptake can result in insufficient chlorophyll production and death (Hewitt, 1953). The potential environmental harm posed by both stable and radioactive isotopes of Co means that it is important to understand how Co^{2+} interacts with soil constituents in order to predict Co mobility and fate in the environment and develop soil remediation methods.

Soils contain a complex mixture of components including water, air, primary and secondary minerals and organic materials in varying proportions (Sparks, 1995). However, it is interactions with relatively low abundance, but high surface area phases such as iron (hyr)oxides, clays and humic substances that typically control the sorption behaviour of many divalent transition element cations in soils, including Co^{2+} (Sparks, 1995). Therefore, a common approach to understanding Co sorption behaviour has been to study its sorption to separate mineral or organic phases (e.g., Ainsworth et al., 1994; Angove et al., 1998; Alvarez and Garrido, 2004). More recently, however, the sorption behaviour of metal cations in different physical mixtures and chemical composites of mineral phases (such as kaolinite and ferrihydrite) and organic materials has been investigated as a way of approaching the complexity expected in natural soil

environments (e.g., Zhu et al., 2010; Moon and Peacock, 2012, 2013; Otero Fariña et al., 2018).

Macroscopic Co^{2+} sorption behaviour to ferrihydrite has been well documented (Forbes et al., 1976; Schenck et al., 1983; Ainsworth et al., 1994; Kanungo, 1994; Landry et al., 2009) . Cobalt is shown to sorb to ferrihydrite over a narrow pH range of ~5.5 to ~7 (Ainsworth et al., 1994; Landry et al., 2009) below which there is minimal to no sorption, and above which sorption reaches 100% of Co concentrations tested. In particular, Landry et al. (2009) reports no significant difference in sorption behaviour over changes in the Co concentration and sorbate/sorbent ratio (with a Co concentration range from 10^{-4} mol L^{-1} to 10^{-6} mol L^{-1} and solid/solution from 2 to 5 g L^{-1}) or ionic strength (between 10^{-3} mol L^{-1} $NaNO_3$ and 10^{-1} mol L^{-1} $NaNO_{3)}$. On the other hand, Kanungo (1994) finds that increasing the Co concentration from 4.1 x 10^{-5} mol L^{-1} to 2.0 x 10^{-4} mol L^{-1} does shift the sorption edge to higher pH values.

The experimental data by both Landry et al. (2009) and Ainsworth et al. (1994) are fit to a thermodynamic surface complexation model in order to quantify the distribution of Co between the mineral and solution phases. These studies use the double layer model (DLM) as presented by Dzombak and Morel (1990) to account for the electrostatics at the mineral surfaces. Landry et al. (2009) show that Co^{2+} sorption data fit by a single sorption site DLM does not provide as good a visual fit to the data as a 2-site DLM. The Dzombak and Morel DLM invokes monodentate Co^{2+} surface complexation to both strong and weak FeOH sorption sites, however, the goodness of fit of the single-site and two-site models are not statistically different (Landry et al., 2009). Ainsworth et al. (1994) find that at low sorbent concentrations the data can be modelled with only one (the strongest) site, but at increased Co^{2+} concentrations a second, weaker FeOH site is required. However, despite these macroscopic observations and modelling inferences, there are no direct spectroscopic observations of Co sorption on any of the iron (hydr)oxides, and the local sorption environment of Co^{2+} on the common soil constituent ferrihydrite is still unconstrained.

The sorption of Co^{2+} to the commonly occurring 1:1 phyllosilicate clay mineral, kaolinite, has also been studied extensively (Spark et al., 1995; Angove et al., 1998; Landry et al., 2009). A two stage sorption process is observed. The initial sorption stage generally shows an increase in sorption between pH 4 and 5.5 (Spark et al., 1995; Angove et al., 1998; Landry et al., 2009). Then between pH 5.5 to 6.5, the amount of Co^{2+} sorbed remains relatively stable and sorption in this pH range is highly dependent on solution ionic strength (Landry et al., 2009; Spark et al., 1995). Indeed the initial sorption stage is completely inhibited by increasing the solution ionic strength from 10^{-3} mol L^{-1} to 10^{-1}

mol L^{-1} with either KNO_3 or NaCl (Spark et al., 1995). The low pH sorption behaviour of Co^{2+} to kaolinite is therefore attributed to complexation of Co^{2+} to the siloxane faces in the kaolinite until these sites become saturated (Spark et al., 1995; Angove et al., 1997; Angove et al., 1998). This is consistent with spectroscopic data that indicate only outer-sphere sorption of Co^{2+} to kaolinite at low pH (O'Day et al., 1994a), and low pH Co^{2+} sorption data that can be adequately predicted by invoking non selective cation exchange involving permanent negative charge on the siloxane sites (Angove et al., 1998). The second sorption stage occurs above pH ~6.5, where Co^{2+} sorption to kaolinite increases to 100% of the concentrations tested at pH ~8 (Spark et al., 1995; Angove et al., 1998; Landry et al., 2009); this second stage is not affected by changes in ionic strength or Co^{2+} concentration (Landry et al., 2009). This behaviour is attributed to cation sorption to the amphoteric alumina faces (Schulthess and Huang, 1990). Spectroscopic data of Co^{2+} sorption to kaolinite above pH ~6.5 suggests that Co-Co second-neighbour atoms at 3.1 ±0.02 Å become increasingly important with increasing surface coverage (O'Day et al., 1994a;b). O'Day et al. (1994a) interpret this behaviour as evidence for the formation of multinuclear surface complexes on the kaolinite surface. At the lowest Co surface coverages, however, EXAFS data suggested that there are also Al or Si backscattering atoms present at 2.7 ±0.5Å and 3.4 ±0.05 Å, with the shorter of these bond lengths consistent with the predicted bond length for inner-sphere bidentate Co^{2+} complexes (Fig. 4.1) on the AlOH surface sites. Experimental data for Co^{2+} to kaolinite is therefore fit using a DLM framework by invoking cation exchange processes in combination with either monodentate or bidentate surface complexes (Landry et al., 2009). Both models fit the data well at ionic strengths of 10^{-2}-10^{-1} mol L^{-1}, but at low ionic strength (10^{-3} mol L^{-1}) Co sorption is overpredicted. Although the model invoking monodentate complexes performs slightly better than the model with bidentate complexes, neither is significantly different at a 95% confidence interval (Landry et al., 2009). Angove et al. (1998) also fitted Co^{2+} sorption data using a two-site model consisting of Co sorption to X^- and SOH sites and the constant capacitance model to account for surface electrostatics. The model produces a good fit across the entire pH range, although the model was only tested at an ionic strength of 5 x 10^{-3} mol L^{-1}.

While several previous studies focus on how Co sorbs to different soil constituents, including ferrihydrite at a macroscopic level and kaolinite at both macro- and microscopic levels, there has been almost no research to understand Co^{2+} sorption behaviour in systems involving organo-mineral composites (Zachara et al., 1994). This is an important knowledge gap to fill because contaminants do not react with soil phases in isolation, rather natural soil phases are present as more complex composites, where, for example, clays and iron (hydr)oxides in natural soils are typically coated with organic matter in the form of humic substances and/or microbial cells (e.g., Davis, 1982; Sposito, 1984; O'Melia, 1989; Fortin and Langley, 2005). Therefore, the purpose of this study is to understand the mechanisms by which Co^{2+} interacts with common soil constituents in the form of isolated end-member phases, ferrihydrite, kaolinite and humic acid, and more complex organo-mineral composites of ferrihydrite-humic acid and kaolinite-

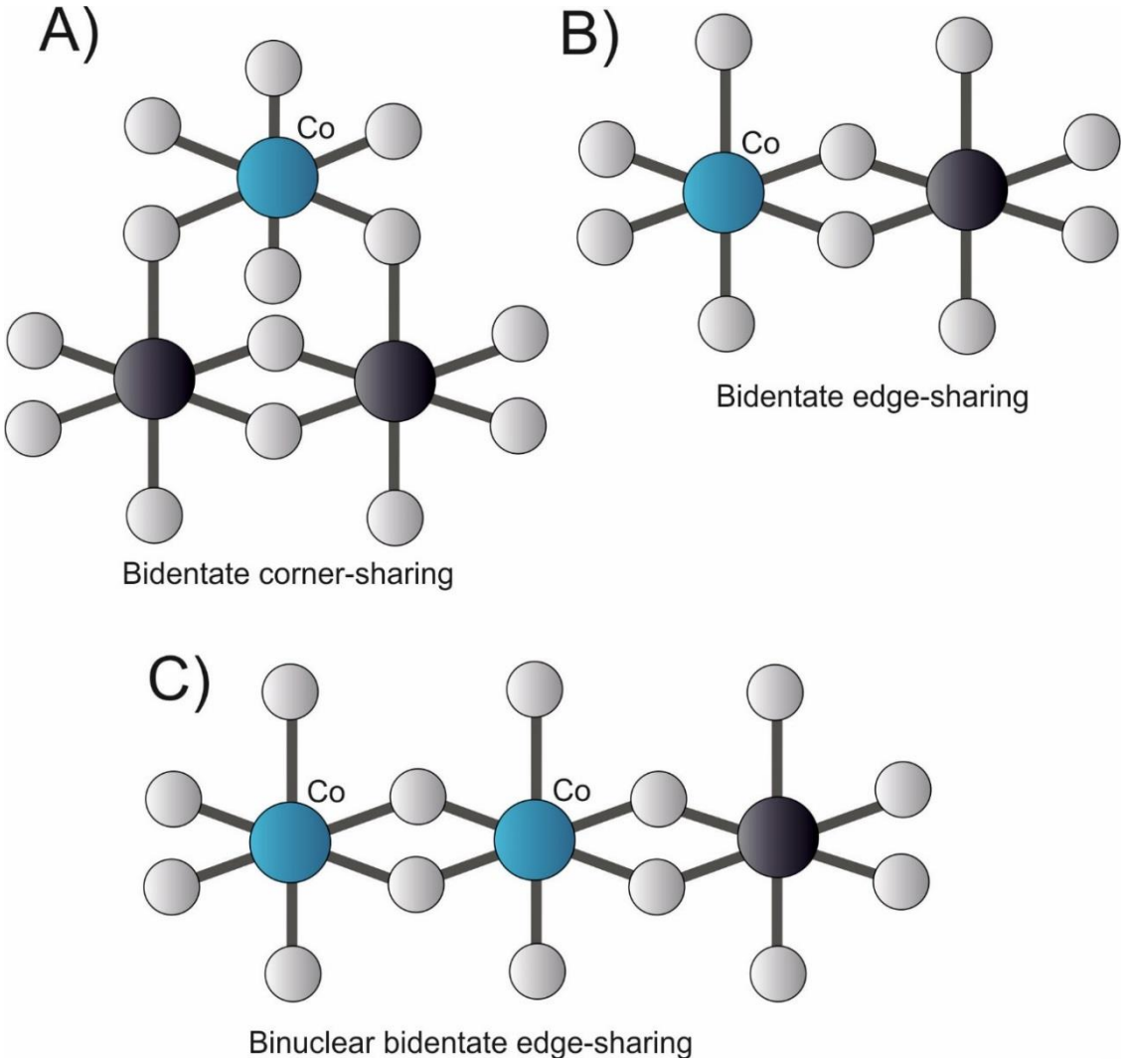

Figure 4.1: Diagrams showing sorption mechanisms discussed in this study. Co atoms are labelled circles, unlabelled large circles are surface metal atoms of a standard mineral, and unlabelled smaller circles are oxygen atoms.

humic acid, made by coating the pure mineral phases with sorbed humic acid. We investigate Co sorption as a function of pH, ionic strength, and Co concentration, and also for the composites as a function of organic carbon concentration, with composites made containing a wide range of organic carbon contents. We determine the molecular sorption mechanisms of Co to the end-member mineral and organic phases and the composites using extended X-ray absorption fine structure (EXAFS) spectroscopy, and transmission electron microscopy (TEM) to visualise Co^{2+} distribution at the nm-scale on the sorbent particles. Our work addresses the lack of underpinning spectroscopic information regarding the nature of Co^{2+} sorption coordination with iron (hydr)oxides and humic substances, in comparison to that observed with kaolinite clay. From our analysis we develop molecularly constrained thermodynamic surface complexation models to investigate the nature of the Co sorption behaviour to the soil constituents, and in particular to determine whether Co^{2+} sorption to the organo-mineral composites adheres to sorption additivity (i.e., can be predicted by assuming a simple mixture of phases).

4. 2 Methods

4. 2. 1 Materials

Humic acid was obtained from an ombrotrophic peat soil in Galicia (NW Spain, 43° 28′ 5.10″ N, 7° 32′ 6.53″ W) (López et al., 2011). Preparation and characterisation of the humic acid is reported in López et al. (2012). Briefly, the soil was acid-washed to remove inorganic components following Smith et al. (2004), and then humic acid was extracted following Swift (1996). ferrihydrite was synthesised as described in Schwertmann and Cornell (1991) by rapid hydrolysis of 0.1 M $Fe(NO_3)_3{\cdot}9H_2O$ (aq) with 1 M NaOH at pH 7. After synthesis ferrihydrite was washed several times over a week in equivalent volumes of 18.2 MΩ·cm MilliQ water, and subsequently stored as a slurry at 4°C, following standard protocols to maintain mineralogical integrity (Schwertmann and Cornell, 1991). Plastic labware and AR grade reagents were used throughout the ferrihydrite preparations. Mineralogically pure kaolinite (KGa-1b) was obtained from the Clay Minerals Society Source Clays Repository. Mineral identity and purity of the ferrihydrite and kaolinite was confirmed by X-ray powder diffraction (XRD) using a Bruker D8 Advance powder diffractometer and Cu–Kα radiation (λ = 1.5406 Å). The BET surface area of the end-member minerals was measured in triplicate using a Micrometrics Gemini VII 2390a using the N_2 sorption method after degassing for 16 hours at room temperature. We report ferrihydrite and kaolinite surface areas of 295 ± 3 and 11.7 ± 0.1 m^2/g, respectively, which are in good agreement with literature values (Schwertmann and Cornell, 1991; Eick and Fendorf, 1998). Three ferrihydrite-humic acid and two kaolinite-humic acid composites with different wt% adsorbed C were prepared following the method suggested by Iglesias et al. (2010a, b). Briefly, 2 dry g equivalent of the pure mineral were suspended in 50 mL of 0.1 mol L^{-1} $NaNO_3$ and then mixed with a varying amounts of humic acid (23, 70, and 140 ml of 5.2 g L^{-1} humic acid slurry for ferrihydrite-humic acid composites, and 10 and 55 ml of 13.99 g L^{-1} humic acid slurry for kaolinite-humic acid composites) and DIW to make up a 500 mL solution. The pH was lowered to ~4 by the addition of dilute HNO_3 to facilitate humic acid sorption and the solutions were agitated for 7 days. To wash the ferrihydrite-humic acid composites, the solutions were repeatedly mixed with equivalent volumes of DIW and centrifuged at 4000 g for 10 minutes until the presence of humic acid in the supernatant was negligible, as determined by UV-Vis performed at 280 nm (Otero-Fariña et al., 2017). The kaolinite-humic acid composite particles were too fine for efficient centrifugation and were therefore washed via dialysis, using excess volumes of DIW and Membra-Cel MD44 14x100 CLR dialysis tubing with a 14 kDa cut off, until the electrical conductivity of the

wash water equalled that of deionised water. All of the composites were stored as a slurry at 4°C. The C content of the humic acid and composites was measured by combustion using a LECO SC-144DR Dual Range Sulfur and Carbon Analyzer 606-000. The three ferrihydrite-humic acid composites were found to have 5, 10, and 17 wt% C, and the kaolinite-humic acid composites had 1.4 and 2.2 wt% C.

4. 2. 2 Sorption Experiments

Batch sorption experiments were carried out in 50 mL plastic centrifuge tubes at room temperature and in aerobic conditions. The pH range for the experiments was 3.5-8.4, representative of the pH of natural soils. 0.03 dry g equivalent weight samples (0.3 dry g equivalent for kaolinite) were mixed with 30 mL solutions of $NaNO_3$ (10^{-1}, 10^{-2}, or 10^{-3} mol L^{-1} $NaNO_3$) and Co so that the sorbents contained either 5.8, 0.58, or 0.058 wt % Co at 100% sorption (0.58, 0.058, or 0.0058 wt % Co for kaolinite). pH was recorded when there was less than 0.01 pH unit change in 15 seconds. Samples were adjusted to the chosen pH by dropwise addition of dilute NaOH or HNO_3. The samples were shaken continuously while the pH was monitored and set back to within ±0.15 of the desired pH. The pH values were then reset twice a day for 4 days until they remained constant for 16-24 hours, after which time the experiments were concluded and the final pH was measured. The samples were centrifuged for 15 minutes at 3000 g. The supernatant was filtered using 0.22 μm filters (10 kDa centrifuge filters in the case of the humic acid) and then 5 mL was added to 5 mL of 2% HNO_3 to maintain Co in solution. The Co concentration was determined (with an analytical uncertainty of < ±3%) on a Thermo iCAP 7400 radial ion-coupled plasma optical emission spectrometer (ICP-OES; ThermoFisher Scientific, USA).

PHREEQC (Parkhurst and Appelo, 1999) was used to calculate Co speciation in solution using the MINTEQ.V4 database (Charlton and Parkhurst, 2002) and is shown in Fig. 4.2 as a function of pH. Up to pH ~8.5, Co^{2+} (aq) dominates Co speciation. At pH 8.3 $Co(OH)_2$ (s) begins to precipitate and by pH 8.5 it accounts for 50% of the Co total. Therefore in our experiments Co(II) is predominantly present as Co^{2+} (aq) throughout the pH range examined.

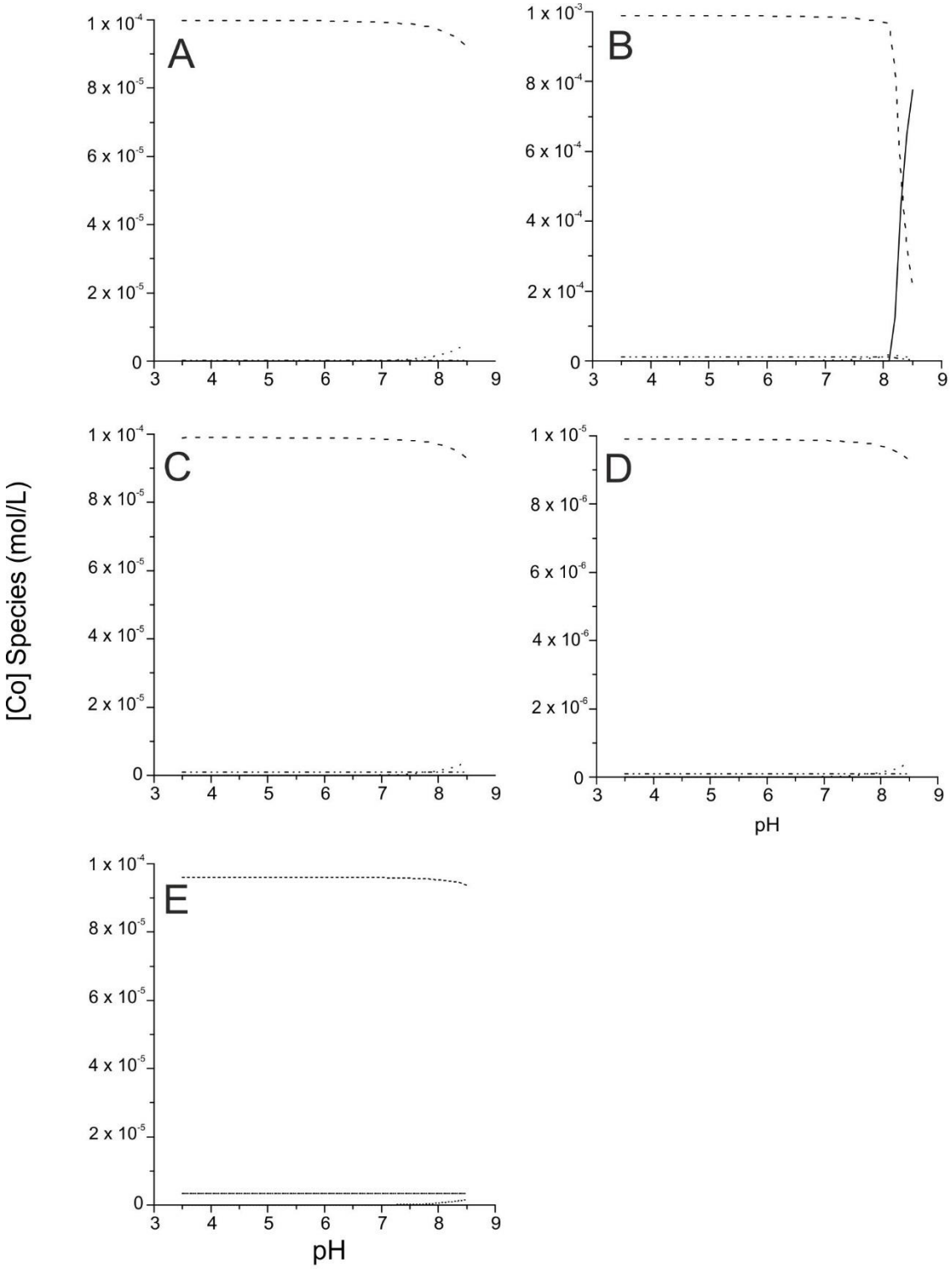

Figure 4.2: Co speciation plots for each of the ionic strength and Co concentrations used in the sorption experiments (solid lines, Co(OH)2, dashes, Co^{+2}, dots, $CoOH^{+}$, and dash-dot-dot, $CoNO_3^{+}$). Panels A, C, and E show 10^{-4} mol L^{-1} Co at 10^{-3}, 10^{-2}, and 10^{-1} mol L^{-1} $NaNO_3$, respectively. Panels B and C show 10^{-3} and 10^{-5} mol L^{-1} Co at 10^{-2} mol L^{-1} $NaNO_3$.

4. 2. 3. EXAFS Spectra Collection and Data Analysis

EXAFS spectra were collected at the Co K-edge (7722 eV) at Beamline B18 at Diamond Light Source Ltd, UK, operating at 3 GeV with a typical current of 300 mA. The X-rays at B18 are generated from a bending magnet source. The beam is vertically collimated by a Si mirror before passing through a double crystal Si monochromator. It was then focused onto the sample to give a spot size of 200x250 μm at the sample. Dried (40 °C) sorption samples were presented to the beam as 8 mm pressed pellets using cellulose as a dilutant to reduce chemical thickness. The sample pellets were held in Kapton™ tape for analysis, and a separate 1000 mg L^{-1} $Co(NO_3)$ solution was also prepared and held in a polythene bag for analysis. Spectra were collected for the samples containing kaolinite and humic acid in fluorescence mode at room temperature (~295 °K) using a 32 element solid state Ge detector, and for the samples containing ferrihydrite in transmission mode at room temperature. Multiple scans were averaged to improve the signal to noise ratio and background subtracted using Athena version 0.9.25 from the Demeter package (Ravel and Newville, 2005). The resultant EXAFS spectra were then fit *ab initio* to model spectra produced by including a series of theoretical single and multiple scattering pathways calculated in Artemis version 0.9.25 (also from the Demeter package). Data were fit in a shell-by-shell manner to construct a structurally realistic best possible fit. Fit quality was assessed using the EXAFS R-factor and the reduced χ^2 function, which were calculated in Artemis for each model fit (the final best fit is reported in Tables 4.1 and 4.2). A fit is deemed to be of acceptable quality when the R-factor is less than or equal to 0.02 (Ravel and Newville, 2005). The reduced Chi^2 value allows comparison of fits with different parameterisation and therefore is only useful when comparing between samples or model fits and does not have its own ideal value. Additional longer backscattering pathways were only included if there was a > 10% reduction in the reduced χ^2 function measure of goodness of fit. Uncertainties in the fitting parameters for each pathway (r, E0, S^2_0, and σ^2) were calculated individually and are also shown in Tables 4.1 and 4.2. For the EXAFS models of the composite samples, the end-member samples were combined and adjusted, if necessary, to produce an acceptable fit.

4. 2. 4. Scanning Transition Electron Microscopy

Separate ferrihydrite, kaolinite and humic acid samples with Co surface loadings of approximately 1 wt% were prepared for (S)TEM analysis in the same way as the sorption experiments. Briefly 0.03 dry g equivalent of sorbent was suspended in 29.5 mL of 10^{-3} mol L^{-1} $NaNO_3$ and 0.6 mL 0.01 mol L^{-1} Co^{2+}. After 16 hrs the final pH was 7.5 ±0.5; consistent with > 90% aqueous Co removal in previous batch sorption experiments. Samples were then dispersed in methanol (or DI water in the case of humic acid) and a

drop was pipetted onto a lacy / holey thin-film across a copper grid using a glass Pasteur pipette. As DI water was used to disperse the humic acid sample, the carbon film and grid underwent plasma treatment in a Fischione 1020 plasma cleaner for 10 seconds to make the film hydrophilic and ensure the sample was evenly distributed. (S)TEM images, energy dispersive X-ray (EDX) microanalysis elemental maps and electron energy loss spectra (EELS) were collected on an FEI Titan^3 Themis 300: X-FEG 300 kV S/TEM. This was fitted with S-TWIN objective lens, monochromator (energy spread 1.1 eV when the monochromator is de-excited), multiple high-angle annular dark-field (HAADF), annular dark-field (ADF), bright-field (BF) STEM detectors, FEI Super-X 4-detector EDX system, Gatan Quantum ER 965 energy filter for EELS and energy filtered TEM and Gatan OneView 4K CMOS digital camera. To minimise potential sample damage (which was most important for kaolinite samples) a low beam current of 0.3 nA was used throughout data acquisition and limited magnification (280k x) BF TEM imaging with short acquisition times (< 1 s) was performed before commencement of HAADF STEM imaging and EDX elemental mapping (using a ~80 pA probe current).

4. 2. 5 Surface Complexation Modelling

The sorption behaviour of Co on end-member ferrihydrite, kaolinite and humic acid and the organo-mineral composites was fit to a thermodynamic surface complexation model using the program EQLFOR (Sherman et al., 2008; Sherman, 2009). The ferrihydrite and kaolinite models were then combined with the humic acid model using a linear component additivity approach to explore Co sorption behaviour on the ferrihydrite and kaolinite organo-mineral composites. The surface electrostatics in all the models were accounted for by adopting the basic Stern model (BSM). The Davies equation was used for activity corrections to the stability constants for aqueous species. Detailed discussion on the development of the end-member ferrihydrite model is available in Moon and Peacock (2013), and for the kaolinite, humic acid and organo-mineral composite models in Section 4.4.3 below.

4. 2. 5. 1 Sensitivity Analysis of the Co-Ferrihydrite, -Kaolinite, and Humic Acid Surface Complexation Models

A sensitivity analysis was performed to evaluate the sensitivity of the end-member models to the input parameters. For each model, the input parameters (C_{stern}, electrolyte binding constants, surface site densities, and surface area) were systematically varied while monitoring the log *K* values for the Co adsorption complexes. The analyses are based on the protocols of Moon and Peacock (2013). The C_{stern} was varied by ±50%, the log *K* electrolyte binding constants between -1.5 and 0.5, and the surface site densities

and the surface areas were varied by a factor of ±3. Log K values for each surface site and their uncertainty are presented in Table 4.5.

4. 3. Results

4. 3 .1 Co Sorption to End-member Ferrihydrite, Kaolinite and Humic Acid

The results from pH sorption edge experiments using ferrihydrite, kaolinite, and humic acid are shown in Figs. 4.3 and 4.4 (n.b. only data from 0.58 wt% Co experiments are shown, where the solid:solution ratio is 1 g L^{-1} in the ferrihydrite and humic acid experiments and 10 g L^{-1} in the kaolinite experiments; data from all Co^{2+} concentrations 0.058 – 5.8 wt% Co for the ferrihydrite and humic acid, and 0.0058 – 0.58 wt% Co for the kaolinite experiments are shown in Fig. 4.5).

For ferrihydrite we observe sigmoid sorption edges that are in agreement with previous studies of Co sorption onto iron (hydr)oxides (Forbes et al., 1976; Schenck et al., 1983; Ainsworth et al., 1994; Kanungo, 1994; Landry et al., 2009). There is no change in the shape or position of the sorption edges in pH space with increases in ionic strength from 10^{-3} to 10^{-1} mol L^{-1} (Fig. 4.4) or with increases in Co concentration from 0.058 to 5.8 wt % Co (Fig. 4.5).

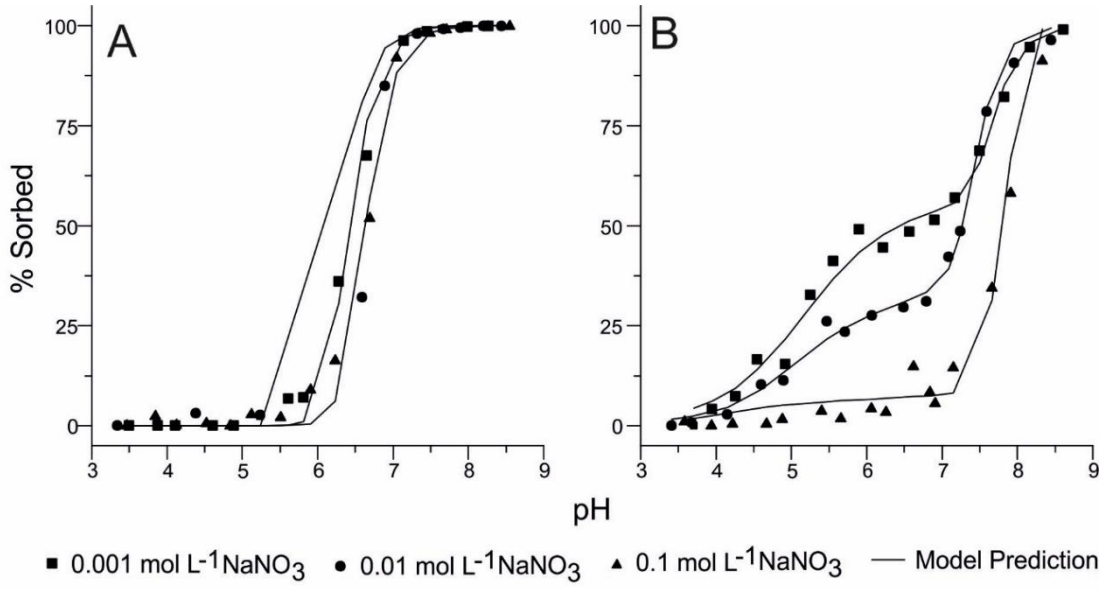

Figure 4.3: Co sorption (at 10^{-4} mol L^{-1} Co total concentration, equating to 0.58 wt% Co sorbed at 100% sorption for ferrihydrite and 0.058 wt% Co sorbed at 100% sorption for kaolinite) to ferrihydrite (A) and kaolinite (B) as a function of pH; conducted at room temperature at a range of ionic strengths.

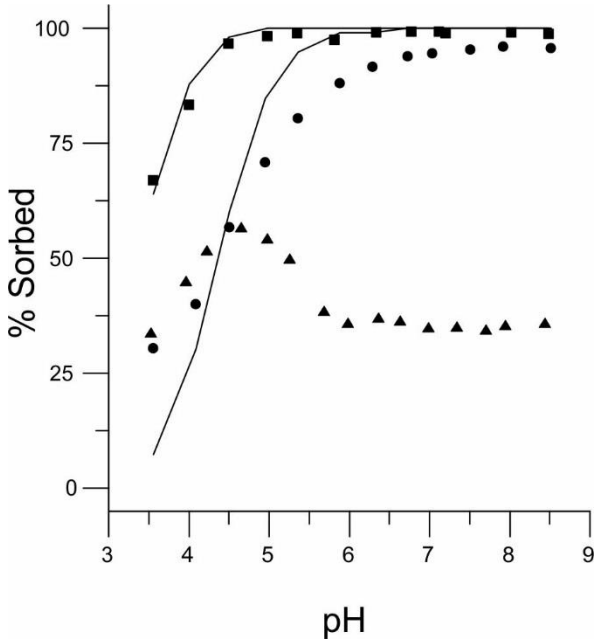

Figure 4.4: Co sorption to humic acid at ionic strengths of 10^{-3} mol L^{-1} and 10^{-1} mol L^{-1}, and using two different filters before analysis (squares, 10^{-3} mol L^{-1} $NaNO_3$; circles, 10^{-1} mol L^{-1} $NaNO_3$ filtered with a 10 kDA centrifuge filter; triangles, 10^{-1} mol L^{-1} $NaNO_3$ filtered at 0.22 µm.) Solid lines represent the surface complexation model fits for each system.

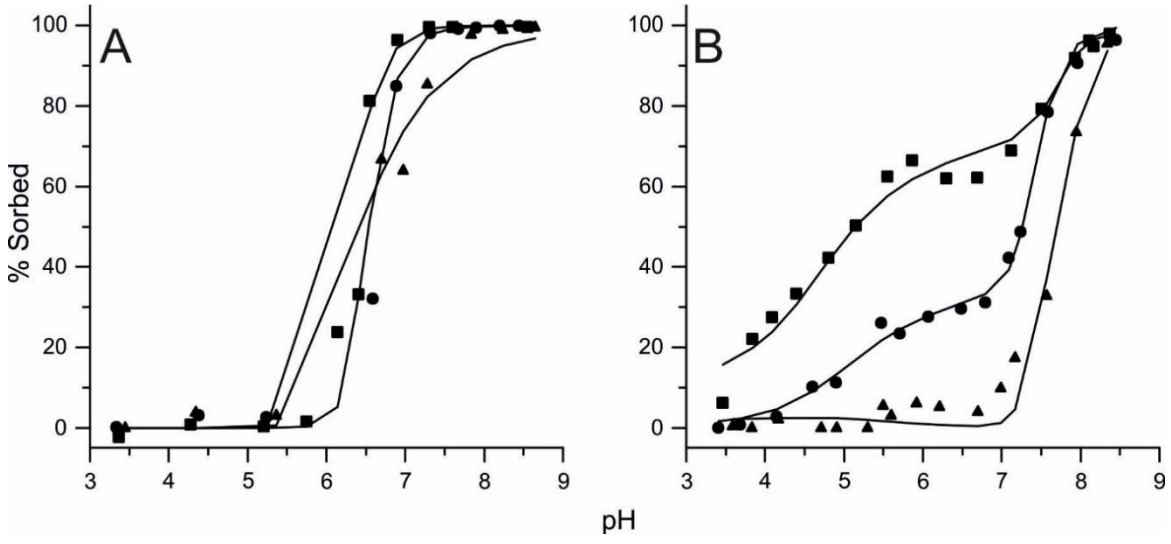

Figure 4.5: Co sorption to ferrihydrite (A) and kaolinite (B) as a function of pH and Co concentration. For ferrihydrite, squares show 0.058 wt% Co, circles show 0.58 wt% Co, and triangles show 5.8 wt% Co systems. For kaolinite, squares show 0.0058 wt% Co, circles show 0.058 wt% Co, and triangles show 0.58 wt% Co. Solid lines represent the EQLFOR fits. The solid:solution ratio was 1 g L^{-1} for ferrihydrite experiments, and 10 g L^{-1} for kaolinite.

The kaolinite sorption edges show two sorption stages which is also in agreement with previous studies of Co sorption onto kaolinite (Spark et al., 1995; Angove et al., 1998; Landry et al., 2009). There is a decrease in the amount of Co sorbed during the initial sorption stage with increasing ionic strength from 10^{-3} to 10^{-1} mol L^{-1} (Fig. 4.3) The percentage of Co sorbed in the initial sorption stage also decreases when increasing the Co concentration from 0.0058 to 0.58 wt% Co (Fig. 4.5).

For humic acid we observe high sorption even at low pH values, which is consistent with previous studies of Co sorption on humic acid (McLaren et al., 1986). The sorption edge shifts to higher pH values when ionic strength is increased from 10^{-3} to 10^{-1} mol L^{-1} (Fig. 4.4). There is also a marked difference in sorption behaviour dependant on the filtration method used for equivalent samples. When the sample is filtered with a 10 kDa filter, sorption reaches 100%, however when it is filtered with a 0.22 μm filter, sorption peaks at ~60% and then decreases back down to ~35% where it remains stable (Fig. 4.4).

4. 3. 2. Co Sorption to Organo-mineral Composites

The sorption of Co to the organo-mineral composites is plotted in Fig. 4.6 as a function of pH. The three ferrihydrite-humic acid composites show a generally sigmoidal shape, but the sorption edges are intermediate between those of the end-member ferrihydrite and humic acid, showing enhanced sorption relative to the end-member ferrihydrite in the mid-low pH regime. In particular at pH 3.5 – 5.5 there is negligible sorption to ferrihydrite, but the composites show 15 – 45% sorption. This is in good agreement with the sorption of other divalent cations to ferrihydrite organo-mineral composites (e.g., Moon and Peacock, 2012, 2013; Zhu et al., 2010).

The two kaolinite-humic acid sorption edges are also intermediate between those of the end-member kaolinite and humic acid, with the 1.4 wt% C composite edge falling below the end-member kaolinite edge only above pH 7. The 1.4 wt% C and 2.2 wt% C composites show enhanced sorption relative to the end-member kaolinite in the low-mid pH regime and over the majority of the pH range studied, respectively.

4. 3. 3. EXAFS of End-member and Composite Phases

Spectra collected from all samples are fit with a series of single and corresponding multiple scattering pathways. The final best model fits are shown in Fig. 4.7 for all sample spectra and an aqueous Co standard solution, and the fit parameters are shown in Table 4.1 and 4.2 for the end-member and composite systems, respectively. Additional ferrihydrite samples (with both very high and very low Co-loadings) that produced EXAFS spectra with high signal to noise ratio are presented in Table 4.3 and Fig. 4.8.

The amplitude reduction factor, S^2_0, determined for the fitting of all EXAFS samples was based on results obtained from the fitting of the EXAFS standard Co^{2+}(aq) solution. In this process, the CN (coordination number) of the Co-O path was set to 6 and the S^2_0 parameter fit to a value of 0.92. This value was used for all S^2_0 in all subsequent fits and models. The CN for the Co-O pathway was fixed at 6 for all samples, and we did not consider non-octahedrally coordinated Co^{2+}. For the sorption coordination we fit the CN's for the Co-Fe and Co-Co pathways iteratively to choose the best fit for the highest quality data. This was then applied to the lower quality data to ensure consistency. Given

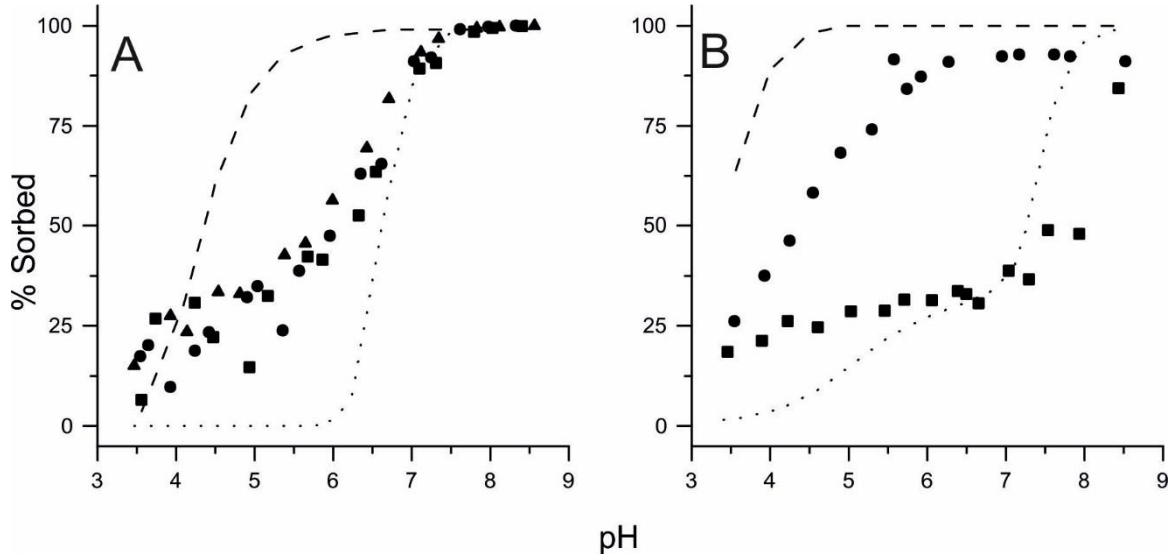

Figure 4.6: Co sorption to ferrihydrite-humic acid (A) and kaolinite-humic acid (B) organo-mineral composites, both at a range of C contents (for the ferrihydrite-humic acid composites, squares show sorption to the composite with 5 wt% C; circles, 10 wt% C; and triangles, 17 wt% C; for the kaolinite-humic acid composites, squares show sorption to the composite with 1.4 wt% C, and circles 2.2 wt% C). In both graphs, the dashed line shows sorption to the humic acid end-member at the ionic strength of each experiment, and the dotted line shows sorption to the mineral end-member (ferrihydrite or kaolinite).

that the error on CNs is ~25% it was sensible to choose an intermediate number close to integer values for the subsequence fits.

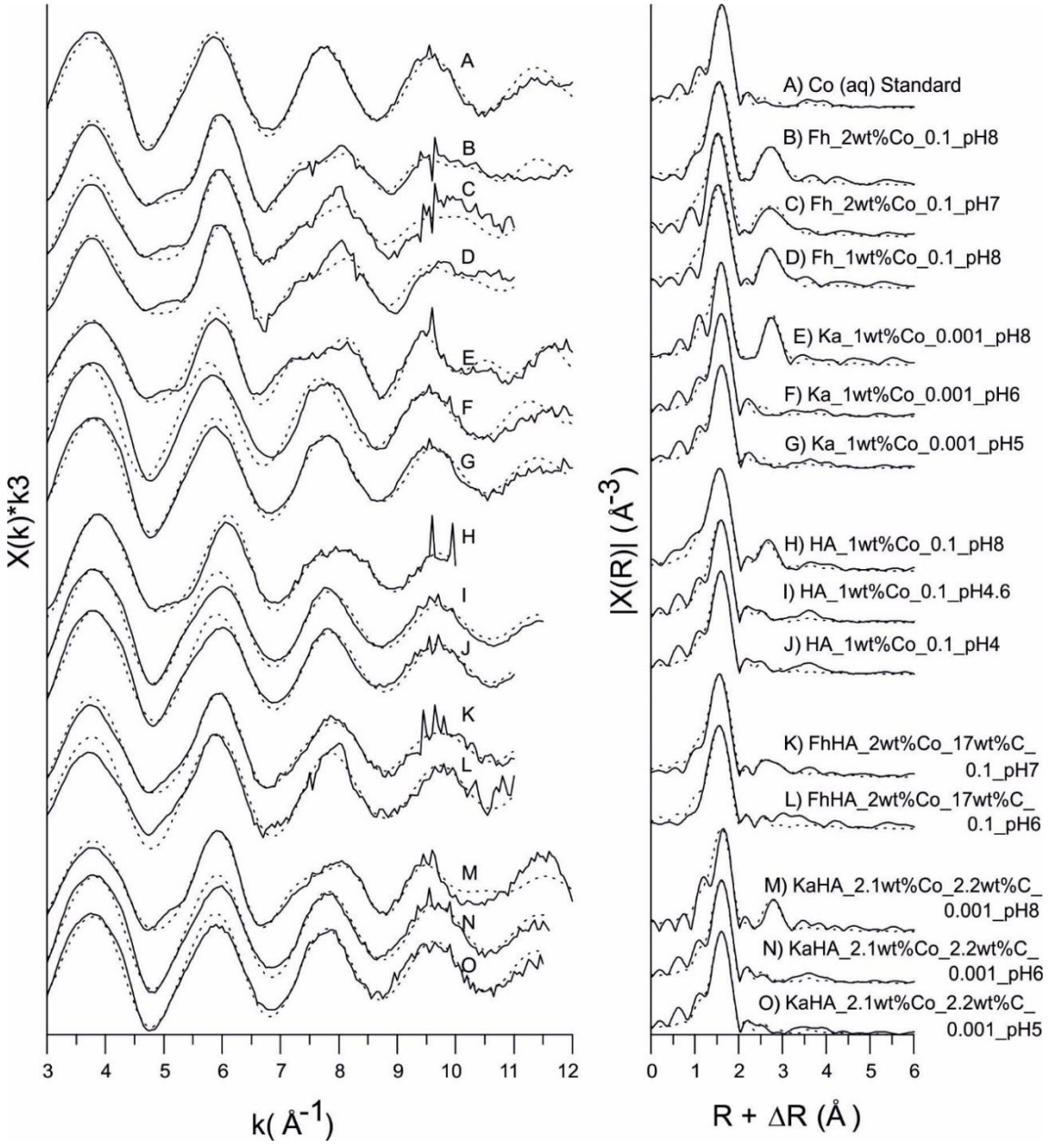

Figure 4.7: EXAFS spectra and resulting Fourier transforms of each sample. Sample names are presented as: adsorbent_wt % Co_wt% C (only necessary for the composite phases)_ionic strength (in mol L^{-1}) and sample pH. The solid line represents the data and dotted line is the best fit. Samples showing signs of low signal:noise and self-absorption have been omitted, but are shown in Fig. 4.8.

Table 4.1: Co K-edge EXAFS fitting parameters for ferrihydrite, kaolinite and humic acid samples, where N is the coordination number (±25%), r is the interatomic distance, σ2 is the Debye–Waller Factor and reduced χ^2 and R are the goodness of fit parameters. Uncertainties in the last digit shown in parentheses. MS = multiple scattering pathways within the CoO_6 octahedral and Co-O-Co linkages. MS pathways are italicised and do not contribute to the structural fit.

Experiment Description	Pathway	N	r (Å)	σ^2 (Å^2)	χ^2; *R*
A: Co (aq) Standard	Co-O	6	2.07(1)	0.005(1)	771;
δe0 = -3(1)	*CoO_6 MS*	*12*	*4.14(2)*	*0.011(2)*	0.019
S^2_0 = 0.92					
B: Fh_2wt%Co_0.1_pH8	Co-O	6	2.06(1)	0.011(1)	120;
δe0 = -2(1)	Co-Fe	1.3(3)	2.99(2)	0.006(3)	0.013
S^2_0 = 0.92	Co-Co	1.6(4)	3.14(1)	0.005(2)	
	CoO_6 MS	*12*	*4.12(2)*	*0.022(2)*	
	Co-O-Co MS	*6(2)*	*3.66(1)*	*0.008(2)*	
C: Fh_2wt%Co_0.1_pH7	Co-O	6	2.04(1)	0.011(1)	288;
δe0 = -3(2)	Co-Fe	1.3(3)	2.99(3)	0.006(5)	0.045
S^2_0= 0.92	Co-Co	1.8(4)	3.14(3)	0.007(4)	
	CoO_6 MS	*12*	*4.09 (2)*	*0.022(2)*	
	Co-O-Co MS	*6(2)*	*3.65(2)*	*0.009(3)*	
D: Fh_1wt%Co_0.1_pH8	Co-O	6	2.04(1)	0.009(1)	
δe0 = -3(1)	Co-Fe	1.1(3)	3.00(4)	0.006(7)	266;
S^2_0 = 0.92	Co-Co	1.7(4)	3.13(3)	0.007(4)	0.022
	CoO_6 MS	*12*	*4.09(2)*	*0.018(2)*	
	Co-O-Co MS	*6(2)*	*3.65(2)*	*0.007(3)*	
E: Ka_1wt%Co_0.001_pH8	Co-O	6	2.06(1)	0.009(1)	121;
	Co-Al	0.5(1)	2.97(10)	0.014(17)	0.017
δe0 = -3(1)	Co-Co	1.2(3)	3.11(1)	0.004(1)	
S^2_0 = 0.92	*CoO_6 MS*	*12*	*4.13(2)*	*0.018(2)*	
	Co-O-Co MS	*4(1)*	*3.64(1)*	*0.006(1)*	
F: Ka_1wt%Co_0.001_pH6	Co-O	6	2.07(1)	0.006(1)	445;
	CoO_6 MS	*12*	*4.14(2)*	*0.013(2)*	0.013
δe0 = -2(1)					
S^2_0 = 0.92					
G: Ka_1wt%Co_0.001_pH5	Co-O	6	2.06(1)	0.007(1)	775;
	CoO_6 MS	*12*	*4.13(2)*	*0.014(2)*	0.015
δe0 = -2(1)					
S^2_0 = 0.92					
H: HA_1wt%Co_0.1_pH8	Co-O	6	2.04(1)	0.010(1)	36;
δe0 = 0(1)	Co-C	2.3(5)	2.92(2)	0.006(4)	0.006
S^2_0 = 0.92	Co-Co	0.9(2)	3.07(2)	0.007(2)	
	CoO_6 MS	*12*	*4.08(2)*	*0.020(2)*	
	Co-O-Co MS	*4(1)*	*3.61(2)*	*0.008(2)*	
I: HA_1wt%Co_0.1_pH4.6	Co-O	6	2.05(1)	0.008(1)	1062;
	CoO_6 MS	*12*	*4.11(2)*	*0.017(2)*	0.024
δe0 = -3(1)					
S^2_0 = 0.92					
J: HA_1wt%Co_0.1_pH4	Co-O	6	2.05(1)	0.007(1)	642;
δe0 = -3(1)					0.017
S^2_0 = 0.92					

Table 4.2: Co K-edge EXAFS fitting parameters for ferrihydrite, kaolinite and humic acid samples, where N is the coordination number (±25%), r is the interatomic distance, σ2 is the Debye–Waller Factor and reduced χ^2 and R are the goodness of fit parameters. Uncertainties in the last digit shown in parentheses. MS = multiple scattering pathways within the CoO_6 octahedral and Co-O-Co linkages. MS pathways are italicised and do not contribute to the structural fit.

Experiment Description	Pathway	N	r (Å)	σ^2 (Å^2)	χ^2; *R*
K:	Co-O	6	2.05(1)	0.009(1)	90;
FhHA_2wt%Co_17wt%C_0.1_pH7	Co-C	1.3(3)	2.95(12)	0.012(27)	0.014
	Co-Fe	0.6(2)	3.02(8)	0.007(13)	
δe0 = -3(1)	Co-Co	0.9(2)	3.17(5)	0.008(9)	
S^2_0 = 0.92	*CoO_6 MS*	*12*	*4.11(2)*	*0.018(2)*	
	Co-O-Co MS	*8(2)*	*3.67(3)*	*0.009(5)*	
L:	Co-O	6	2.04(1)	0.007(1)	185;
FhHA_2wt%Co_17wt%C_0.1_pH6	*CoO_6 MS*	*12*	*4.09(2)*	*0.014(2)*	0.025
δe0 = -5(1)					
S^2_0 = 0.92					
M:	Co-O	6	2.07(1)	0.009(1)	363;
KaHA_2.1wt%Co_2.2wt%C_0.001_pH8	Co-C	2.5(6)	3.09(6)	0.011(12)	0.031
	Co-Co	1(2)	3.12(3)	0.007(4)	
δe0 = -2(2)	*CoO_6 MS*	*12*	*4.14(2)*	*0.019(2)*	
S^2_0 = 0.92	*Co-O-Co MS*	*4(1)*	*3.65(2)*	*0.008(3)*	
N:	Co-O	6	2.06(1)	0.006(1)	306;
KaHA_2.1wt%Co_2.2wt%C_0.001_pH6	*CoO_6 MS*	*12*	*4.12(2)*	*0.013(2)*	0.013
δe0 = -2(1)					
S^2_0 = 0.92					
O:	Co-O	6	2.06(1)	0.006(1)	279;
KaHA_2.1wt%Co_2.2wt%C_0.001_pH4	*CoO_6 MS*	*12*	*4.13(2)*	*0.012(2)*	0.014
δe0 = -3(1)					
S^2_0 = 0.92					

The FEFF paths for the model were created from the basic atom coordinates of cobalt hydroxide, goethite, kaolinite, and Co-acetate, which account for Jahn-Teller distortions. A potential problem with this approach is that increasing the number of variables to be determined in the fitting minimization can make the uncertainties in the fitted variables intolerably large. However, the parameters for the additional MS paths (*R,* σ^2) can all be expanded quantitatively in terms of the single scattering paths that make up the individual legs of each of the multiple scattering paths. Thus the added multiple scattering paths do not need any additional variable parameters added to the fit and instead they add constraints to better define the single scattering paths, reducing the uncertainty of the first shell Co-O and Co-Co paths making such a fit attainable (Webb et al., 2005).

The spectra collected from the Co-sorbed ferrihydrite samples at all pH and Co concentrations are fit with the same molecular model, consisting of 6 O at

Table 4.3: Co K-edge EXAFS fitting parameters for high signal: noise ferrihydrite samples, where N is the Occupancy, r is the interatomic distance, σ^2 is the Debye–Waller Factor and reduced χ^2 and R are the goodness of fit parameters. Uncertainties in the last digit shown in parentheses. MS = multiple scattering pathways within the CoO_6 octahedral and Co-O-Co linkages. MS pathways are italicised and do not contribute to the structural fit.

Experiment Description	Pathway	N	r (Å)	σ^2 (Å^2)	χ^2; *R*
A: Fh_5wt%Co_0.1_pH8 $\delta e0 = -2(1)$ $S^2_0 = 0.92$	Co-O	6(2)	2.05(1)	0.013(8)	851; 0.011
	Co-Fe	1.2(3)	2.98(2)	0.006(3)	
	Co-Co	1.6(4)	3.14(1)	0.006(2)	
	CoO_6 MS	*12(3)*	*4.10(2)*	*0.026(16)*	
	Co-O-Co MS	*6(2)*	*3.65(2)*	*0.009(5)*	
B: Fh_2wt%Co_0.1_pH 6.5 $\delta e0 = -4(2)$ $S^2_0 = 0.92$	Co-O	6(2)	2.04(1)	0.006(1)	299; 0.086
	Co-Co	1.7(4)	3.09(4)	0.010(5)	
	CoO_6 MS	*12(3)*	*4.08(1)*	*0.013(1)*	
	Co-O-Co MS	*6(2)*	*3.62(3)*	*0.008(3)*	
C: Fh_1wt%Co_0.1_pH7 $\delta e0 = -2(2)$ $S^2_0 = 0.92$	Co-O	6(2)	2.04(2)	0.009(1)	66; 0.065
	Co-Co	1.8(4)	3.09(3)	0.008(4)	
D: Fh_0.5wt%Co_0.1_pH8 $\delta e0 = -4(2)$ $S^2_0 = 0.92$	Co-O	6(2)	2.04(1)	0.004(1)	532; 0.058
	Co-Co	1.6(4)	3.08(2)	0.006(3)	

~2.05 Å, ~1 Fe at ~3 Å and ~1.5 Co at 3.1 – 3.2 Å. The Co-sorbed kaolinite spectra at low pH (pH 5 and 6) are fit with only 6 O at ~2.05 Å, similar to the $Co_{(aq)}$ standard, while at high pH (pH 8), the best fit model includes ~0.5 Al at ~2.9 Å and ~1 Co at ~3.1 Å. The Co-sorbed humic acid spectra at low pH (pH 4 and 4.6) are also fit with only 6 O, similar to the $Co_{(aq)}$ standard and the low pH sorption to kaolinite, while at high pH (pH 8) there are also ~2 C at ~2.9 Å and ~1 Co at ~3.1 Å. Co sorption to the ferrihydrite-humic acid composite spectrum at pH 6, is fit with 6 O at ~2.05 Å, ~1 Fe at ~3.02 Å and ~1.5 Co at ~3.2 Å, while at pH 7, the fit also includes ~1 C at ~2.9 Å. Sorption to the kaolinite-humic acid composite spectrum at pH 4 and 6 is fit with only 6 O at ~2.05 Å, while at pH 8, there are also contributions from ~2 C at ~3.04 Å and ~1 Co at ~3.14 Å.

4. 3. 4. TEM Imaging of Co-Sorbed End-member Ferrihydrite, Kaolinite and Humic Acid

In low magnification imaging the Co-sorbed ferrihydrite sample is seen to consist of small (2 - 5 nm) particles that form much larger aggregates between 500 – 800 nm in

size (Fig. 4.9). Relatively high magnification analysis of 5 areas of interest shows that none of these areas contain any nano-scale Co-containing particles. In all 5 areas of interest EDS mapping shows the Co to be homogenously distributed on the sample, though areas that are deemed to be thicker through observation of the HAADF image appear to have a higher concentration of Co (Fig. 4.9). Due to the possibility of overlap in the Fe K_β and Co K_α peaks in EDS analysis, the presence of Co associated with the ferrihydrite was confirmed using electron energy loss spectroscopy (EELS) and a distinct Co L_3-edge is detected at 780 eV.

In low magnification imaging the Co-sorbed kaolinite sample consists of hexagonal crystalline platelets between 100 – 400 nm in size with a depth of 10 – 50 nm (Fig. 4.10). Thirteen regions of interest were selected for relatively high magnification analysis, 2 imaging the planar platelet surface and the remainder imaging edge-on views of the crystals. No nano-scale Co-containing particles are observed in any region of interest. In EDS mapping Co is found to be heterogeneously distributed on the sample and in 5 regions of interest was detected specifically associated with the crystal edges. In these 5 regions, Co appears to be distributed such that it is found predominately on one face of

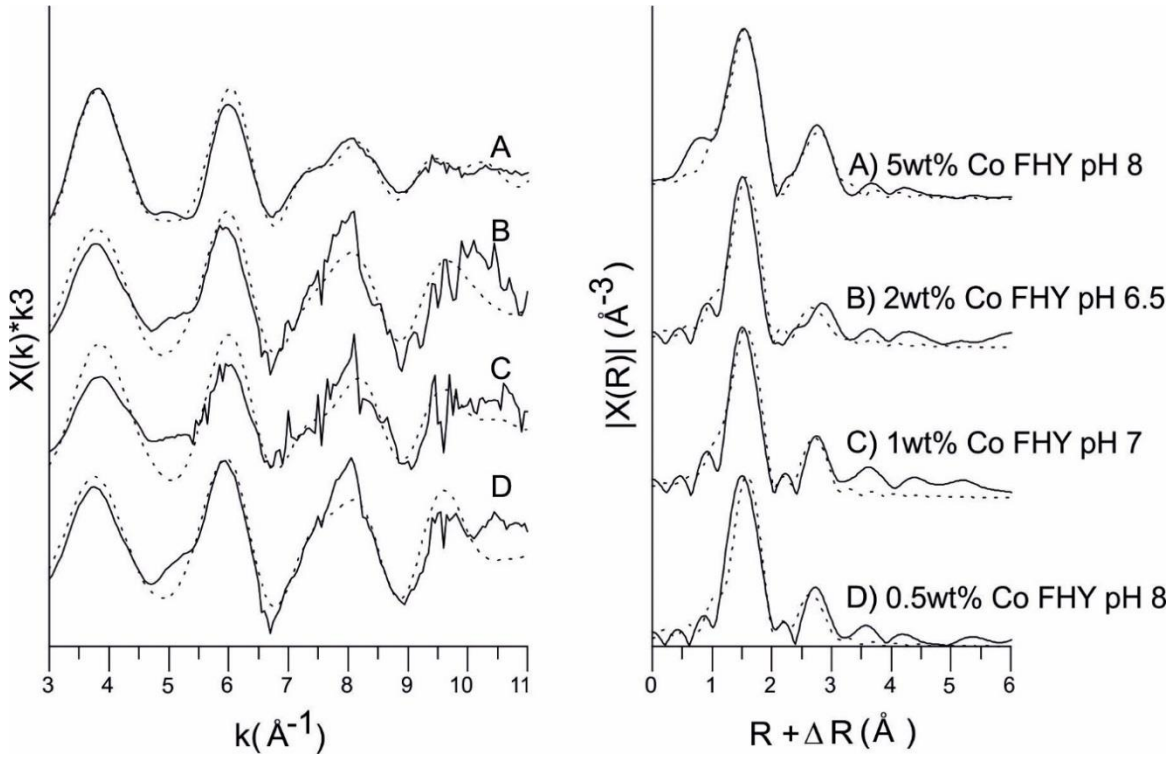

Figure 4.8: EXAFS spectra and resulting Fourier Transform for samples with low signal:noise and high self-absorption. Sample names are presented as: adsorbent_wt % Co_ionic strength (in mol L^{-1})_sample pH. The solid line represents the data and dotted line is the best fit. All samples were fit to a similar model to that of the 2 wt% Co ferrihydrite pH 8 sample in Fig. 4.7.

each crystal. In high resolution imaging these Co-rich faces appear to be regions where the kaolinite cleavage planes are rougher and less coherent than Co-free areas (Fig. 4.10).

In low magnification imaging the Co-sorbed humic acid sample consists of rounded amorphous particles displaying a very wide range of particle sizes (<100 nm – > 2000 nm) (Fig. 4.11). Three areas of interest were studied at a high resolution and in all of these areas EDS mapping shows Co homogenously distributed on the sample with no nano-scale Co-containing particles (Fig. 4.11).

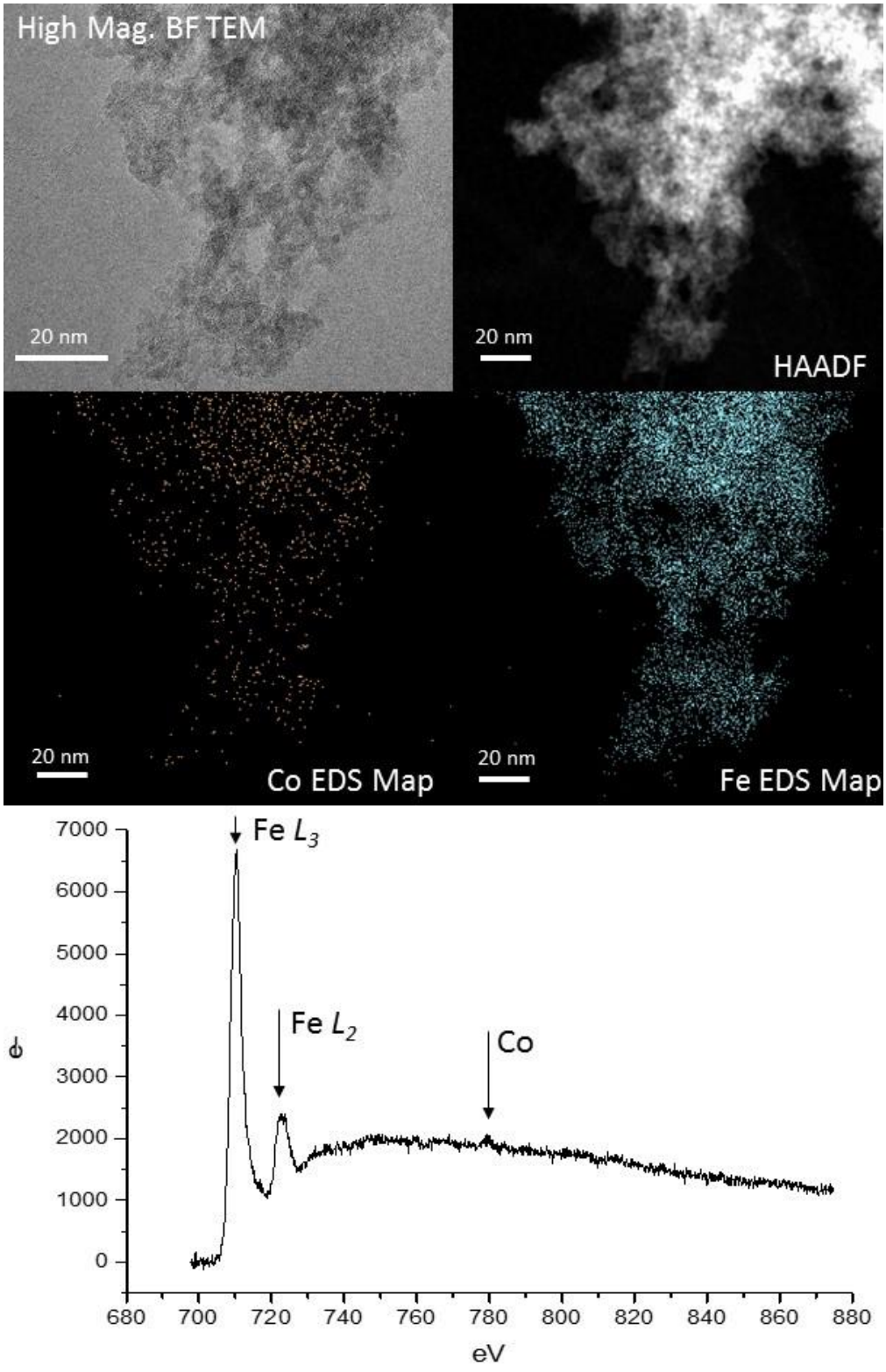

Figure 4.9: High resolution bright field TEM image showing ferrihydrite particles after Co sorption at pH 8, with corresponding HAADF image and Co and Fe EDS maps of the same region. An electron energy loss spectrum collected from the ferrihydrite is also shown (bottom panel) with the position of the Fe $L_{3,2}$ and Co L_3-edges indicated.

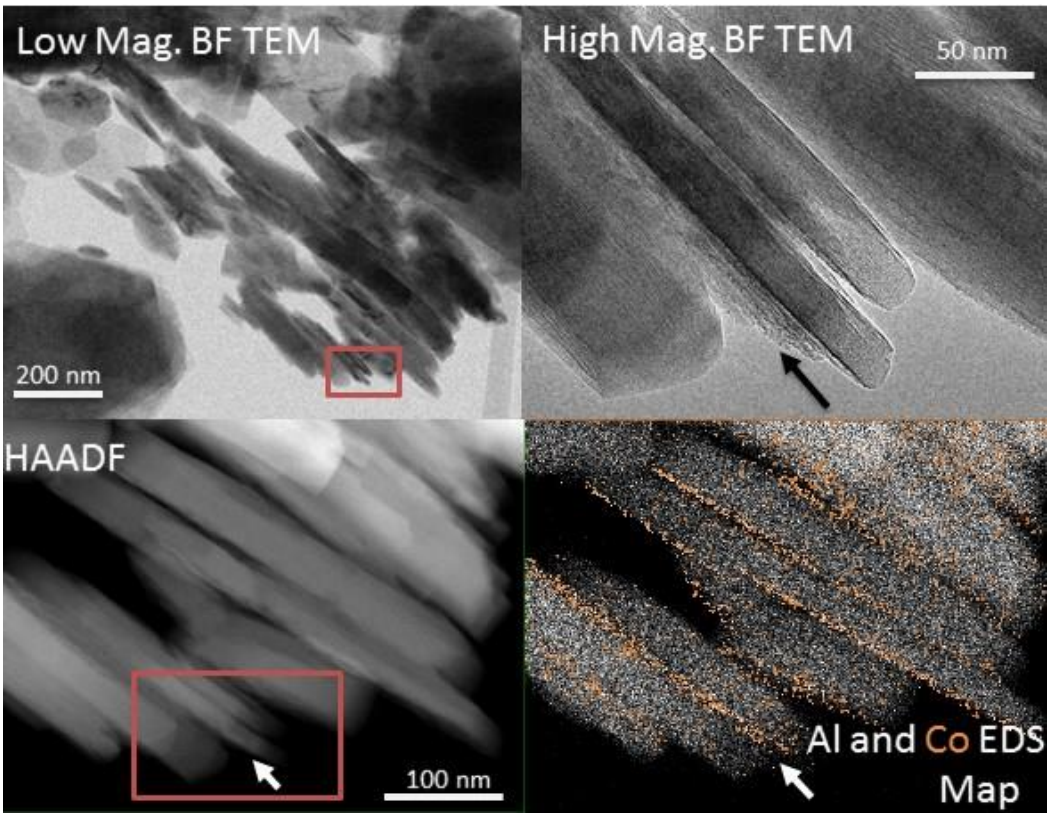

Figure 4.10: Low resolution bright field TEM images show kaolinite crystals after Co sorption. Red box shows region chosen for high resolution TEM imaging. HAADF image of same region and Al and Co EDS elemental maps are also show. Arrows denote a specific Co-containing laminae and

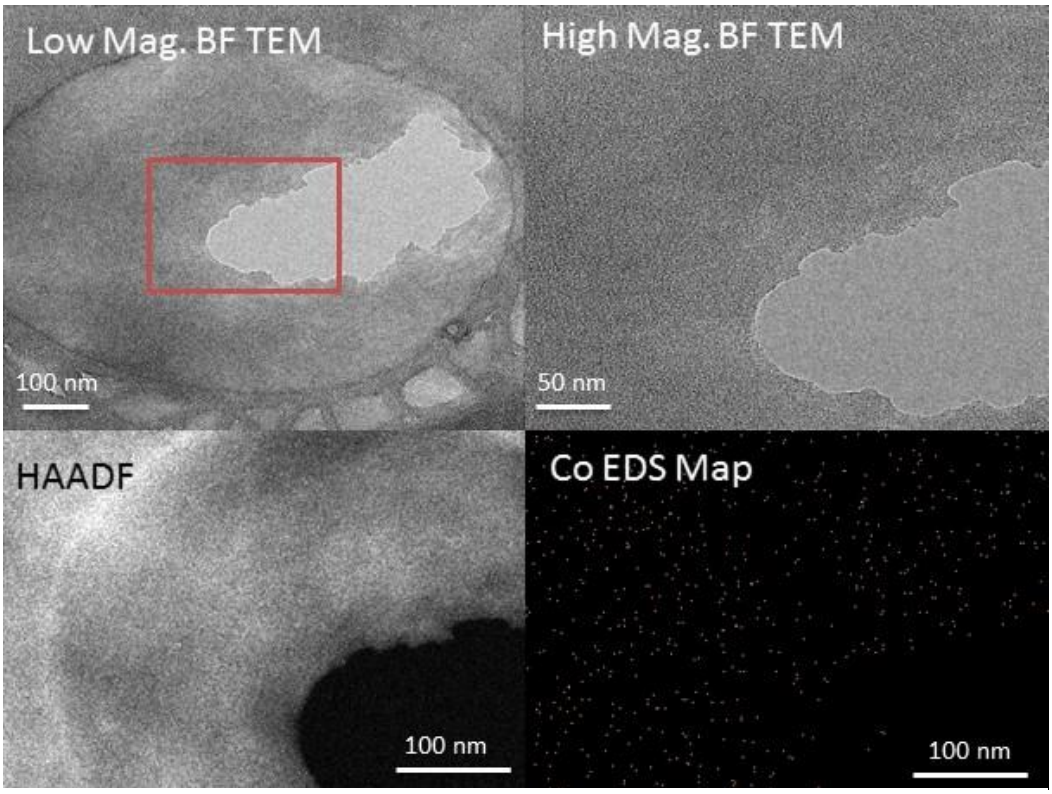

Figure 4.11: Low resolution bright field TEM image showing HA after Co sorption at pH 8. Red box shows region show in the adjacent high resolution image with corresponding HAADF image of same region and the Co EDS elemental map.

4. 4. Discussion

4. 4. 1. Co Sorption to End-member Ferrihydrite, Kaolinite and Humic Acid

4. 4 .1 .1 . Co sorption to ferrihydrite

The sorption edge data for ferrihydrite (Figs. 4.3A and 4.5A) compare well with that reported in the literature for Co sorption to iron (hydr)oxides, with sorption edges in the range pH 6 – 7 (Ainsworth et al., 1994; Landry et al., 2009). The percentage of Co sorbed is independent of initial Co concentration (Fig. 4.5A), suggesting that in our sorption systems there is an excess of surface sorption sites, consistent with the large surface area for ferrihydrite (~295 ± 3 m^2/g). The Co sorption behaviour is also independent of ionic strength (Fig. 4.3A) suggesting that Co binds to ferrihydrite via inner-sphere surface complexation. This is confirmed by EXAFS analysis of Co sorbed to ferrihydrite at pH 7 and 8 as all samples are fit with 1 Fe at ~3.0 Å (Table 4.1). The number of Fe backscatterrers and the Co-Fe interatomic distance indicates that octahedral Co-O moieties form inner-sphere bidentate edge-sharing complexes with FeOH octahedral surface groups at the pH values investigated (e.g., for copper sorption to ferrihydrite; Scheinost et al., 2001; Moon and Peacock, 2012; Otero Fariña et al., 2018). EXAFS data were also fit with ~1.5 Co at ~3.14 Å (Table 4.1) indicating the presence of Co hydroxide-like linkages as opposed to Co hydroxide surface precipitates in which the CN for the Co-Co pathway would be higher. As the Co-Co CN is between 1 and 2, it is possible that Co is forming a mixture of bi- and tri-nuclear surface complexes, as the CN will tend towards 2 as the chain length increases. Although Fe and Co are similar X-ray backscatterers, the modelled Co-Fe and Co-Co pathways as calculated in FEFF have sufficiently different distances (~0.1 Å) that they can be resolved in the EXAFS fit. Addition of both Co-Fe and Co-Co pathways improved the model fits despite also increasing the total degrees of freedom when compared to models with either Co-Fe or Co-Co. TEM observations (Fig. 4.9) however, show that even at relatively high Co loadings Co is evenly dispersed on the ferrihydrite surfaces and does not form discrete $Co(OH)_2$ nanoparticles. Furthermore, 1.5 Co-Co bonds is significantly below the 6 Co-Co bonds present in $Co(OH)_2$ (O'Day et al., 1994a). Therefore we propose that Co binds to ferrihydrite via bi- or tri-nuclear surface complexes, and thus in summary via inner-sphere bidentate multinuclear edge-sharing complexes (Fig. 4.1).

4. 4 .1 .2 Co sorption to kaolinite

The sorption edge data for kaolinite (Fig. 4.3B) is similar to results found in previous studies (Spark et al., 1995; Angove et al., 1998; Landry et al., 2009). Our data sets all show increasing sorption between pH 4 and 5.5, and 6.5 and 8. In contrast to the ferrihydrite samples, the percentage of Co sorbed is somewhat dependent on initial Co concentration below pH ~7 (Fig. 4.5B), suggesting that our sorption systems are surface sorption site limited in the low-mid pH regime, consistent with the relatively low surface area for kaolinite (11.7 ± 0.1 m^2/g). Again in contrast to ferrihydrite, the Co sorption behaviour is also dependent on ionic strength mainly below pH ~7 (Fig. 4.3B), suggesting that Co binds to kaolinite via outer-sphere surface complexation in the low-mid pH regime. Taken together and in agreement with previous studies, these results suggest that Co binds to kaolinite via outer-sphere complexation during the initial sorption stage in the low-mid pH regime, where sorption is generally attributed to Co uptake onto permanently negatively charged surface sorption sites present on the siloxane faces (Spark et al. 1995; Landry et al. 2009), and then above pH ~7 during the second sorption stage Co binds via inner-sphere complexation onto the variable charge sites present on the alumina faces that are increasingly deprotonated and thus negatively charged in the mid-high pH regime (Schulthess and Huang, 1990).

The above inferences about Co-kaolinite sorption behaviour based on our macroscopic sorption data are confirmed by our EXAFS analysis of Co sorbed to kaolinite, where at low-mid pH (pH 5 and 6) the best fits do not include Co-Al bonds, while at high pH (pH 8) the best fit includes 0.5 Al at ~2.9 Å. The number of Al backscatterrers and the Co-Al interatomic distance indicates that octahedral Co-O moieties form inner-sphere bidentate edge-sharing complexes with AlOH octahedral surface groups at the pH value investigated (e.g., O'Day, et al., 1994a;b). The absence and presence of Co-Al bonds at low-mid and high pH, respectively, also agrees with previous work on the sorption of Co to kaolinite (O'Day et al., 1994b). In addition to previous work however, our EDS map (Fig. 4.10) appears to show Co distributed across the edges of the kaolinite particles, and in particular concentrated onto one side of the edges of the kaolinite particles. The distribution of Co across the particle edges is likely due to the presence of highly reactive edge sites created when crystallites break apart (Sposito, 1984) which Co can bind to (O'Day et al, 1994b). Additionally, kaolinite is a 1:1 clay that readily cleaves between octahedral Al and tetrahedral Si layers (Spark et al., 1995) to produce exposed AlOH and SiOH sites on opposite sides of the resultant crystallites. While the exposed SiOH sites are likely to provide outer-sphere sorption sites for Co, the exposed AlOH sites are known to provide inner-sphere sorption sites (O'Day, et al., 1994b), and so we propose

that the observed concentration of Co onto one side of the edges of the kaolinite particles is caused by a "depth profile" created when Co preferentially sorbs to cleavage planes containing exposed AlOH sites. As with ferrihydrite, the EXAFS analysis also indicates there are multiple (~1.5) Co-Co bonds at ~3.1 Å, but the CN for the Co-Co pathway is not high enough to imply surface precipitation and there is no evidence of $Co(OH)_2$ nanoparticles present in the TEM images (Fig. 4.10). As with ferrihydrite, a Co-Co CN of ~1.5 suggests a mixture of bi- and tri-nuclear surface complexes are forming. Overall we therefore propose that at low-mid pH, Co sorbs via outer-sphere complexation, likely associated with the permanently negatively charged sites present on the siloxane faces, while at high pH Co sorbs via inner-sphere bidentate binuclear edge-sharing complexes onto the variable charge alumina sites present at the kaolinite crystal edges and on exposed cleavage plains (Fig. 4.10).

4. 4 .1 .3 Co sorption to humic acid

Our results show that there are significant differences in the apparent amount of Co sorbed to humic acid after filtration through 0.22 μm or 10 kDa filters (Fig. 4.4). The marked decrease in solid-associated Co above pH 5, which is only observed when using 0.22 μm filters, is attributed to humic acid solvation and dispersal processes occurring at higher pH values. Humic acid solvation increases progressively as pH is raised from pH 2 to pH 12, with initially the low molecular weight (MW) fraction being dispersed at lower pH (cf. full dispersion of humic acid molecules is operationally defined at pH 12) (Ritchie and Posner, 1982). Therefore, at pH values > 5, a fraction of the sorbed Co present is not solid associated, but rather is bound to a relatively low MW (<220 nm) Co-humic acid phase that is dispersed in solution. The 10 kDa filter, in contrast, removed all humic acid particles larger than 3 nm (Pan et al., 2017) and represents the best estimate of true sorption behaviour (i.e. ~90% above pH 6.5 for the 0.1 mol L^{-1} ionic strength system).

Co sorption to humic acid at low pH (pH 4 and 4.6) is reduced when the ionic strength is increased (Fig. 4.4), in good agreement with previous studies on the sorption of other heavy metals onto purified Aldrich humic acid (Liu & Gonzalez, 2000), and our EXAFS analysis shows that at low pH (pH < 5) no Co-C bonds are required to fit the data (Table 4.1). This suggests that Co is bound through outer-sphere complexation at low pH. However, at higher pH Co sorption is unaffected by changes in ionic strength (Fig. 4.4) and our EXAFS fitting also includes 2 C at ~2.9 Å, indicative of inner-sphere complexation to C-containing functional groups present in humic acid. This is in good agreement with previous EXAFS studies reporting that Co is bound to humic acid via inner-sphere complexation to C atoms (Ghabbour et al., 2007; Xia et al., 1997). The

presence of the Co-Co bond at 3.07 Å at pH 8 indicates the presence of a hydroxide-like precipitate, but again, the CN for the Co-Co pathway is not high enough to imply surface precipitation and the TEM images (Fig. 4.11) provide no evidence of Co-Co nanoclusters. This is consistent with other work on heavy metal interactions with organic matter, where Gustafsson et al. (2014) found that Cr(III) formed dimers when sorbed to soil above pH 5, with each Cr atom bound to two carboxyl groups at 2.85-2.87 Å, which is similar to the Co-C path length used in this study. Overall we propose that Co sorbs to humic acid at low pH via outer-sphere surface complexation, and at high pH via inner-sphere bidentate binuclear surface complexation, likely involving carboxyl groups present in the humic acid moiety.

4. 4. 2. Co sorption to organo-mineral composites

Sorption to all ferrihydrite-humic acid composites is enhanced relative to the pure ferrihydrite phase, particularly at low pH (Fig. 4.6A). This is typically attributed to the fact that, in contrast to ferrihydrite, the majority of humic acid surface functional groups are deprotonated at low pH and thus possess a negative charge, which when present in a ferrihydrite-humic acid composite results in enhanced sorption in the low-mid pH regime, over the pure end-member ferrihydrite phase (Tipping et al., 1983; Murphy and Zachara, 1995; Zhu et al., 2010). The combined sorption edge and EXAFS data for the ferrihydrite-humic acid system indicates that Co binds to each of the composite fractions, and does so via the same molecular mechanisms as to the end-member ferrihydrite and humic acid phases. Specifically, at pH 6 we see enhanced Co sorption relative to the end-member ferrihydrite (Fig. 4.6A), suggesting that Co binds to both the ferrihydrite and humic acid fractions, and the best fit EXAFS model includes ~1 Fe at ~3.0 Å and ~1.5 Co at ~3.2 Å (Table 4.2), suggesting that Co binds to the ferrihydrite fraction via the inner-sphere bidentate multinuclear surface complex identified for ferrihydrite. The absence of a Co-C interatomic distance for the pH 6 ferrihydrite-humic acid sample is consistent with our EXAFS data for Co sorption to end-member humic acid which indicates that Co binds to humic acid via outer-sphere surface complexation at low-mid pH. In contrast at pH 7 the best fit EXAFS model includes 0.5 Fe at ~3.0 Å, 1.25 Co at ~3.17 Å and 1.1 C at ~2.87 Å, suggesting that Co binds to both the ferrihydrite fraction and the humic acid fraction, via the ferrihydrite inner-sphere multidentate binuclear surface complex and the humic acid inner-sphere bidentate binuclear surface complex. Our results indicate that the sorption behaviour of Co with respect to humic acid is the same for end-member humic acid, and humic acid that is sorbed to ferrihydrite surfaces.

Sorption to the kaolinite-humic acid composites is generally enhanced relative to the pure kaolinite phase, except for the 1.4 wt% C kaolinite-humic acid composite above pH

~7 (Fig. 4.6B), and again this is typically attributed to the presence of additional negatively charged sorption sites in the low-mid pH regime that are associated with the organic moieties (e.g., Heidmann et al. 2005a) who found that introducing fulvic acid to kaolinite increased Cu and Pb sorption at low to mid pH values). Consistent with the outer-sphere sorption of Co to end-member kaolinite and humic acid at low-mid pH, the best fit EXAFS models for Co sorption to kaolinite-humic acid at similar pH include only 6 O at ~ 2.0 Å. At higher pH (pH 8) the best fit EXAFS model includes 2 C at ~3.0 Å and 1 Co at ~3.14 Å (Table 4.2), suggesting that Co binds to the humic acid fraction via the inner-sphere bidentate binuclear surface complex identified for end-member humic acid. The pH 8 best fit EXAFS model does not however include any Co-Al bonds (Table 4.2), which suggests that either Co has a higher affinity for humic acid and is only sorbed to the humic acid phase in the composite, or because the Co-C and Co-Al bond lengths are similar they are not resolvable during the EXAFS analysis.

It is noteworthy that the extent to which Co sorption is enhanced in our mineral-organic composites over the pure end-member mineral phases appears to depend on the surface area of the end-member mineral phase. With relatively high surface area ferrihydrite (~ 295 ± 3 m^2/g) the percentage of Co sorbed by ferrihydrite-humic acid appears to be independent of composite C content, while with relatively low surface area kaolinite (~ 11.7 ± 0.1 m^2/g) the percentage of Co sorbed by kaolinite-humic acid appears to increase with increasing composite C content. This is observed in other heavy metal composite sorption systems, where studies using high surface area ferrihydrite in ferrihydrite-organic composites also show the enhanced low-mid pH regime sorption to be independent of composite C content (Moon and Peacock, 2012, 2013; Otero Fariña et al., 2018), while studies using relatively low surface area goethite (~42.1 m^2/g; Jönsson et al., 2006) in goethite-organic composites show increasingly enhanced low-mid pH regime sorption with increasing composite C content (Jönsson et al., 2006; Otero Fariña et al., 2017). We suggest that with a lower surface area, the organic surface coverage on a kaolinite composite will be significantly higher than for a ferrihydrite composite, and as such, cation sorption in the mid-low pH regime, where sorption onto the humic acid fraction dominates, will increasingly resemble the sorption of the cation onto pure end-member humic acid, and will thus increase with increasing humic acid fraction.

4. 4 .3 Surface Complexation Modelling of Co Sorption to End-member Ferrihydrite, Kaolinite and Humic Acid

4. 4. 3. 1 Model framework and input parameters

Surface complexation models were developed for the sorption of Co onto end-member ferrihydrite, kaolinite and humic acid that are consistent with the EXAFS data. The model framework for Co sorption to ferrihydrite is based on the model for copper sorption to ferrihydrite by Moon and Peacock (2013) and Otero Fariña et al. (2018), the framework for Co sorption to kaolinite is adapted from the model for Co sorption to kaolinite by Heidmann et al. (2005b), and the framework for Co sorption to humic acid is based on the model for copper sorption to humic acid by Otero Fariña et al., (2018). The model input parameters were obtained either through fitting potentiometric titration data for the sorbent acid-base behaviour, or from direct measurement of the sorbent physiochemical characteristics, and are detailed in Moon and Peacock (2013) for ferrihydrite, Heidmann et al. (2005b) for kaolinite and López et al. (2012) for humic acid; the input parameters are reported here in Table 4.4.

The basic stern model (BSM) is used to model surface electrostatics in the ferrihydrite, kaolinite and humic acid sorption systems. For ferrihydrite, a 3-site 1 p*K* formalism is assumed for the protonation of the ferrihydrite surface, involving two types of singly-coordinated surface oxygens (sorbing cations in edge-sharing ($\equiv FeOH^{-0.5}(e)$) and corner-sharing ($\equiv FeOH^{-0.5}(c)$) configuration), and the triply coordinated oxygens ($\equiv Fe_3O^{-0.5}$) (e.g., Hiemstra et al., 1989; Hiemstra and van Riemsdijk, 2009; Moon and Peacock, 2013; Otero Fariña et al., 2018). A 2-site, 1p*K* formalism is used for the protonation of the kaolinite surface. This involves a singly-coordinated surface oxygen ($\equiv AlOH^{-0.5}$) representing the pH-dependent charge, and negatively charged sites ($\equiv X^-$) to represent the permanent negative charge (e.g., Heidmann et al. 2005b). For the humic acid, a 1-site 1 p*K* formalism is used, involving $\equiv RCOO^-$ sites where the stability constants for the protonation of these sites and the site densities are constrained using the NICA-Donnan model (Kinniburgh et al., 1999), calibrated on multiple data sets (López et al. (2012).

The sorption data are fit by iterating the log *K* for the surface complexation reaction that represents the formation of the Co-ferrihydrite, -kaolinite or -humic acid complexes that were identified by EXAFS analysis. The three ferrihydrite systems that contained 10^{-2} mol L^{-1} ionic strength (5.8, 0.58 and 0.058 wt% Co) and two of the kaolinite systems that contained 10^{-2} mol L^{-1} ionic strength (0.058 and 0.0058 wt% Co) are fit simultaneously. Due to the limitations of EQLFOR, systems with different ionic strengths are fit

Table 4.4: Input parameters for the surface complexation models for Co sorbed to ferrihydrite, kaolinite and humic acid. Parameters for the ≡FeOH$^{-0.5}$ site are from Moon and Peacock (2013); the ≡AlOH$^{-0.5}$ and ≡X^{-} sites are from Heidmann et al. (2005b); and the ≡RCOO^{-} site are from López et al. (2012).

Site	Parameter	
≡FeOH$^{-0.5}$	Site Density (mol sites g^{-1})	1.25x10^{-3}
	Capacitance (C) (F m^{-2})	1.1
	$Log\ K_{FeOH_2}$ ≡FeOH$^{-0.5}$ + H^{+} ⇌ ≡FeOH$_2^{+0.5}$	7.99
	$Log\ K_{FeOH\_Na}$ ≡FeOH$^{-0.5}$ + Na^{+} ⇌ ≡FeOH$^{-0.5}$ – Na$^{+0.5}$	-1.00
	$Log\ K_{FeOH2\_NO_3}$ ≡FeOH$_2^{+0.5}$ + NO$_3^{-}$ ⇌ ≡FeOH$_2^{+0.5}$ – NO$_3^{-}$	-1.00
≡AlOH$^{-0.5}$	Site Density (mol sites g^{-1})	8.78x10^{-4}
	Capacitance (C) (F m^{-2})	1.1
	$Log\ K_{AlOH_2}$ ≡AlOH$^{-0.5}$ + H^{+} ⇌ ≡AlOH$_2^{+0.5}$	4.8
	$Log\ K_{AlOH\_Na}$ ≡AlOH$^{-0.5}$ + Na^{+} ⇌ ≡AlOH$^{-0.5}$ – Na^{+}0.5	-2.1
	$Log\ K_{AlOH2\_NO_3}$ ≡AlOH$_2^{+0.5}$ + NO$_3^{-}$ ⇌ ≡AlOH$_2^{+0.5}$ – NO$_3^{-}$	4.9
≡X^{-}	Site Density (mol sites g^{-1})	5.44x10^{-5}
	Capacitance (C) (F m^{-2})	1.1
	$Log\ K_{X\_Na}$ ≡X^{-} + Na^{+} ⇌ ≡X^{-} - Na$^{+0.5}$	2.9
	$Log\ K_{X\_H}$ ≡X^{-} + H^{+} ⇌ ≡XH	5.9
≡RCOO^{-}	Site Density (mol sites g^{-1})	1.94x10^{-3}
	Capacitance (C) (F m^{-2})	8.0

separately. The best fit log *K* values for the sorption of Co in all the end-member systems are shown in Table 4.5. The model fits to the data are shown in Figs. 4.3 and 4.4.

4. 4. 3. 2. Model for Co sorption to end-member ferrihydrite

Our EXAFS data indicate that Co sorbs to ferrihydrite via an inner-sphere bidentate bi- or tri-nuclear edge-sharing complex over the entire pH range investigated. Both bidentate bi- and tri-nuclear edge-sharing complexes were used to model the sorption edge data, however, models invoking a bidentate binuclear edge-sharing complex produce the best fits across all the ferrihydrite sorption data sets investigated. Model fits to the data are shown in Fig. 4.3 and our model produces adequate fits to the data over the range of ionic strengths studied. We therefore model our ferrihydrite sorption data with:

Table 4.5: Log K values for Co sorbed to ferrihydrite, kaolinite and humic acid with the error (±) as derived from the sensitivity analysis.

Phase	Ionic Strength (mol L^{-1})	Co concentration (wt% Co)	Complex	Log *K*
ferrihydrite	10^{-1}	0.58	$(\equiv FeOH(e))_2Co^{+3}$	13.11±0.58
	10^{-2}	0.058, 0.58, 5.8	$(\equiv FeOH(e))_2Co^{+3}$	14.33±2.07
	10^{-3}	0.58	$(\equiv FeOH(e))_2Co^{+3}$	13.90±0.57
kaolinite	10^{-1}	0.058	$(\equiv AlOH^{-0.5})_2Co_2(OH)_6^{-2}$	-33.86±0.58
			X^- -- Co^{+2}	3.99±0.49
	10^{-2}	0.58	$(\equiv AlOH^{-0.5})_2Co_2(OH)_6^{-2}$	-33.97±0.97
			$\equiv XH$	9.60±1.17
		0.058	$(\equiv AlOH^{-0.5})_2Co_2(OH)_6^{-2}$	-32.12±0.8
			XH -- Co^{+2}	9.23±1.54
			X^- -- Co^{+2}	4.59±3.02
		0.0058	$(\equiv AlOH^{-0.5})_2Co_2(OH)_6^{-2}$	-31.46±0.81
			XH -- Co^{+2}	10.41±1.62
			X^- -- Co^{+2}	5.20±2.42
	10^{-3}	0.058	$(\equiv AlOH^{-0.5})_2Co_2(OH)_6^{-2}$	-32.93±1.58
			XH -- Co^{+2}	11.72±1.66
			X^- -- Co^{+2}	3.81±5.85
humic acid	10^{-1}	0.58	$(\equiv RCOO)_2Co_2$	-0.58±2.25
			$\equiv RCOO^-$ -- Co^{+2}	0.75±0.94
	10^{-3}	0.58	$(\equiv RCOO)_2Co_2$	2.04±0.83
			$\equiv RCOO^-$ -- Co^{+2}	2.03±1.07

$$2\equiv FeOH^{-0.5}(e) + 2Co^{2+} \rightleftharpoons (\equiv FeOH(e))_2Co_2^{+3}$$

$$\log K_{\left(\equiv FeOH(e)\right)_2 Co_2^{+3}} \qquad (4.1)$$

$$K_{\left(\equiv FeOH(e)\right)_2 Co_2^{+3}} = \frac{X_{\left(\equiv FeOH(e)\right)_2 Co_2^{+3}}}{(X_{\equiv FeOH^{-0.5}(e)})^2[Co^{2+}]} \exp\left(\frac{(-2\psi_0)F}{RT}\right) \qquad (4.2)$$

Where X represents the mole fraction of surface sites that the protonated or deprotonated surface complex occupies, ψ_0 is the electrostatic potential at the 0-plane (defined from the surface charge distribution (σ) using the BSM), *F* is the Faraday

constant, *R* is the gas constant and *T* is temperature. It should be noted that bidentate binuclear edge-sharing complexation is technically represented by $\equiv Fe(OH^{-0.5}(e))_2 + 2Co^{2+} \rightleftharpoons \equiv Fe(OH(e))_2Co_2^{3+}$. However, in surface complexation modelling formalism, $\equiv FeOH^{-0.5}$ is the operational surface site and thus both bidentate binuclear edge- and corner-sharing are represented by Eq. (4.1).

4. 4. 3. 2. Model for Co sorption to end-member kaolinite

Our EXAFS data indicate that Co sorbs to kaolinite via an outer-sphere complex at low-mid pH and an inner-sphere bidentate binuclear edge-sharing complex associated with the alumina sorption sites at high pH. In agreement with previous modelling studies (e.g., Heidmann et al., 2005b; Peacock and Sherman, 2005) outer-sphere sorption is invoked onto the permanently negatively charged sites present on the siloxane faces ($\equiv X^-$), and we find that the best fits to the data generally involve Co sorption onto these sites in both their deprotonated ($\equiv X^-$) and protonated ($\equiv XH$) forms. The inner-sphere sorption is invoked onto the variable charge alumina sites ($\equiv AlOH^{-0.5}$). The total model fits to the data are shown in Fig. 4.3 while the contribution of the different surface sites to the total sorption is shown in Fig. 4.12. The protonated form of the permanently negatively charged site ($\equiv XH$) only significantly contributes to sorption at low ionic strength (Fig. 4.12A) and low wt% Co (Fig. 4.13) and in the very low pH regime, reflecting the log K for the deprotonation of these sites (log K = 5.9; Table 4.4). Overall the models produce good fits to the data over the range of ionic strengths studied, and the contribution of the different surface complexes to the total sorption as a function of pH is consistent with our EXAFS data. We therefore model our kaolinite sorption data with:

$$2\equiv AlOH^{-0.5} + 2Co^{2+} + 6H_2O \rightleftharpoons (\equiv AlOH)_2Co_2(OH)_6 + 6H \qquad \log K_{(\equiv AlOH)_2Co_2(OH)_6^{-2}} \quad (4.3)$$

$$K_{(\equiv AlOH)_2Co_2(OH)_6^{-2}} = \frac{X_{(\equiv AlOH)_2Co_2(OH)_6^{-2}}}{(X_{\equiv AlOH^{-0.5}})^2[Co^{2+}]} \exp\left(\frac{(2\psi_0)F}{RT}\right) \quad (4.4)$$

$$\equiv X^- + Co^{2+} \rightleftharpoons \equiv X^- -- Co^{2+} \qquad \log K_{\equiv X^- -- Co^{2+}} \quad (4.5)$$

$$K_{\equiv X^- -- Co^{2+}} = \frac{X_{\equiv X^- -- Co^{2+}}}{(X_{\equiv X^-})^2[Co^{2+}]} \exp\left(\frac{(-2\psi_1)F}{RT}\right) \quad (4.6)$$

$$\equiv XH + Co^{2+} \rightleftharpoons \equiv XH -- Co^{2+} \qquad \log K_{\equiv XH -- Co^{2+}} \quad (4.7)$$

$$K_{\equiv XH -- Co^{2+}} = \frac{X_{\equiv XH -- Co^{2+}}}{(X_{\equiv XH})^2[Co^{2+}]} \exp\left(\frac{(-3\psi_1)F}{RT}\right) \quad (4.8)$$

Where X represents the mole fraction of surface sites that the protonated or deprotonated surface complex occupies, ψ_0 is the electrostatic potential at the 0-plane and ψ_1 is the electrostatic potential at the 1-plane (as defined from the surface charge distribution (σ) using the BSM), *F* is the Faraday constant, *R* is the gas constant and *T* is temperature. Again it should be noted that bidentate binuclear edge-sharing complexation is technically represented by $\equiv Al(OH^{-0.5})_2 + 2Co^{2+} + 6H_20 \rightleftharpoons \equiv Al(OH)_2Co_2(OH)_6 + 6H^+$. However, as above, in surface complexation modelling formalism $\equiv AlOH^{-0.5}$ is the operational surface site and thus both bidentate binuclear edge- and corner-sharing are represented by Eq. (4.3).

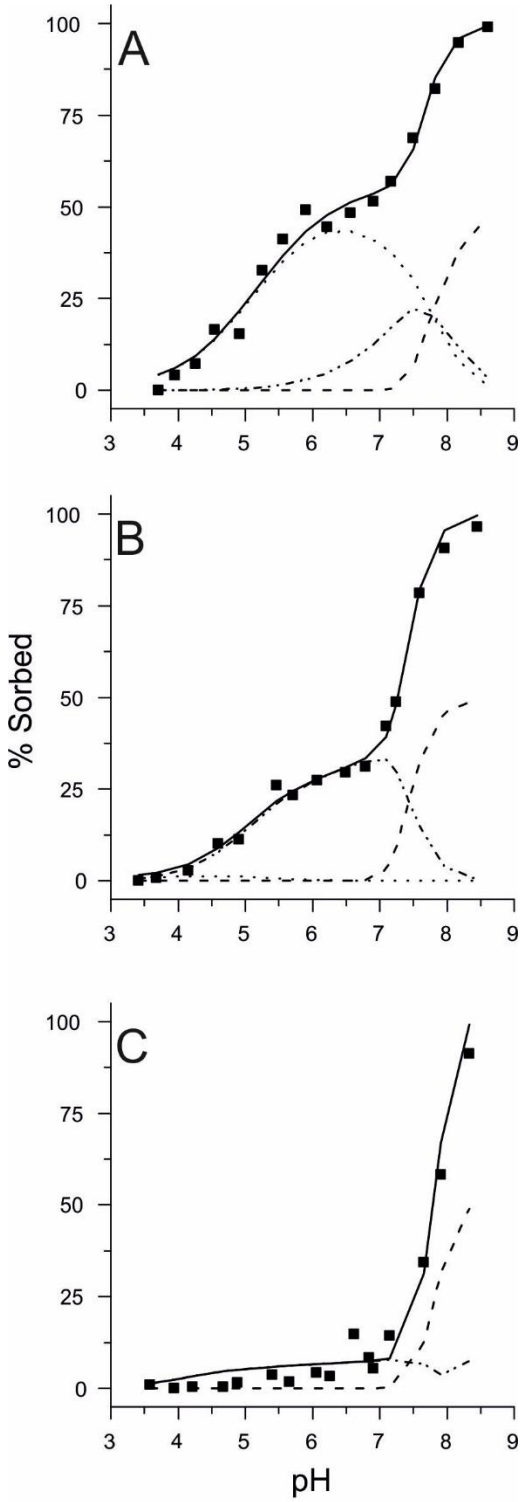

Figure 4.12: Iterated surface complexation model predictions for Co sorption to kaolinite surface sites. Panel A shows Co sorption with an ionic strength of 10^{-3} mol L^{-1}; panel B, 10^{-2} mol L^{-1}; and panel C, 10^{-1} mol L^{-1}. Squares are data; solid lines show total predicted sorption; dashed lines, ≡AlOH sites; dotted lines, ≡XH sites; and dash-dot-dot lines, $\equiv X^-$ sites.

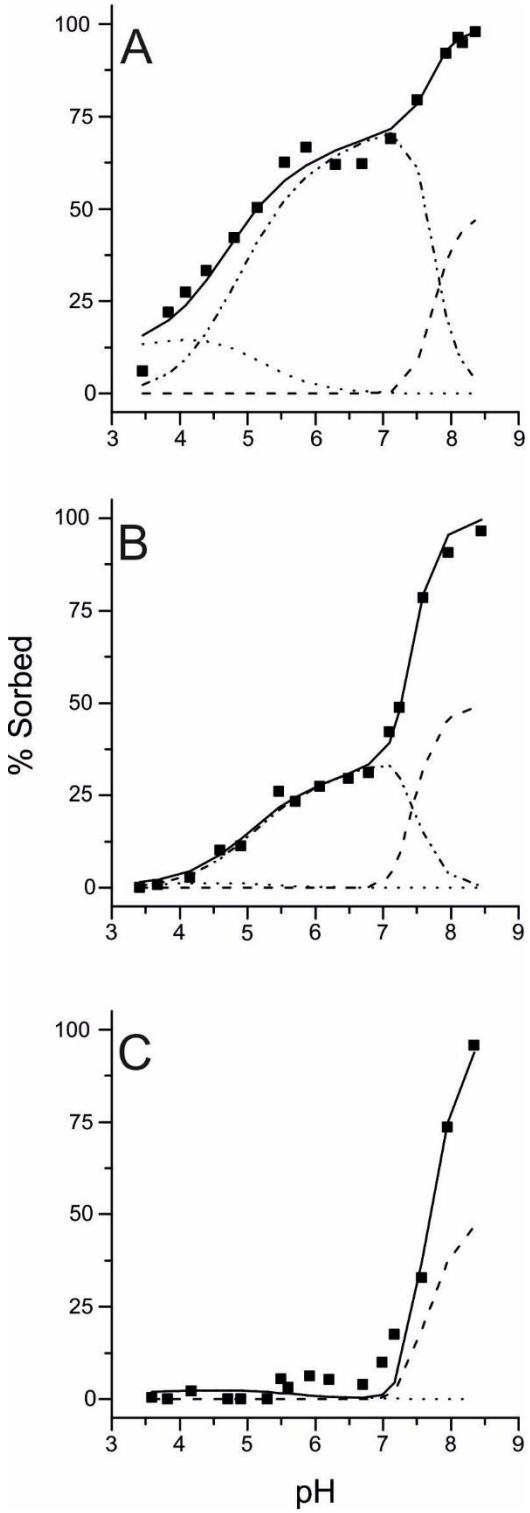

Figure 4.13: EQLFOR model predictions for Co sorption to kaolinite surface sites. Panel A shows predicted sorption at 0.0058 wt% Co, panel B at 0.058 wt% Co, and panel C at 0.58 wt% Co. Solid lines represent total amount of Co predicted to be sorbed, dashed lines show sorption to ≡AlOH sites, dotted lines show sorption to ≡XH sites, and dash-dot-dot lines show sorption to $\equiv X^-$ sites.

4. 4. 3. 3 Model for Co sorption to end-member humic acid

Our EXAFS data indicate that Co sorbs to humic acid at low pH via outer-sphere surface complexation, and at high pH via inner-sphere bidentate binuclear surface complexation that likely involves carboxyl groups present in the humic acid moiety. It is not possible to determine from the EXAFS which sorption site(s) are most associated with the outer-sphere complex, and unlike kaolinite, humic acid has a number of different sorption sites which could be responsible for the electrostatic and hence outer-sphere sorption of Co (including carboxyl, phosphoryl, methoxyl, carbonyl, and alcoholic hydroxyl groups (Tsutsuki and Kuwatsuka, 1978; Yonebayashi and Hattori, 1988)). Given this we nominally assign the outer-sphere sorption to the carboxyl ≡RCOO$^-$ sites in the modelling, which is at least consistent with the fact that Co is already known to interact with these sites during sorption to humic acid via inner-sphere complexation (as identified for our high pH Co-humic acid sorption sample and by Xia et al. (1997) and by Ghabbour et al. (2007) during their studies of Co sorption to humic acid). The total model fits to the data are shown in Fig. 4.4 while the contribution of the different surface sites to the total sorption is shown in Fig. 4.14. Overall the models produce adequate fits to the data at the two ionic strengths studied, and the contribution of the different surface complexes to the total sorption as a function of pH is consistent with our EXAFS data. We therefore model our humic acid sorption data with:

$$2{\equiv}RCOO^- + 2Co^{2+} \rightleftharpoons ({\equiv}RCOO)_2Co_2 \qquad \log K_{(\equiv RCOO)_2Co_2} \qquad (4.9)$$

$$K_{(\equiv RCOO)_2Co_2} = \frac{X_{(\equiv RCOO)_2Co_2}}{(X_{\equiv RCOO^-})^2[Co^{2+}]} \exp\left(\frac{(-4\psi_0)F}{RT}\right) \qquad (4.10)$$

$${\equiv}RCOO^- + Co^{2+} \rightleftharpoons {\equiv}RCOO^- \text{ -- } Co^{2+} \qquad \log K_{\equiv CROO^- -- Co^{2+}} \qquad (4.11)$$

$$K_{\equiv RCOO^- -- Co^{2+}} = \frac{X_{\equiv RCOO^- -- Co^{2+}}}{(X_{\equiv RCOO^-})^2[Co^{2+}]} \exp\left(\frac{(-2\psi_1)F}{RT}\right) \qquad (4.12)$$

As for the ferrihydrite and kaolinite equations, X represents the the mole fraction of surface sites that the protonated or deprotonated surface complex occupies, ψ_0 is the electrostatic potential at the 0-plane and ψ_1 is the electrostatic potential at the 1-plane (as defined from the surface charge distribution (σ) using the BSM), *F* is the Faraday constant, *R* is the gas constant and *T* is temperature.

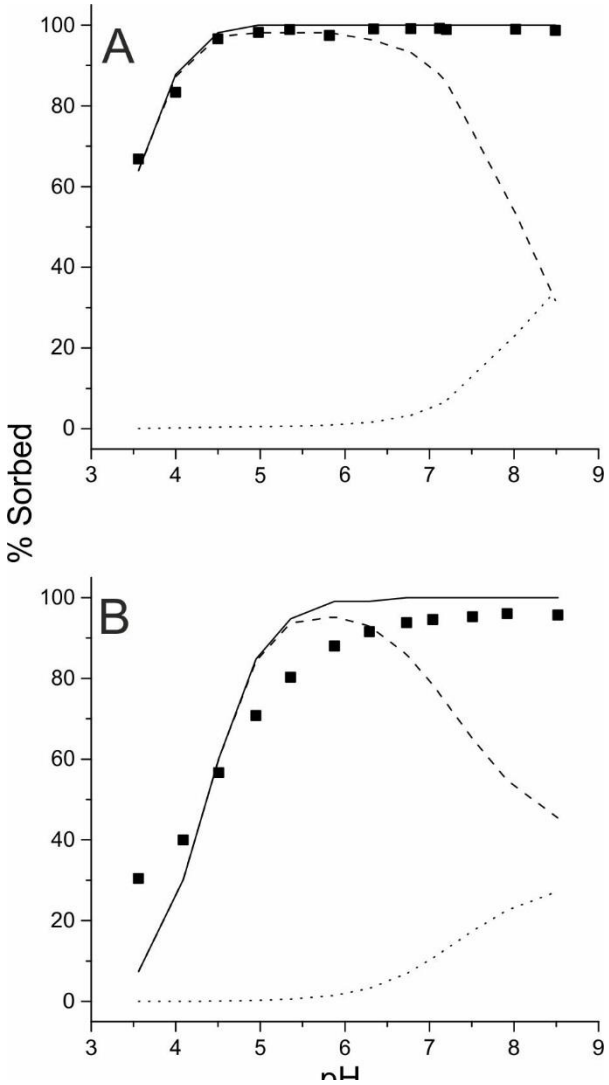

Figure 4.14: Iterated surface complexation model predictions for Co onto humic acid surface sites at 10^{-3} mol L^{-1} $NaNO_3$ (panel A) and 10^{-1} mol L^{-1} $NaNO_3$ (panel B). Squares are data; solid lines, total predicted sorption; dashes, outer-sphere sorption to ≡$RCOO^-$ sites; and dots, inner-sphere sorption to ≡$RCOO^-$ sites.

4. 4. 3. 4 Sensitivity analysis

A sensitivity analysis of the systems, to test the models' sensitivity to the input parameters, was conducted, in which the input parameters are varied over a range of reasonable experimental and theoretical values. The process for this is described fully in Chapter 4.2.5.1, and the results of the analysis are shown in Table 4.5 as the error (±). The errors provide an estimate of the range that the log *K* values may vary due to inherent uncertainties in the parameterisation of the ferrihydrite, kaolinite, and humic acid sorption properties in the models. Overall, based on our EXAFS identified surface complexes, the average log *K* for Co sorption onto ferrihydrite is log *K* $(\equiv FeOH(e))_2Co_2^{+3}$ = 13.78; onto kaolinite is log *K* $\equiv X^-$ -- Co^{+2} = 4.4, log *K* $\equiv XH$ -- Co^{+2} = 10.24 and log *K* $(\equiv AlOH)_2Co_2(OH)_6$ = -32.868; and onto humic acid is log *K* $\equiv RCOO^-$ -- Co^{+2} = 1.39 and log *K* $(\equiv RCOO)_2Co_2$ = 0.73.

4. 4. 4 Surface Complexation Modelling of Co Sorption to Organo-mineral Composites

4. 4. 4. 1 Model framework and input parameters

Sorption edge data for the ferrihydrite-humic acid and kaolinite-humic acid composites are intermediate between the end member phases (Fig. 4.6), and the EXAFS data show the Co sorption to the composites occurs via the same molecular mechanisms as to the end-member phases (Tables 4.1 and 4.2, Fig. 4.7). This suggests that Co sorption to these composites shows a degree of additivity, and therefore a component additivity approach was used to fit the ferrihydrite-humic acid and kaolinite-humic acid composite sorption data. In this approach the models for Co sorbed to ferrihydrite and humic acid, and kaolinite and humic acid are combined linearly in order to create a single sorption model for each composite. The model input parameters are reported here in Table 4.4 and the model fits are shown in Figs. 4.15 (panels A, C, and E) and 4.16 (panels A and C). As with the end-member models, the BSM is used to model the composite electrostatics. As the linear combination of the ferrihydrite and humic acid end-member models, the ferrihydrite composite adopted a 4-site 1 p*K* formalism (containing the 3 ferrihydrite sites and the 1 humic acid site) while the kaolinite composite adopted a 3 p*K* formalism (the 2 kaolinite sites and the 1 humic acid site). In this approach the log *K*'s for the protonation and binding of electrolyte ions to these sites, and absolute site densities, are fixed to the values of the end-member ferrihydrite or kaolinite and humic acid models. Operational site densities for each site, and a surface area and Stern layer capacitance for each composite, are then calculated from the end-member values weighted to the appropriate ferrihydrite:humic acid or kaolinite:humic acid mass ratio (Table 4.6).

Initially Co sorption to the composites is modelled with the best fit log *K* values from the end-member systems (Figs. 4.15A, C, E and 4.16A, C). The end-member log *K* values are then iterated whilst keeping all other parameters constant (Figs. 4.15B, D, F and 4.16B, D). If the composites behave in an additive manner then the optimised log *K* values should fall within the uncertainties on the end-member values.

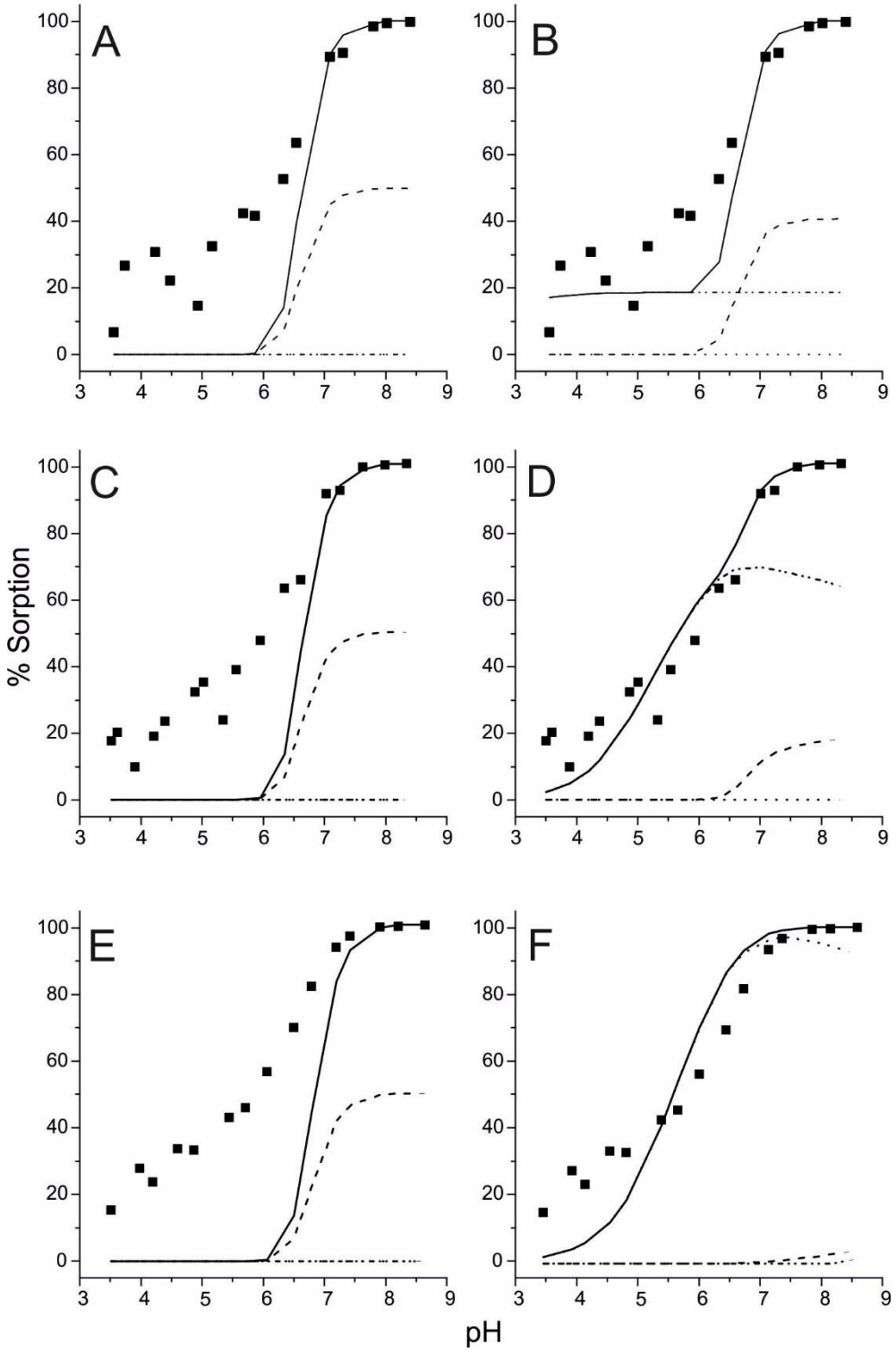

Figure 4.15: Surface complexation model predictions of Co sorption to ferrihydrite-humic acid surface sites. Panels A and B show the composite with 5 wt% C; panels C and D, 10 wt% C; and panels E and F, 17 wt% C composite. Panels A, C, and E show predicted sorption using log *K*s fixed to those from the two end--member phases. Panels B, D, and F show predicted sorption with iterated log *K*s. Solid lines show total predicted sorption; dashed lines, sorption to ≡FeOH sites; dash-dot-dot, outer-sphere sorption to ≡RCOO$^-$ sites; and dotted lines, inner-sphere sorption to ≡RCOO$^-$ sites.

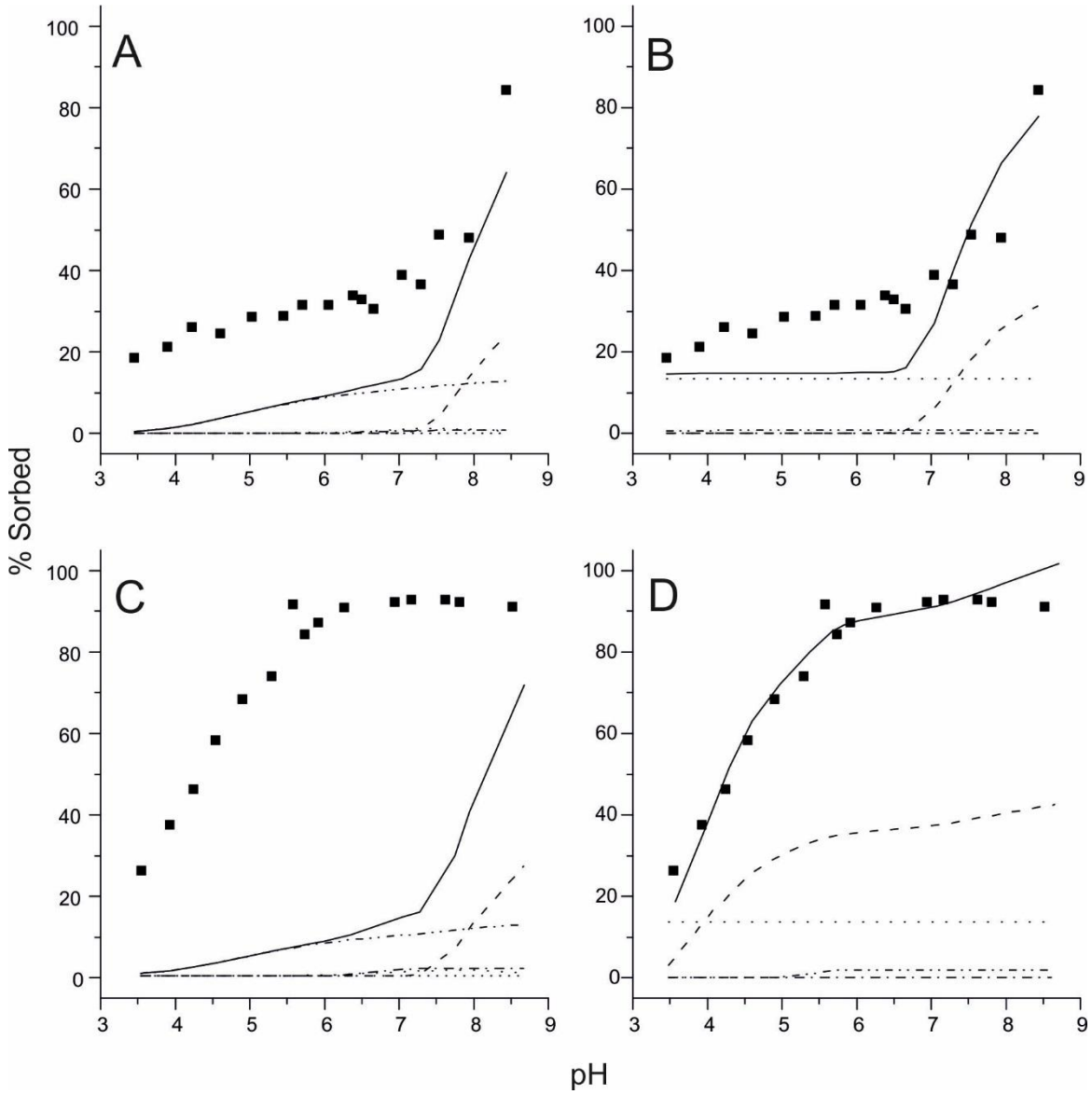

Figure 4.16: Surface complexation model predictions of Co sorption to kaolinite-humic acid surface sites. Panels A and B show the results for the 1.4 wt% C composite, and panels C and D show the 2.2 wt% C composite. Panels A and C show predicted sorption using log *K*s fixed to those from the two end-member phases. Panels B and D show predicted sorption with iterated log *K*s. Solid lines show total predicted sorption; dashed lines, sorption to the ≡AlOH sites; dotted lines, sorption to ≡XH sites; dash-dot-dot lines, inner-sphere sorption to ≡RCOO$^-$ sites; and dash-dot, outer-sphere sorption to ≡RCOO$^-$ sites.

Table 4.6: Input parameters for the surface complexation models for Co sorbed to ferrihydrite and kaolinite organo-mineral composites. Operational site densities for each site, and a surface area and Stern layer capacitance for each composite, are then calculated from the end-member values weighted to the appropriate ferrihydrite:humic acid or kaolinite:humic acid mass ratio. ferrihydrite data is from Moon and Peacock (2013), kaolinite from Heidmann et al. (2005b), and humic acid from López et al. (2012).

Composite		**Site Densities (mol sites L^{-1})**				**Surface Area** (m^2 L^{-1})	**Stern Layer Capacitance** (F m^{-2})
		FeOHe	**FeOHc**	**Fe3O**	**R-COO$^-$**		
Ferrihydrite-humic acid	5 wt% C	$1.13x10^{-3}$	$1.58x10^{-3}$	$5.4x10^{-4}$	$1.93x10^{-5}$	291.62	1.8
	10 wt% C	$9.96x10^{-3}$	$1.39x10^{-3}$	$4.79x10^{-4}$	$3.85x10^{-5}$	281.23	2.5
	17 wt% C	$8.35x10^{-4}$	$1.17x10^{-3}$	$4.02x10^{-4}$	$6.27x10^{-5}$	268.14	3.39
		X$^-$	**AlOH**		**R-COO$^-$**		
Kaolinite-humic acid	1.4 wt% C	$1.33x10^{-5}$	$2.14x10^{-3}$		$1.45x10^{-6}$	16.86	1.83
	2.2 wt% C	$1.3x10^{-5}$	$2.1x10^{-3}$		$2.28x10^{-6}$	19.81	1.4

4. 4. 4. 2 Model for Co sorption to ferrihydrite-humic acid composite

Model fits for Co sorption to the 3 ferrihydrite-humic acid composites are shown in Fig. 4.15. Using the exact end-member log *K*s, the model underestimates Co sorption to the 5, 10, and 17 wt% C ferrihydrite-humic acid composites below pH 6.5 (Fig. 4.15A). When the log *K* values are iterated the fit improves, but for the 5 wt% C composite there is still a significant underestimation between pH 5 and 6.5 (Fig. 4.15B). Iterated log *K* values are presented in Table 4.7. Furthermore, the log *K* for the outer-sphere humic acid complex in the iterated fits for all composites is far outside the uncertainty on the end-member value (Table 4.5). This implies that the model formalism for the outer-sphere complexation of Co to the end-member humic acid does not accurately describe the outer-sphere complexation of Co to the humic acid fraction of the composite. This could be because the functional groups available for outer-sphere complexation in the composite are modified as a result of humic acid interaction with the ferrihydrite surface. The model also fails to accurately predict the distribution of the adsorbed Co between the ferrihydrite and humic acid fractions, where, based on our EXAFS, the model fits should show inner-sphere bidentate binuclear sorption to the ferrihydrite fraction, either no sorption or outer-sphere sorption to the humic acid fraction at mid-low pH and inner-sphere bidentate binuclear sorption to both the ferrihydrite and humic acid fractions at mid-high pH. As such Co sorption to our ferrihydrite organo-mineral composites is non-additive and cannot be modelled assuming a component additivity approach. This could be caused by the HA chemically altering the surface sites on the Fh (or vice versa) meaning that Co is not binding to the surface sites accounted for in the model. Alternatively, Co could have a higher affinity to one of the phases so it preferentially binds to that, while the model assumes sorption to each of the phases that is proportional to the number of surface sites of that phase. This is in contrast to previous work on Cu sorption to ferrihydrite-humic acid composites, where iterated log *K* values (resulting in log *K* values of 9.27 and 3.31 for Cu sorption to ferrihydrite and humic acid, respectively) remained within the range of error determined by a sensitivity analysis and produced a good fit to the data, showing that a component additivity approach was able to accurately predict the sorption behaviour (Otero-Fariña et al., 2018).

Table 4.7: Iterated log K values for Co sorbed to ferrihydrite and kaolinite and humic acid organo-mineral composites.

System	Complex	Log *K*
Ferrihydrite-humic acid 5 wt% C	$(\equiv FeOH(e))_2 2Co^{+3}$	13.11
	$(\equiv RCOO)_2Co_2$	-0.58
	$\equiv RCOO^- -- Co^{+2}$	10.73
Ferrihydrite-humic acid 10 wt% C	$(\equiv FeOH(e))_2 2Co^{+3}$	13.11
	$(\equiv RCOO)_2Co_2$	-0.58
	$\equiv RCOO^- -- Co^{+2}$	9.23
Ferrihydrite-humic acid 17 wt% C	$(\equiv FeOH(e))_2 2Co^{+3}$	13.11
	$(\equiv RCOO)_2Co_2$	-0.58
	$\equiv RCOO^- -- Co^{+2}$	8.86
Kaolinite-humic acid 1.4 wt% C	2AlOH-2Co	-30.67
	$XH--Co^{+2}$	18.31
	$X^- -- Co^{+2}$	4.22
	$(\equiv RCOO)_2Co_2$	15.35
	$\equiv RCOO^- -- Co^{+2}$	2.10
Kaolinite-humic acid 2.2 wt% C	2AlOH-2Co	-16.82
	$XH--Co^{+2}$	26.49
	$X^- -- Co^{+2}$	5.17

4. 4. 4. 3 Model for Co sorption to kaolinite-humic acid composite

The model fits for Co sorption to the 2 kaolinite-humic acid composites are shown in Fig. 4.16. Using the exact end-member log *K*s, the model underestimates Co sorption to the 1.4 and 2.2 wt% C kaolinite-humic acid composite over the entire pH range (Fig. 4.16). When the log *K* values are iterated the fit improves, but there is still an underestimation between pH 4 and 7 for the 1.4 wt% C composite. Iterated log *K* values are presented in Table 4.7. Furthermore, for the 1.4 wt% C composite the log *K* values for the $XH -- Co^{+2}$ and inner-sphere humic acid complex are outside the uncertainty on the end-member values (Table 4), and for the 2.2 wt% C composite the log K values for the $XH -- Co^{+2}$ and inner-sphere kaolinite complex are outside the uncertainty on the end-member values (Table 4). As for the ferrihydrite-humic acid composite, this suggests that these surface

functional groups behave differently in the composite system compared to the single phase systems. For both composites the model also fails to accurately predict the distribution of the adsorbed Co between the kaolinite and humic acid fractions, where, based on our EXAFS, the model fits should show outer-sphere sorption to either the kaolinite or humic acid fractions at mid-low pH and bidentate binuclear inner-sphere sorption to the humic acid fraction and either no sorption or outer-sphere sorption to the kaolinite fraction at mid-high pH. As such Co sorption to our kaolinite organo-mineral composites is non-additive and cannot be modelled assuming a component additivity approach. As with the Fh-HA composite, this could be explained by the HA chemically altering the surface sites on the Fh (or vice versa), or Co having a higher affinity to one of the phases so it preferentially binds to that.

4. 4. 5. Implications for Co Behaviour in Natural Environments

In all end-member and organo-mineral composite systems studied in this work, inner-sphere bidentate binuclear sorption complexes were found to occur at mid-high pH. We propose that this is a universal uptake mechanism for Co in soils and sediments at neutral and alkaline pH values. This universal sorption mechanism controls Co uptake onto ferrihydrite, kaolinite and humic acid and their associated organo-mineral composites, and limits Co mobility in natural and contaminated environments. Our work unifies previous studies that have worked on similar systems individually yet reported similar sorption mechanisms (O'Day, et al., 1994a;b; Xia et al., 1997; Ghabbour et al., 2007), but also reconciles direct observations of Co sorption mechanisms, observed with EXAFS, with indirect Co sorption modelling studies, by developing the first thermodynamic surface complexation models for Co sorption to ferrihydrite, kaolinite and humic acid that are completely consistent with EXAFS results.

Our results indicate that Co sorption behaviour is likely to differ between environments where the organic matter content varies. In soils that are low in organic matter such as some alluvial sediments and desert areas, Co will behave similarly to how it does in the pure mineral systems as there is no organic matter to influence sorption. This means that Co will be mobile below pH ~ 6.5 because below this pH there is no significant sorption to solid phases likely to be present such as iron (hydr)oxides and clay minerals. In contrast to mineral soils, in peat soils and other organic matter dominated environments, Co will be less mobile at lower pH values due to higher sorption to humic substances and will likely be mobile as Co^{2+} only at very low pH values. At neutral to high pH, humic acid may also be present as colloids and the association of Co with low MW humic acid colloids is a potential transport vector for contamination in organic rich environments at neutral to alkaline pH values where high Co sorption would be expected. In temperate

regions, soils that contain both minerals and modest amounts of organic matter are much more common than either mineral or peat soils and are likely to show sorption behaviour that is composite between pure mineral and organic dominated systems. This is especially true at low pH, where enhanced sorption may be expected due to interaction of Co with humic materials. Also, in composite systems discrete humic acid colloids do not appear to form, most likely due to the strong bonding of humic acid to mineral surfaces reducing the propensity for humic acid solvation and dispersion in solution. In addition, in soils where there is a high amount of humic substances relative to clays, sorption to the clay fraction may be completely inhibited due to all AlOH sites being involved in clay-humic acid bonding and none being available for cation sorption. This would result in Co binding solely to the humic acid coating and thus sorption behaviour would be most similar to that of the pure humic acid system.

Finally these organo-mineral composite systems cannot be modelled in a component additivity approach. Therefore, the physiochemical characteristics of the composite must be so significantly different from the end-member phases that adsorption is not the simple linear combination of the end-member adsorptivities. This means that Co sorption to these composites cannot currently be predicted and more research is necessary in order to fully understand how organic and mineral phases in organo-mineral composites interact to potentially change the composite adsorptive properties.

4. 5 Conclusion

The addition of humic acid to ferrihydrite and kaolinite enhances the amount of Co sorbed below pH 6, where there is typically little sorption. For the first time, Co sorption onto an iron (oxy)hydroxide was studied using EXAFS and its local molecular environment analysed. EXAFS and TEM data suggests that Co sorbs to all soil components through formation of similar inner-sphere bidentate multinuclear surface complexes at high pH, but at low pH on kaolinite and humic acid sorption is via outer-sphere complexation. We conclude that the formation of these inner-sphere bidentate multinuclear surface complexes at high pH constitute a universal uptake mechanism of Co onto soil materials. It was possible to fit the sorption data for the pure end-member systems invoking the sorption mechanisms identified by the EXAFS data. However, fixing the log *K*s in the composite models to the values from the pure end-member systems did not produce a good fit to the composite sorption data. Therefore, we conclude that Co sorption to ferrihydrite-humic acid and kaolinite-humic acid composites is non-additive and further work is required to understand how organic and mineral phases in organo-mineral composites interact and how this interaction potentially changes composite adsorptive properties.

4.6 References

Ainsworth C. C., Pilon J. L., Gassman P. L., Van W. G. and Sluys D. (1994) Cobalt, Cadmium, and Lead Sorption to Hydrous Iron Oxide: Residence Time Effect. *Soil Sci. Soc. Am. J.* **58**, 1615–1623.

Alvarez A. and Garrido J. (2004) Retention of Co (II), Ni (II), and Cu (II) on a Purified Brown Humic Acid . Modeling and Characterization of the Sorption Process. *Langmuir* **20**, 3657–3664.

Angove M. J., Johnson B. B. and Wells J. D. (1997) Adsorption of cadmium(II) on kaolinite. *Colloids Surfaces A Physicochem. Eng. Asp.* **126**, 137–147.

Angove M. J., Johnson B. B. and Wells J. D. (1998) The Influence of Temperature on the Adsorption of Cadmium(II) and Cobalt(II) on Kaolinite. *J. Colloid Interface Sci.* **204**, 93–103.

CEFAS (2005) Radioactivity in Food and the Environment, 2004.

Charlton S. R. and Parkhurst D. L. (2002) *PHREEQCI – A Graphical User Interface to the Geochemical Model PHREEQC.*, U.S. Geological Survey Fact Sheet FS-031–02.

Covelo E. F., Vega F. A. and Andrade M. L. (2007) Competitive sorption and desorption of heavy metals by individual soil components. *J. Hazard. Mater.* **140**, 308–315.

Dzombak D. A. and Morel F. (1990) *Surface Complexation Modeling: Hydrous Ferric Oxide.*, John Wiley & Sons Inc, New York.

Eick M. J. and Fendorf S. E. (1998) Reaction Sequence of Nickel(II) with Kaolinite: Mineral Dissolution and Surface Complexation and Precipitation. *Soil Sci. Soc. Am. J.* **62**, 1257–1267.

Forbes E. A., Posner A. M. and Quirk J. P. (1976) The Specific Adsorption of Divalent Cd, Co, Cu, Pb, and Zn on Goethite. *J. Soil Sci.* **27**, 154–166.

Gál J., Hursthouse A., Tatner P., Stewart F. and Welton R. (2008) Cobalt and secondary poisoning in the terrestrial food chain: Data review and research gaps to support risk assessment. *Environ. Int.* **34**, 821–838.

Ghabbour E. A., Scheinost A. C. and Davies G. (2007) XAFS studies of cobalt(II) binding by solid peat and soil-derived humic acids and plant-derived humic acid-like substances. *Chemosphere* **67**, 285–291.

Gustafsson J. P., Persson I., Oromieh A. G., Van Schaik J. W. J., Sjö C. and Kleja D. B. (2014) Chromium(III) Complexation to Natural Organic Matter: Mechanisms and Modeling. *Environ. Sci. Technol.* **48**, 1753–1761.

Heidmann I., Christl I. and Kretzschmar R. (2005a) Sorption of Cu and Pb to kaolinite-fulvic acid

colloids: Assessment of sorbent interactions. *Geochim. Cosmochim. Acta* **69**, 1675–1686.

Heidmann I., Christl I., Leu C. and Kretzschmar R. (2005b) Competitive sorption of protons and metal cations onto kaolinite: experiments and modeling. *J. Colloid Interface Sci.* **282**, 270–282.

Hewitt E. J. (1953) Metal Interrelationships in Plant Nutrition. *J. Exp. Bot.* **4**, 59–64.

Hizal J. and Apak R. (2006) Modeling of copper(II) and lead(II) adsorption on kaolinite-based clay minerals individually and in the presence of humic acid. *J. Colloid Interface Sci.* **295**, 1–13.

Jönsson J., Sjöberg S. and Lövgren L. (2006) Adsorption of Cu(II) to schwertmannite and goethite in presence of dissolved organic matter. *Water Res.* **40**, 969–974.

Kanungo S. B. (1994) Adsorption of Cations on Hydrous Oxides of Iron. *J. Colloid Interface Sci.* **162**, 93–102.

Landry C. J., Koretsky C. M., Lund T. J., Schaller M. and Das S. (2009) Surface complexation modeling of Co(II) adsorption on mixtures of hydrous ferric oxide, quartz and kaolinite. *Geochim. Cosmochim. Acta* **73**, 3723–3737.

Liu A. and Gonzalez R. D. (2000) Modeling Adsorption of Copper(II), Cadmium(II) and Lead (II) on Purified Humic Acid. *Adsorpt. J. Int. Adsorpt. Soc.* **16**, 3902–3909.

López R., Gondar D., Antelo J., Fiol S. and Arce F. (2012) Study of the acid-base properties of a peat soil and its humin and humic acid fractions. *Eur. J. Soil Sci.* **63**, 487–494.

McLaren R. G., Lawson D. M. and Swift R. S. (1986) Sorption and desorption of cobalt by soils and soil components. *J. Soil Sci.* **37**, 413–426.

Moon E. M. and Peacock C. L. (2012) Adsorption of Cu(II) to ferrihydrite and ferrihydrite-bacteria composites: Importance of the carboxyl group for Cu mobility in natural environments. *Geochim. Cosmochim. Acta* **92**, 203–219.

Moon E. M. and Peacock C. L. (2013) Modelling Cu(II) adsorption to ferrihydrite and ferrihydrite-bacteria composites: Deviation from additive adsorption in the composite sorption system. *Geochim. Cosmochim. Acta* **104**, 148–164.

Murphy E. M. and Zachara J. M. (1995) The role of sorbed humic substances on the distribution of organic and inorganic contaminants in groundwater. *Geoderma*, 103–124.

O'Day P. A., Brown JR G. E. and Parks G. A. (1994a) X-Ray Absorption Spectroscopy of Cobalt(II) Multinuclear Surface Complexes and Surface Precipitates on Kaolinite. *J. Colloid Interface Sci.* **165**, 269–289.

O'Day P. A., Parks G. A. and Brown Jr G. E. (1994b) Molecular Structure and Binding Sites of Cobalt(II) Surface Complexes on Kaolinte from X-Ray Absorption Spectroscopy. *Clays Clay*

Miner. **42**, 337–355.

O'Day P. A., Chisholm-brause C. J., Towle S. N., Parks G. A. and Brown Jr G. E. (1996) X-Ray absorption spectroscopy of Co (II) sorption complexes on quartz (~-SiO2) and rutile (TiO2). *Geochim. Cosmochim. Acta* **60**, 2515–2532.

Otero-Fariña A., Fiol S., Arce F. and Antelo J. (2017) Effects of natural organic matter on the binding of arsenate and copper onto goethite.

Otero-Fariña A., Peacock C. L., Fiol S., Antelo J. and Carvin B. (2018) A universal adsorption behaviour for Cu uptake by iron (hydr)oxide organo-mineral composites. *Chem. Geol.*

Pan C., Troyer L. D., Liao P., Catalano J. G., Li W. and Giammar D. E. (2017) Effect of Humic Acid on the Removal of Chromium(VI) and the Production of Solids in Iron Electrocoagulation. *Environ. Sci. Technol* **51**.

Parkhurst D. L. and Appelo C. A. J. (1999) *User's Guide to PHREEQC (version 2) – A Computer Program for Speciation, Batch-Reaction, One-Dimensional Transport, and Inverse Geochemical Calculations*., U.S. Geological Survey Water- Resources Investigations Report 99–4259.

Peacock C. L. and Sherman D. M. (2005) Surface complexation model for multisite adsorption of copper(II) onto kaolinite. *Geochim. Cosmochim. Acta*.

Ravel B. and Newville M. (2005) ATHENA, ARTEMIS, HEPHAESTUS: data analysis for X-ray absorption spectroscopy using IFEFFIT. *J. Synchrotron Rad* **12**, 537–541.

Ritchie G. S. P. and Posner A. M. (1982) The effect of pH and metal binding on the transport properties of humic acids. *J. Soil Sci.* **33**, 233–247.

Rout K., Mohapatra M. and Anand S. (2012) 2-Line Ferrihydrite: Synthesis, Characterization and its Adsorption Behaviour for Removal of Pb(II), Cd(II), Cu(II) and Zn(II) from Aqueous Solutions. *Dalt. Trans.* **41**, 3302–3312.

Scheinost A. C., Abend S., Pandya K. and Sparks D. L. (2001) Kinetic Controls on Cu and Pb Sorption by Ferrihydrite. *Environ. Sci. Technol.* **35**.

Schenck C. V, Dillard J. G. and Murray J. W. (1983) Surface Analysis and the Adsorption of Co(ll) on Goethite. *J. Colloid Interface Sci.* **95**, 398–409.

Schulthess C. P. and Huang C. P. (1990) Adsorption of Heavy Metals by Silicon and Aluminum Oxide Surfaces on Clay Minerals. *Soil Sci. Soc. Am. J.* **54**, 679–688.

Schwertmann U. and Cornell R. M. (1991) *Iron Oxides in the Laboratory: Preparation and Characteristics*., VCH, Weinheim.

Sherman D. M. (2009) Surface Complexation Modeling: Mineral Fluid Equilbria at the Molecular Scale. *Rev. Mineral. Geochemistry* **70**, 181–205.

Sherman D. M., Peacock C. L. and Hubbard C. G. (2008) Surface complexation of U(VI) on goethite (α-FeOOH). *Geochim. Cosmochim. Acta* **72**, 298–310.

Smith E. J., Rey-Castro C., Longworth H., Lofts S., Lawlor A. J. and Tipping E. (2004) Cation binding by acid-washed peat, interpreted with Humic Ion-Binding Model VI-FD. *Eur. J. Soil Sci.* **55**, 433–447.

Spark K. M., Wells J. D. and Johnson B. B. (1995) Characterizing trace metal adsorption on kaolinite. *Eur. J. Soil Sci.* **46**, 633–640.

Sparks D. L. (1995) *Environmental Soil Chemistry*., Academic Press, London.

Sposito G. (1984) *The Surface Chemistry of Soils*., Oxford University Press, New York.

Swift R. S. (1996) Organic Matter Characterisation. In *Methods of Soil Analysis: Part 3. Chemical Methods* (ed. D. L. Sparks). Soil Science Society of America, Madison, WI.

Tipping E., Griffith J. R. and Hilton J. (1983) The effect of adsorbed humic substances on the uptake of copper(II) by goethite. *Croat. Chem. Acta* **56**.

Tsutsuki K. and Kuwatsuka S. (1978) Chemical studies on soil humic acids. *Soil Sci. Plant Nutr.* **24**, 547–560.

Webb S. M., Tebo B. M. and Bargar J. R. (2005) Structural characterization of biogenic Mn oxides produced in seawater by the marine bacillus sp. strain SG-1. *Am. Mineral.* **90**, 1342–1357.

Xia K., Bleam W. and Helmke P. a. (1997) Studies of the nature of binding sites of first row transition elements bound to aquatic and soil humic substances using X-ray absorption spectroscopy. *Geochim. Cosmochim. Acta* **61**, 2223–2235.

Yonebayashi K. and Hattori T. (1988) Chemical and biological studies on environmental humic acids. *Soil Sci. Plant Nutr.* **34**, 571–584.

Zachara J. M., Resch C. T. and Smith S. C. (1994) Influence of humic substances on Co2+ sorption by a subsurface mineral separate and its mineralogic components. *Geochim. Cosmochim. Acta* **58**, 553–566.

Zhu J., Pigna M., Cozzolino V., Caporale A. G. and Violante A. (2010) Competitive sorption of copper(II), chromium(III) and lead(II) on ferrihydrite and two organomineral complexes. *Geoderma* **159**, 409–416.

Chapter 5: Cobalt sorption to soils with a range of organic matter contents

This second experimental chapter presents results of an investigation into Co sorption onto 3 soils of different origins to determine whether sorption to soils can be modelled using the surface complexation models developed in Chapter 4.

5. 1. Introduction

Cobalt is a transition metal that has a range of industrial uses and its radioactive form (cobalt-60) is a by-product in nuclear reactors. While it is a micronutrient at low concentration levels, in high doses it is toxic to both plants and animals (Aubert and Pinta, 1977; Palit et al., 1994; Tokaz et al., 2013). Therefore it is important to understand how it behaves in typical environmental conditions if it were to be released into the wider environment.

Previous studies have sorbed Co to a range of soils in an attempt to determine how different compositions of the soil affect sorption behaviour, and therefore which is the dominant phase in controlling Co sorption.

The clay content of the soil has been found to largely impact Co sorption, with more Co sorbing to the soils with a higher clay content (Anderson and Christensen, 1988; Rawat et al., 1996). This is due to clay providing high energy binding sites and therefore having a high capacity to bind Co and an increased cation exchange capacity (CEC). Co sorption has been found to have a good correlation with the CEC of agricultural soils (Yasuda et al., 1995).

This high dependence on soil clay content could explain the dependence on ionic strength. As previously studied in Chapter 4, sorption to clay minerals such as kaolinite is dependent on ionic strength. Co sorption to a loamy sand showed dependence on ionic strength that was more prominent at pH values above 5.5 (Barrow and Whelan, 1998)

Soil carbon content was found to have a limited effect on Co sorption (Anderson and Christensen, 1988). In a study between sandy loam and silt clay loam soils, the silt clay loam soil sorbed more Co, despite the sandy loam having a higher carbon content (Barrow and Whelan, 1998).

Despite these studies on Co sorption to a variety of soils, the dominant sorption phase and which characteristics of the soil contribute most to sorption behaviour is still uncertain.

Co sorption to the common soil constituents ferrihydrite, kaolinite, and humic acid and their organo-mineral composites has been previously studied and modelled in Chapter 4. The purpose of this study is to determine how Co sorbs to natural soils with different organic matter contents rather than synthetic organo-mineral composites, and to determine whether this sorption can be modelled as either ferrihydrite, kaolinite, humic acid sorption, or a mixture. This will aid the prediction of the main sorbing phase in each of the soils.

5. 2. Methods

5. 2. 1. Materials

Irish moss peat (Westland Horticulture Ltd. UK) was used in this study. Agricultural soil was collected from Leeds University farm (53°51'48.8"N and 1°20'36.1"W) which is on an Mg limestone catchment. It contains 0.0175% plant available Fe, which was extracted using Mehlich 3. Briefly, this method involves extracting the Fe using a solution of acetic acid, ammonium nitrate, ammonium fluoride, nitric acid, and EDTA. 20 mL of this solution is added to 2 g of powdered soil and then shaken. The soil suspension is filtered and the solution analysed by ICP-OES (Mehlich, 1984). Glacial outwash sediment was acquired from a borehole located on the Sellafield site, West Cumbria, from a radioactively uncontaminated area. Total Fe content was 2%, as determined by X-ray fluorescence (XRF) carried out at the University of Leicester using a PANalytical Axios Advanced XRF spectrometer. Fe analysis was conducted on fused glass beads prepared from igniting 15 g powdered sediment sample. The agricultural soil and sediment were collected and Fe content analysed by Nicholas Humphries and Emma James (both University of Leeds), respectively.

Due to the high pH buffering capacity of the agricultural soil, 35 g was mixed with DIW to make a slurry and a Titrando 907 autotitrator with a 800 Dosino doser and Tiamo v2.5 software was used to lower the pH with the addition of 1 mol L^{-1} HCl at a flow rate of 1.5 mL min^{-1} until the pH remained between 3.5 and 4.0 for 30 minutes. The soil was then dried at 35°C.

Surface area of the soils was measured using the BET method. The analyses were performed in triplicate, yielding average surface area values of 1.51 m^2 g^{-1} for the peat soil, 13.79 m^2 g^{-1} for the agricultural soil, and 11.13 m^2 g^{-1} for the sediment.

Carbon content of the 3 soils was measured in triplicate by combustion using an Elementar vario MICRO cube. The peat soil was found to have an average C content of 49.05%, the agricultural soil was 4.45%, and the sediment was 0.07%.

5. 2. 2. Sorption Experiments

Batch sorption experiments were carried out in triplicate, as described in Chapter 3.1. The pH range for the experiments was 3.5 – 8.4, representative of the natural

range of soil pH. 1 g of soil was mixed with 27 mL of 10^{-1} mol L^{-1} $NaNO_3$ and 3 mL 10^{-2} mol L^{-1} Co stock solution. Samples were adjusted to the desired pH by dropwise addition of dilute NaOH or HNO_3. The pH values were then reset twice a day for 4 days until they remained constant for 16 – 24 hours, after which time the experiments were concluded and the final pH was measured. The samples were then prepared for ICP-AES analysis as reported in Chapter 3.2. The samples were first centrifuged for 15 minutes at 3000 g. For the peat, 5ml of the supernatant was then filtered via 10 kDa centrifuge filters. The sediment and agricultural soils were filtered using 0.22 μm filters. Then, 5ml of the filtered samples was added to 5 mL of 2% HNO_3 to maintain Co in solution. The Co concentration was determined (with an analytical uncertainty of < ±3%) on a Thermo iCAP 7400 radial ion-coupled plasma atomic emission spectrometer (ICP-AES; ThermoFisher Scientific, USA).

5.2.3. XRD analysis

The three soils were crushed using a mortar and pestle and prepared for XRD analysis as described in Chapter 3.3.

5. 2. 4. Surface Complexation Modelling

The sorption behaviour of Co on the three soils was fit to a thermodynamic surface complexation model using the program EQLFOR (Sherman et al., 2008; Sherman, 2009). The models are based on the end-member ferrihydrite, kaolinite, and humic acid models developed in Chapter 4. These were combined using a linear component additivity approach to explore how far sorption to these phases explains sorption to the natural soils. The surface electrostatics in all the models were accounted for by adopting the basic Stern model (BSM). The Davies equation was used for activity corrections to the stability constants for aqueous species.

5. 3. Results

5.3.1 Batch sorption experiments

Results for Co sorbed to the three types of soil are shown in Fig. 5.1.

For the peat soil, high sorption was found across the entire pH range, with a sorption edge between pH 3.5 and 6 where sorption increased from ~60 to 100%.

The sorption edge for the agricultural soil shows low sorption (10 – 20%) between pH 3.5 and 6. Above pH 6, sorption rises to 100% by pH 8.

The sediment had low amounts of sorption (10 – 20%) at pH <6. From pH 6 to 8.4, Co sorption increased from ~20% to 100%.

5.3.2 XRD analysis

The spectra from the XRD analysis of the three soils are shown in Fig. 5.2.

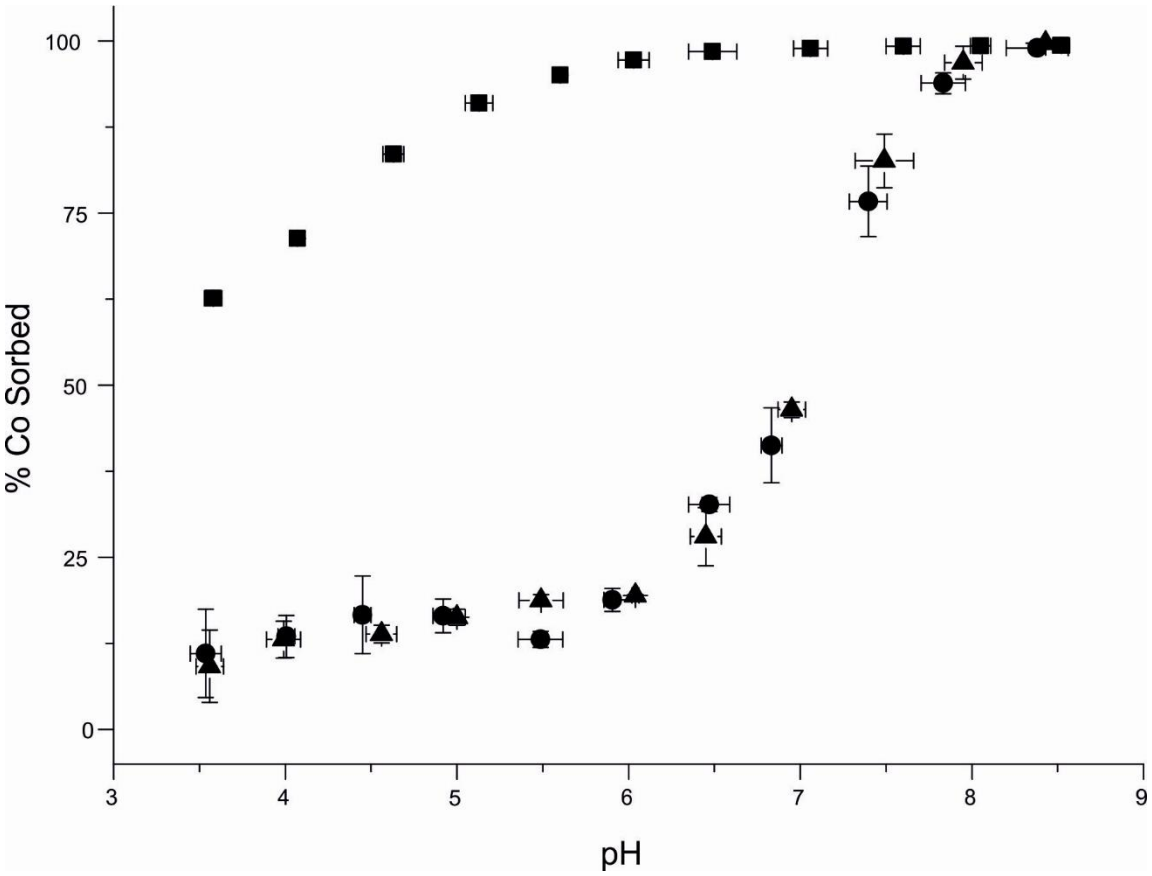

Figure 5.1: Co sorption to 3 soils from different environments: peat (squares), agricultural (circles), and sediment (triangles). Error bars represent the standard deviation of the triplicate sets.

The spectrum for peat shows a large sharp peak at ~26.5° 2θ. This was identified as quartz.

In the spectrum for agricultural soil, two quartz peaks at 21° and 26.5° 2θ were present. The peaks at 31° and 41° 2θ were identified as dolomite. A number of smaller peaks not visible in Fig 5.2 were identified to be albite, microcline, and clays belonging to the mica group.

The sediment XRD spectrum shows two quartz peaks at 21° and 26.5° 2θ (Fig. 5.2). Peaks at 6°, 12°, and 25°were identified at chlorite. The two peaks at 8° and 17° were identified as muscovite.

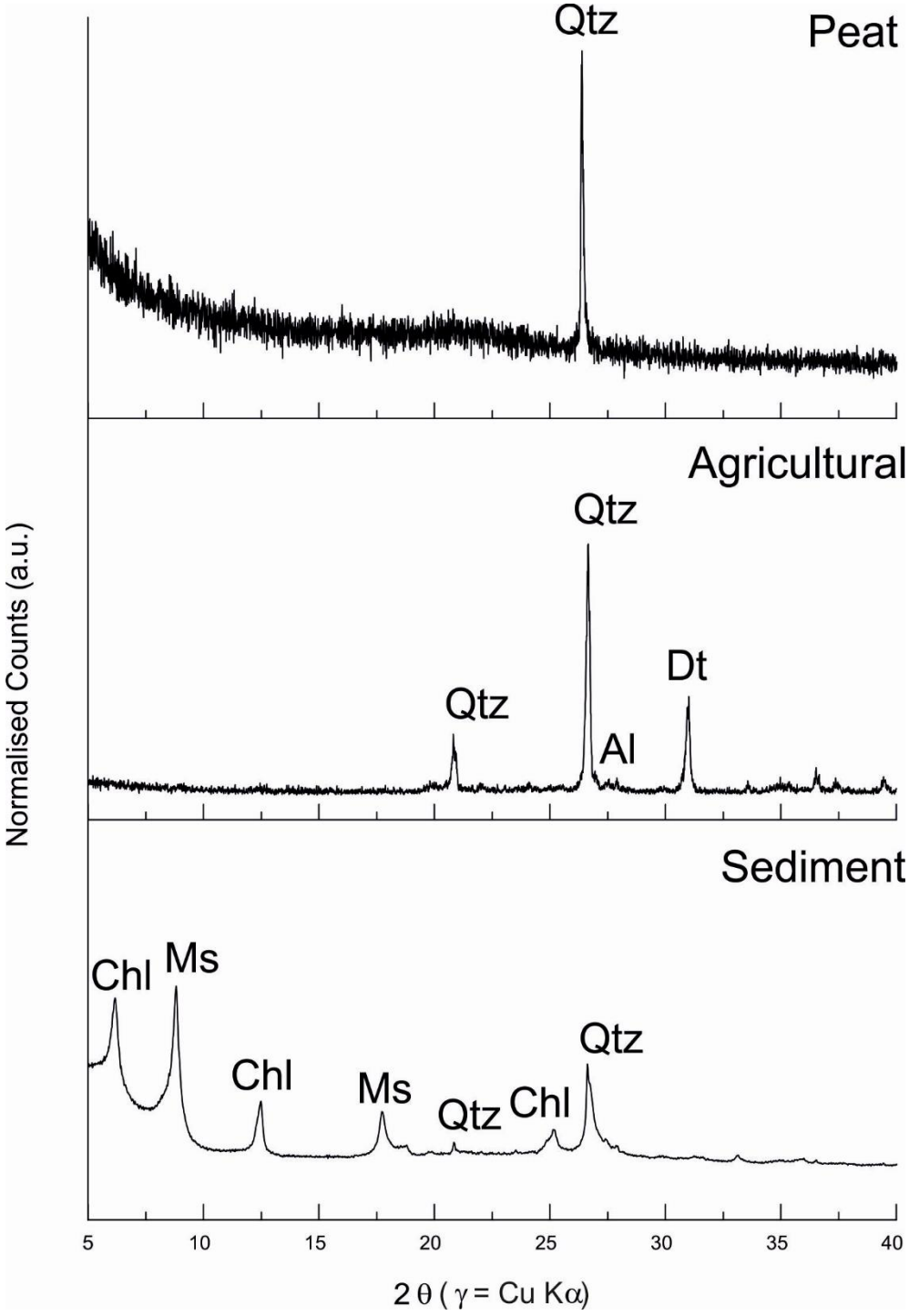

Figure 5.2: XRD spectra of the peat, agricultural soil, and sediment. Dominant mineral phases are identified as: Qtz, quartz; Al, albite; Dt, dolomite; Chl, chlorite; and Ms, muscovite.

5. 4. Discussion

5.4.1 Cobalt sorption to soils

Co sorption to peat soil was higher than sorption to the agricultural and sediment soils across the entire pH range. The peat sorption edge is similar to that of Co sorption to humic acid (Chapter 4), which implies that humic acid is a dominant sorption phase in soils with a high organic matter content.

The sorption edges for agricultural and sediment soil are similar, despite the agricultural soil having 4.45% C and the sediment having 0.07%. It is possible that the high ionic strength of the experiments reduced the effect of sorption to the organic matter in the agricultural soil, as it was found to reduce sorption to pure humic acid (Chapter 4). A system with a lower ionic strength (~10^{-3} mol L^{-1}) could have produced a sorption edge that was more intermediate between the peat and sediment sorption edges. The other phases found in the XRD spectrum of the agricultural soil – dolomite and albite – also show reduced sorption of cations in high ionic strength solutions (Syed Ahmad, 1995; Brady et al., 1999). Despite the Fe content only being 0.0175%, any Fe oxides in the soil would have a great impact on Co sorption as they have high sorption capacity. However, sorption to Fe oxides only increases above pH ~6 and is not affected by high ionic strength, so this would not have affected reduced sorption below pH 6.

XRD spectra for the sediment shows the presence of chlorite, muscovite, and quartz. High ionic strength only reduces the amount of cation sorption to chlorite, while muscovite and quartz are not affected (Chen and Hayes, 1999; Yang et al., 2010; Fuller et al., 2016). This could explain why there is some sorption below pH 6. As the sediment also contains high amounts of Fe (2%), this would account for the steep sorption edge between pH 6.5 and 8.

As the agricultural soil contains a high number of phases that show reduced sorption at high ionic strength, this is likely to be why the Co sorption edge is similar to that of the sediment, rather than being intermediate between the peat and sediment sorption edges.

5.4.2 Surface Complexation Modelling

Surface complexation models were used for the sorption of Co onto the soils that are consistent with the EXAFS data for Co sorption to the main contributing phases in the soil. These end-member models, their input parameters and surface electrostatics, were discussed in Chapter 4.

The sorption data are fit by iterating the log *K* for the surface complexation reaction that represents the formation of the Co-humic acid (for the peat), Co-ferrihydrite and –humic acid (for the agricultural soil), or Co-kaolinite (for the sediment) complexes that were identified by EXAFS analysis.

Carbon content analysis showed that the peat soil contained 49% C, and therefore it was modelled using the humic acid surface complexation model developed in Chapter 4. Model fits are shown in Fig 5.3. Using the humic acid end member log *K* values from Chapter 4, the model underestimated sorption at pH values below 5 (Fig 5.3). When the log *K* value was iterated, the fit improved. However, the iterated log *K* value for the outer-sphere complex (Table 5.1) is outside of the range provided by the sensitivity analysis (Table 5.1). This suggests that humic acid is not the only surface that Co was outer-spherically sorbed to and there must be other phases (such as humin or clays,) present. Previous studies that

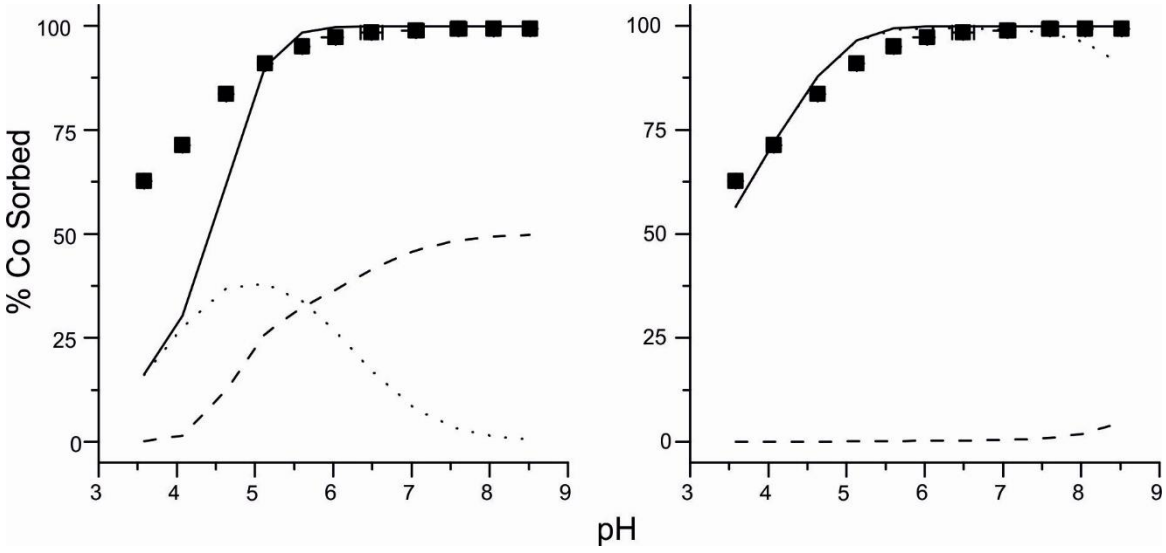

Figure 5.3: Surface complexation model predictions of Co sorption to peat soil. Panel on the left shows predicted sorption using log K values fixed to those from the two end member phases. Panel on the right shows predicted sorption with iterated log K values. Solid lines show total predicted sorption; dashed lines, inner sphere sorption to ≡RCOO$^-$ sites; and dotted lines, outer-sphere sorption to ≡RCOO$^-$ sites.

Table 5.1: The iterated log K values for Co sorption to the peat, agricultural, and sediment soils, as well as the end member log K values and the error from the sensitivity analysis in Chapter 4.

Soil	Complex	Log *K*	End member log *K*
Peat	$(\equiv RCOO)_2Co_2$	-2.17	-0.58±2.25
	$\equiv RCOO^-$ -- Co^{+2}	3.36	0.75±0.94
Agricultural	$(\equiv FeOH^{-0.5})_2Co_2(OH)_6^{-2}$	11.35	13.11±0.58
	$(\equiv RCOO)_2Co_2$	11.75	-0.58±2.25
	$\equiv RCOO^-$ -- Co^{+2}	6.50	0.75±0.94
Sediment	$(\equiv AlOH^{-0.5})_2Co_2(OH)_6^{-2}$	-31.72	-33.86±0.58
	X^- -- Co^{+2}	5.00	3.99±0.49

have characterised peat have found silicates such as quartz, and small amounts of feldspars, and Fe, Al and Mn (López-Buendía et al., 2007; Muller et al., 2008; López et al., 2012). However, Mn and Fe form compounds that are soluble in acidic peat soil and so are not present in large quantities and are unlikely to affect the sorption behaviour of Co (Holynska et al., 1998). XRD analysis shows a large quartz peak, and although quartz has a low surface area (4.5 – 5 $m^2\ g^{-1}$; Fubini et al., 1987) and surface site density, it is possible that some Co was sorbed to quartz, which was not accounted for in the model. The poor fit of the data to the humic acid model could also be caused by the model assuming sorption was only to the carboxyl groups in the humic acid. Humic acid has a range of different surface groups that it is possible for cations to sorb to (e.g. phenolic and quinones). Including these in the model could have improved the fit by making the model similar to natural humic acid, and therefore, natural soil.

The agricultural soil contains organic matter and some clay phases. However, despite the small Fe content (0.02%) it was modelled using the ferrihydrite-humic acid model from Chapter 4. This is because of the high sorption capacity of Fe oxides meaning that small amounts contribute significantly to the sorption of cations. The model was adjusted for the different C content of the agricultural soil. Model fits are shown in Fig 5.4. Sorption was underpredicted at low to mid pH values when the log *K* values were fixed to the ferrihydrite and humic acid end member values, and only show inner-sphere sorption to ferrihydrite starting at pH 6. When the log *K* values were iterated (Table 5.1) the fit improved above pH 5.5 and outer-sphere sorption to the humic acid was present as well as inner-sphere sorption to ferrihydrite. The iterated log *K* values were outside the range provided by the sensitivity analysis by a large amount (Table 5.1). This suggests

that sorption to the agricultural soil cannot be modelled using the ferrihydrite-humic acid model and there are other phases in the soil that need to be taken into account. The phases that need to be considered are possibly other Fe oxides, as unaltered ferrihydrite is rare in soils and Fe oxides are more likely to be present as goethite. The model could also benefit from including clay phases that sorb cations via outer-sphere complexation at low pH (e.g. kaolinite), as this is a pH range where the model underpredicted sorption.

XRD analysis showed that the sediment primarily contained clays with a negligible C content (<0.1%) . Whereas XRF analysis showed a 2% Fe content. As the FeOH sites behave similarly to the AlOH sites in clays, for simplicity the sediment soil was modelled assuming the kaolinite surface complexation model (Chapter 4). Despite kaolinite not being present in the soil, it is assumed that the clays identified have similar sorption sites (i.e. an X^- site that forms outer-sphere bonds and AlOH sites that form inner-sphere bonds). Model fits are presented in fig. 5.5. Sorption was underpredicted across the entire pH range when using the kaolinite end member log *K* values. When the log *K* values were iterated the fit improved, although the iterated log *K* values are outside of the range provided by the sensitivity analysis (Table 5.1). The log *K* for the AlOH complex did not

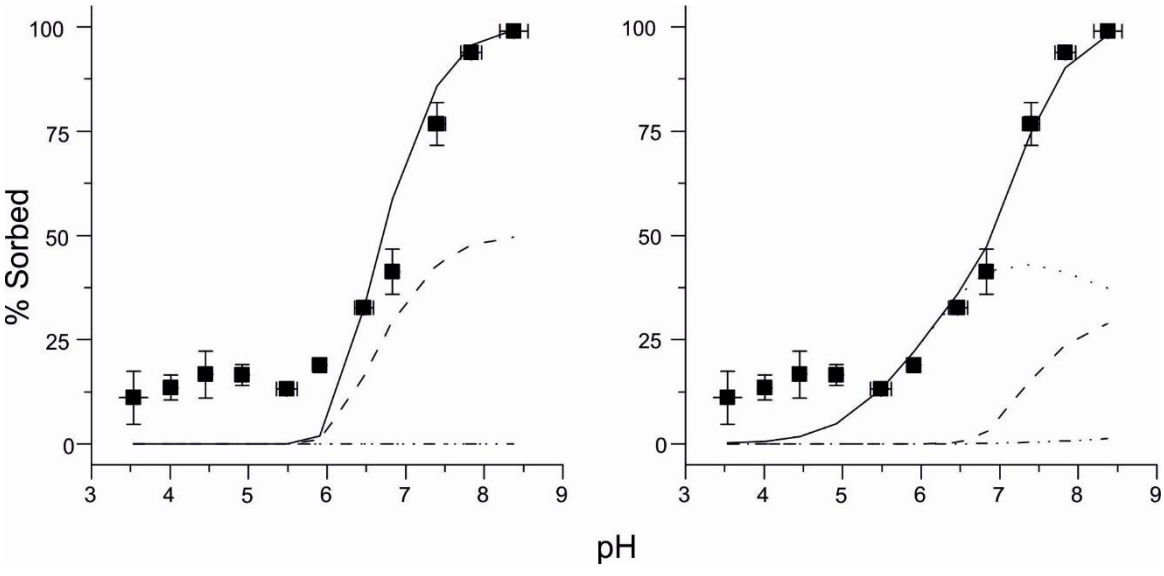

Figure 5.4: Surface complexation model predictions of Co sorption to agricultural soil. Panel on the left shows predicted sorption using log K values fixed to those from the two end member phases. Panel on the right shows predicted sorption with iterated log K values. Solid lines show total predicted sorption; dashed lines inner-sphere sorption to ≡FeOH sites; dotted lines, outer-sphere sorption to $\equiv RCOO^-$ sites; dash-dot-dot, inner-sphere sorption to $\equiv RCOO^-$ sites.

change to be dramatically more intermediate between the AlOH and FeOH end member log *K* values, suggesting that the clays do provide a dominant sorption site. However, the iterated log *K* values being outside the range suggested by the sensitivity analysis implies that kaolinite does not provide a good representation of the clay minerals identified in the sediment soil. This is not surprising, as the Fe content of the sediment would have contributed to the change in log *K* in providing surface sites that could have behaved slightly differently, and because the identified clay minerals do not appear to have inhibited sorption when in a system with high ionic strength, and Co sorption to kaolinite is reduced with high ionic strength (Chapter 4). The clays present in the sediment (muscovite and chlorite) are also chemically different to kaolinite, as kaolinite is a 1:1 dioctahedral clay whereas muscovite and chlorite are 2:1 clays. This extra silica layer would provide extra X^- sites while at the same time reducing cation access to Al^{3+} sites, thus changing the surface site concentrations and Co sorption behaviour. This behaviour is not accounted for in the model and thus is likely to contribute towards the iterated log *K*s not fitting within the sensitivity range.

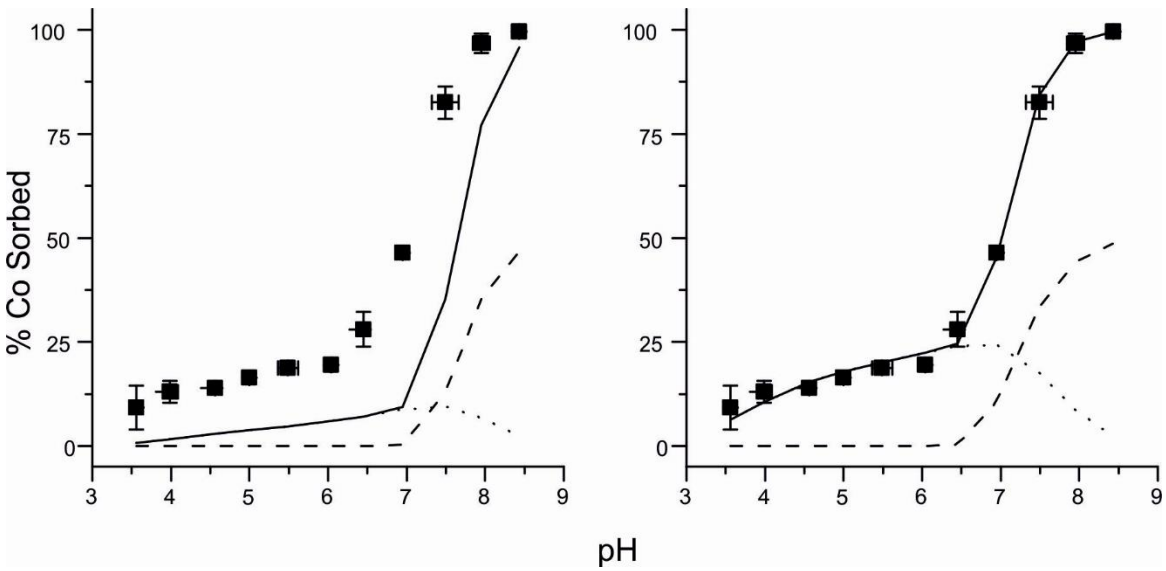

Figure 5.5: Surface complexation model predictions of Co sorption to sediment. Panel on the left shows predicted sorption using log K values fixed to those from the two end member phases. Panel on the right shows predicted sorption with iterated log K values. Solid lines show total predicted sorption; dashed lines inner-sphere sorption to ≡AlOH sites; dotted lines, sorption to $\equiv X^-$ sites.

5. 5. Conclusion

Co sorption to the peat soil was the highest of the three soils across the pH range studied. Sorption to the agricultural and sediment soils were similar, and this is likely to be because sorption to the phases in the agricultural soil were reduced due to high ionic strength. Modelling suggests that while iterating the values of the complexes in each of the systems does provide a reasonable fit, the log *K* values are outside the range of the sensitivity analysis and the complexes used in the models do not necessarily represent the dominant sorption phase.

5.6 References

Anderson P. R. and Christensen T. H. (1988) Distribution coefficients of Cd, Co, Ni, and Zn in soils. *J. Soil Sci.* **39**.

Aubert H. and Pinta M. (1977) *Trace Elements in Soils*., Elsevier Scientific Publishing Company, Oxford.

Barrow N. J. and Whelan B. R. (1998) Comparing the effects of pH on the sorption of metals by soil and by goethite, and on uptake by plants. *Eur. J. Soil Sci.* **49**, 683–692.

Brady P. V, Papenguth H. W., Kelly J. W. and Raiswell P. (1999) Metal sorption to dolomite surfaces. *Appl. Geochemistry1* **14**.

Chen C. C. and Hayes K. F. (1999) X-Ray absorption spectroscopy investigation of aqueous Co(II) and Sr(II) sorption at clay-water interfaces. *Geochim. Cosmochim. Acta* **63**, 3205–3215.

Fubini B., Bolis V. and Giamello E. (1987) The Surface Chemistry of Crushed Quartz Dust in Relation to its Pathogenicity. *Inorganica Chim. Acta* **138**, 193–197.

Fuller A. J., Shaw S., Peacock C. L., Trivedi D. and Burke I. T. (2016) EXAFS Study of Sr sorption to Illite, Goethite, Chlorite, and Mixed Sediment under Hyperalkaline Conditions. *Langmuir* **32**.

Holynska B., Ostachowicz B., Ostachowicz J., Samek L., Wachniew P., Obidowicz A., Wobrauschek P., Streli C. and Halmetschlager G. (1998) Characterisation of 210Pb dated peat core by various X-ray fluorescence techniques. *Sci. Total Environ.* **218**, 239–248.

López-Buendía A. M., Whateley M. K. G., Bastida J. and Urquiola M. M. (2007) Origins of mineral matter in peat marsh and peat bog deposits, Spain. *Int. J. Coal Geol.* **71**, 246–262.

López R., Gondar D., Antelo J., Fiol S. and Arce F. (2012) Study of the acid-base properties of a peat soil and its humin and humic acid fractions. *Eur. J. Soil Sci.* **63**, 487–494.

Mehlich A. (1984) Mehlich 3 soil test extractant: Amodification of Mehlich 2 extractant. *Commun. Soil Sci. Plant Anal.* **15**.

Muller J., Kylander M., Martinez-Cortizas A., Wüst R. A. J., Weiss D., Blake K., Coles B. and Garcia-Sanchez R. (2008) The use of principle component analyses in characterising trace and major elemental distribution in a 55 kyr peat deposit in tropical Australia: Implications to paleoclimate. *Geochim. Cosmochim. Acta* **72**, 449–463.

Palit S., Sharma A. and Talukder G. (1994) Effects of Cobalt on Plants. *Bot. Rev.* **60**.

Rawat J. P., Umar Iraqi S. M. and Singh R. P. (1996) Sorption equilibria of cobalt(n) on two types of Indian soils --the natural ion exchangers. *Physicochem. Eng. Asp.* **117**, 183–188.

Sherman D. M. (2009) Surface Complexation Modeling: Mineral Fluid Equilbria at the Molecular

Scale. *Rev. Mineral. Geochemistry* **70**, 181–205.

Sherman D. M., Peacock C. L. and Hubbard C. G. (2008) Surface complexation of U(VI) on goethite (α-FeOOH). *Geochim. Cosmochim. Acta* **72**, 298–310.

Syed Ahmad S. H. S. (1995) Competitive Adsorption of 9°Sr on Soil Sediments, Pure Clay Phases and Feldspar Minerals. *AppL Radiat. Isot* **46**, 287–292.

Tokaz E. J., Boyd W. A., Freedman J. H. and Waalkers M. P. (2013) Toxic Effects of Metals. In *Casarett & Doull's Toxicology: The Basic Science of Poisons* (ed. C. D. Klaassen). McGraw-Hill, Hightstown, NJ.

Yang J.-S., Lee J. Y., Park Y.-T., Baek K. and Choi J. (2010) Adsorption of As(III), As(V), Cd(II), Cu(II), and Pb(II) from aqueous solutions by natural muscovite. *Sep. Sci. Technol.* **45**.

Yasuda H., Uchida S., Muramatsu Y. and Yoshida S. (1995) SORPTION OF MANGANESE, COBALT, ZINC, STRONTIUM, AND CESIUM ONTO AGRICULTURAL SOILS: STATISTICAL ANALYSIS ON EFFECTS OF SOIL PROPERTIES. *Water. Air. Soil Pollut.* **83**.

Chapter 6: The Effect of Ageing on Desorption of Co from Common Soil Constituents

This chapter presents the work of a series of experiments that aimed to understand the behaviour of Co when in equilibrium with soil constituents for long periods of time, and how this affects the ability to remove Co from the surface of those constituents.

6. 1. Introduction

Cobalt has the potential to be released into the environment in its stable form as waste from industrial processes, or in its radioactive form as ^{60}Co by contamination from nuclear waste waters or from a radiological dispersion device. Once it has been released, it may not initially be known which contaminant has leaked into the environment, therefore first responders need to determine what has been released and the best decontamination method for that particular environment. This means that decontamination may not occur immediately following a contamination event, and aging processes can occur, such as surface precipitation, surface oxidation, and incorporation into crystal lattices (Wendling et al., 2009), which affects the ability of Co to be removed from the soil.

There is limited research on the effect of ageing on Co sorption to common soil components (Ainsworth et al., 1994; McLaren et al., 1998), though what there is suggests no change in the amount of Co sorbed to clays and iron oxides with increases in the equilibration time (for time periods of longer than 1 day).

However, increasing the ageing time does appear to affect desorption. Desorption of Co from kaolinite (Thompson et al., 2000), goethite (Backes et al., 1995), and ferrihydrite (Ainsworth et al., 1994) was found to have decreased when the sorption systems had been aged. The decrease in sorption with ageing time could be caused by the metal ions being incorporated into the oxides during this time, and this limits the metal's ability to desorb (Backes et al., 1995).

Different desorption agents can have an effect on the amount of Co desorbed. Desorption of Co from HA was studied (Rashid, 1974) and it was found that ammonium acetate desorbed 49.1% of Co, but EDTA desorbed 90.8%. This

suggests that different desorption agents use different mechanisms to remove the Co from the sorbent surface. Similarly, ~95% of Co was desorbed from ferrihydrite when HNO_3 was used to reduce the pH of the system (Ainsworth et al., 1994), but only 37% of sorbed Co was removed after peristaltic pumping with $CaCl_2$ (Backes et al., 1995).

Soil washing is a common remediation technique that can be used either *in situ* or in another location that the soil has been moved to (Tadesse et al., 1994). This process involves using a chemical to wash the soil that has been proven to remove the contaminant. Chemicals used include EDTA, NTA, HNO_3, ammonium oxalate, ammonium acetate, and $CaCl_2$, plus many more (Rashid, 1974; McLaren et al., 1986; Elliott and Brown, 1989; Ford et al., 1997; Thompson et al., 2000). These work in a variety of ways:

- Chelating agents such as EDTA and NTA remove contaminants by forming two bonds with a single central atom. These bonds are incredibly strong and create a soluble complex, thereby releasing the contaminant from the mineral surface.
- Ammonium acetate and $CaCl_2$ compete with the contaminants bound to the mineral's surface functional groups. If they have a higher affinity to the mineral, they will replace the contaminant on the surface functional group and the contaminant will be released back into the environment.
- Acids such as HNO_3 work by simply decreasing the pH of the system. Cation sorption increases with pH, so decreasing the pH can trigger the release of cations back into solution.

With a wide variety of potential desorption agents it is important to determine which chemical is most effective at desorbing Co from soil components. There is also a lack of research on the effect of ageing on Co sorption to humic substances and how this affects desorption. This is an important knowledge gap to fill because humic substances can make up to 95% of soil (Jackson, 1969) and understanding factors that can affect sorption to it will help to understand desorption processes.

The objectives of this study were to sorb Co^{2+} to ferrihydrite, kaolinite, and soil derived HA for different periods of time, ranging from 1 day to 12 weeks, in order to determine whether sorption behaviour changed with ageing. Co^{2+} was then

desorbed from the sorbent using one of four desorption agents: deionised water, EDTA - ethylenediamine tetraacetic acid - citric acid, or hydrochloric acid. These were chosen as they are commonly used in the UK nuclear industry and have low intrinsic toxicity (Harvey, 2015). A desorption agent with a competing ion mechanism (e.g. CaCl2) was not used because Co sorbs via inner-sphere complexation at pH 8 and was therefore expected to be ineffective (Backes et al., 1995). These desorption agents were used to determine whether they were viable options for desorbing Co^{2+} from solids, which was the most effective, and finally, whether their effectiveness changed depending on how long Co^{2+} had been aged in contact with specific solids.

6.2. Methods

6.2.1. Materials

Ferrihydrite was synthesised by following the method described in Schwertmann and Cornell (2003). $Fe(NO_3)_3.9H_2O$ was dissolved in deionised (DI) water and NaOH was added to raise the pH to ~7. The ferrihydrite was washed by allowing the precipitate to settle, and then decanting the excess water and replacing it with DI water. This was repeated 3 times a day for 7 days. The pH was then readjusted to ~7, the precipitate was allowed to settle again, and the excess water was decanted before centrifuging the precipitate at 3000 RPM for 15 minutes to produce a homogenous solution.

Humic acid was extracted from Irish moss peat (Westland Horticulture Ltd, UK). The method was taken from Stevenson (1994) and consisted of washing the soil, extracting the HA, and purifying the HA. To wash the soil, it was first air dried before washing it with 0.1 mol L^{-1} HCl and shaking it on a shaker table at 200 RPM for 4 hours. The solution was then centrifuged at 4000 RPM for 30 minutes and the supernatant was discarded.

Extraction was then carried out by shaking the solid in 0.5 mol L^{-1} NaOH for 24 hours and centrifuging the sample at 4000 RPM for 45 minutes. The supernatant was collected and the solid fraction was extracted again through shaking it in 0.5 mol L^{-1} and shaken for 1 hour. It was then centrifuged again and the supernatant added to the previously collection of supernatant. The solid was finally washed with DI water, shaken for another hour, and centrifuged again. The supernatant was added to the collection of supernatant and the solid was discarded. 4 mol L^{-1} HCl was added to the supernatant until the pH was lowered to 2 and was left to stand for an hour, after which it was centrifuged at 4000 RPM for 45 min. The supernatant was discarded and solid collected.

The solid was purified by redissolving it (raising pH to ~12 with NaOH), shaking it for an hour and then centrifuging it at 4000 RPM for 45 minutes. The precipitate was discarded and soluble fraction collected, which was acidified (pH lowered to ~2) and then shaken for an hour before being centrifuged for 45 minutes at 4000 RPM. The liquid was discarded and solid collected. The solid was redissolved (pH raised to ~12), shaken for an hour, and centrifuged. The

supernatant was acidified again, shaken for an hour, centrifuged, and then the solid was collected. This was washed with DI water so the pH was reduced to pH 2. It was shaken for an hour, centrifuged, and the solid was collected. DI water was added to produce a slurry.

Mineralogically pure Ka (KGa-1b) was obtained from the Clay Minerals Society Source Clays Repository.

6.2.2. Aging Sorption Experiments

Batch sorption experiments were carried out in triplicate in 50 mL plastic centrifuge tubes at room temperature and in aerobic conditions. Each experiment was carried out in triplicate. 0.03 g of each soil constituent was mixed with 30 ml solution and the pH was set to ~8.5 by the dropwise addition of NaOH. The samples were shaken continuously while the pH was monitored and set back to the desired pH. This occurred until the pH remained constant for 16 – 24 hours, after which time the samples were aged for a set period of time (1 day, 7 days, 28 days, or 84 days). During this time the pH was allowed to drift.

After the ferrihydrite and kaolinite samples had been aged for the desired period of time, they were centrifuged at 3000 RPM for 10 minutes and the supernatant filtered using 0.2 μm syringe filters and 5 ml of supernatant was added to 5 ml of 2% HNO3. The rest of the supernatant was decanted, leaving the solid sample in the centrifuge tube.

The HA samples were filtered through 10 kDA centrifuge filters for 20 min at 4000 RPM and then 5 ml was added to 5 ml of 2% HNO3. The rest of the supernatant was discarded and the filtered solid was removed from the filter with a glass pipette and returned to the original centrifuge tube.

The Co concentration was determined (with an analytical uncertainty of < ±3%) on a Thermo iCAP 7400 radial ion-coupled plasma optical emission spectrometer (ICP-OES; ThermoFisher Scientific, USA,).

6.2.3. Desorption

Four desorption agents were used to test their effectiveness: DI water, 0.01 mol L^{-1} EDTA, 0.01 mol L^{-1} citric acid, and 0.01 mol L^{-1} HCl. 30 ml of these were added to the solid sorption sample leftover from the aging experiments, therefore these

experiments were also carried out in triplicate. The samples were then shaken for 24 hours, after which the pH was measured and the samples were centrifuged at 4000 RPM for 10 minutes. 5 mL of supernatant was then filtered through a 0.22 μm syringe filter and added to 5 ml HNO_3. As with the sorption experiments, the HA samples were centrifuged in 10 kDa centrifuge filters at 4000 RPM for 20 minutes and then 5 mL of supernatant was added to 5 mL HNO_3.

6.2.4 Ferrihydrite dissolution

In order to determine the effect of the desorption agents on ferrihydrite the ferrihydrite was aged for 1, 7, 28, and 84 days at room temperature. After each ageing period, 0.03 g of ferrihydrite was removed and mixed in a 50 mL centrifuge tube with 30 mL of either DIW, EDTA, citric acid, or HCl. These experiments were performed in triplicate for each desorption agent. The samples were then shaken for 16-24 hours, after which they were centrifuged at 3000 RPM for 10 minutes and the supernatant filtered using 0.2 μm syringe filters. 5 ml of supernatant was added to 5 ml of 2% HNO3 in preparation for ICP-OES analysis.

6.2.5 Ferrihydrite XRD analysis

After each ageing period a sub sample of room temperature aged ferrihydrite was dried at 40°C. They were then ground into a powder and prepared for XRD analysis as described in Chapter 3.3.

6.3. Results

6.3.1. Sorption and desorption experiments

Co sorption to ferrihydrite, kaolinite and HA after 1, 7, 12, and 84 days of sorption is shown in Fig. 6.1. Sorption to ferrihydrite and HA was 100% after 1 day and remained at this level at 84 days. Co sorption to kaolinite increased from ~65% sorption after 1 day to ~80% after 28 days where it remained for the 84 day equilibration period.

When DIW was used to desorb the Co from ferrihydrite, only 5-10% Co was desorbed from the mineral regardless of the aging period of the system (Fig 6.2). For EDTA,

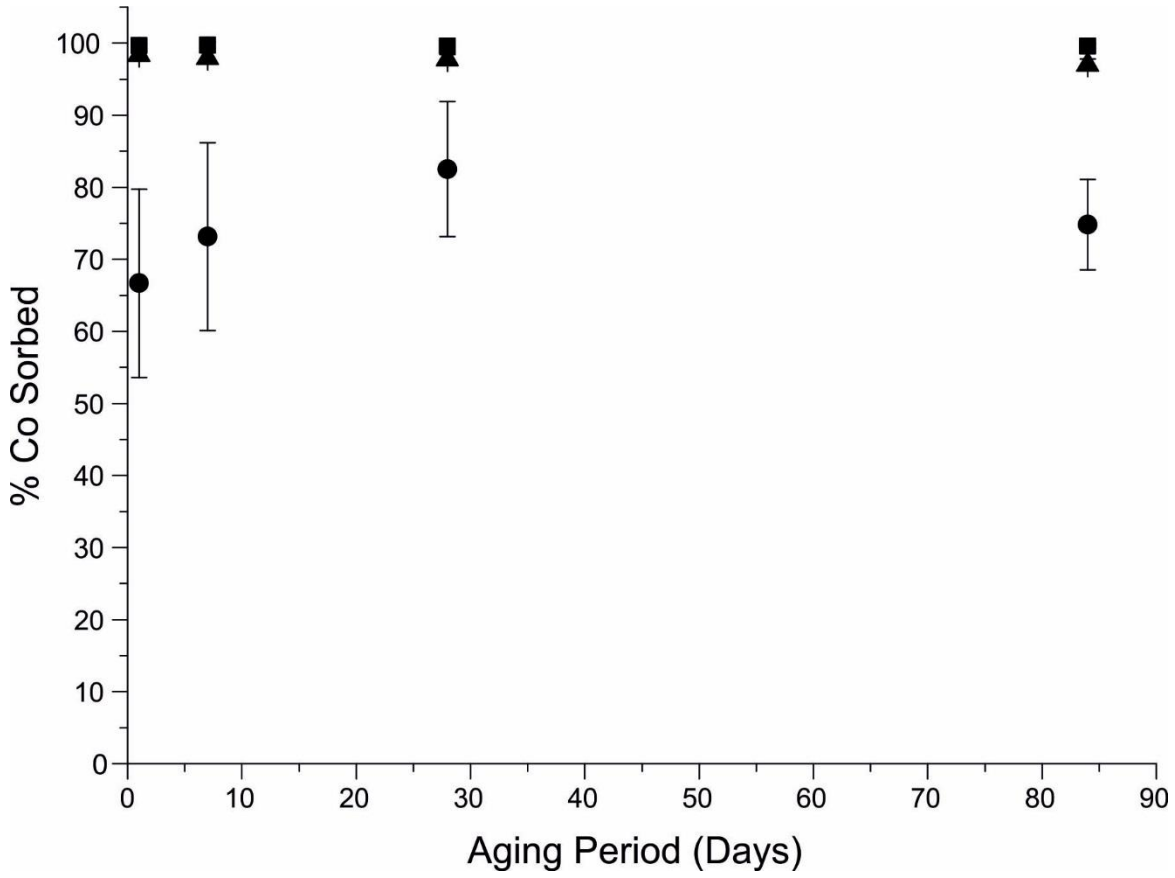

Figure 6.1: Co sorption (at 10^{-3} mol L^{-1}Co total concentration, equating to 5.893 wt% Co sorbed at 100% sorption) to ferrihydrite (squares), kaolinite (circles), and humic acid (triangles); conducted at room temperature and ionic strength of 10^{-3} mol L^{-1} $NaNO_3$. Error bars represent one standard deviation in the amount of Co sorbed and are not visible for the ferrihydrite and humic acid systems.

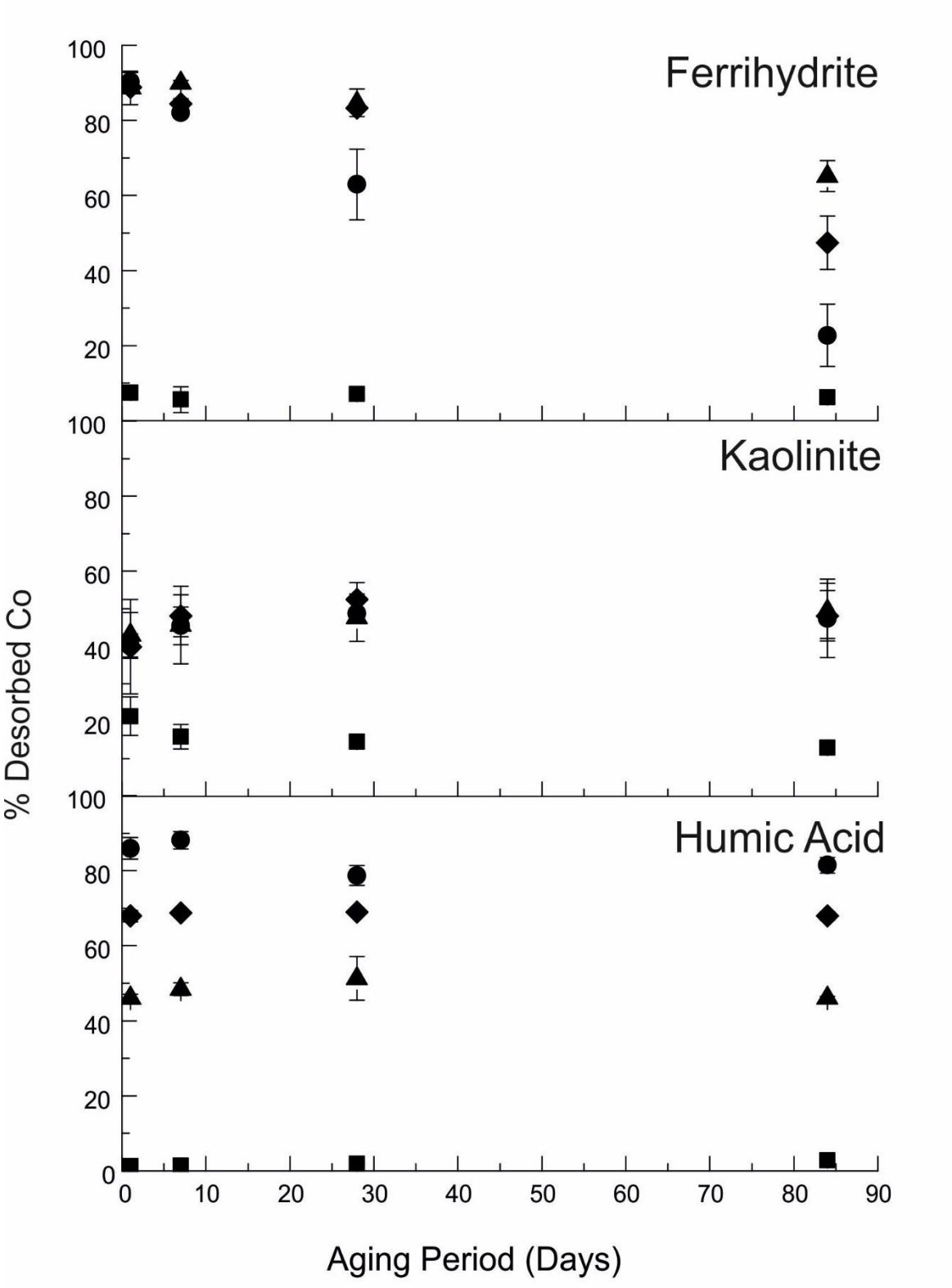

Figure 6.2: Co desorption from ferrihydrite, kaolinite, and humic acid as a function of a variety of desorption agents: DIW (squares), EDTA (circles), citric acid (triangles), and HCl (diamonds). Error bars represent the standard deviation in Co desorbed. Where they are not present indicates data ranges where the standard deviation is too small to be visible.

almost all (>95%) the Co was removed from the mineral after one day of aging. This decreased to ~90% Co desorbed on the sample aged in contact with Co^{2+} for 7 days, and the sample aged for 28 days had ~70% Co desorbed. After a sorption aging period of 84 days, ~25% Co was desorbed. After 1 and 7 days of aging, citric acid was able to remove almost all of the Co sorbed to ferrihydrite. After 28 days of aging, less than 10% sorbed Co was still sorbed to the mineral after citric acid was added to the system. Citric acid was able to remove >70% of sorbed Co after an 84 day aging period. As with EDTA and citric acid, HCl removed almost all of the sorbed Co after a one day aging period. After 7 and 28 days, less than 10% sorbed Co remained on the ferrihydrite, however, after 84 days only 50% Co had been removed.

DIW removed the least Co from kaolinite over the full 84 day period (Fig. 6.2). After 1 day, ~20% sorbed Co was removed which decreased to ~15% after 7 days and remained at this level after 28 and 84 days. EDTA, citric acid, and HCl all released the same amount of Co back into solution. After 1 day 40-45% of sorbed Co was released back into solution. This increased slightly to 45-50% desorption after 7 days and remained at this after 28 and 84 days.

Using DIW to desorb Co from HA resulted in none being removed after all aging periods (Fig 6.2). After aging for 1 and 7 days, ~5% sorbed Co was left on the HA after desorption with EDTA, after 28 days ~15% was left, and after 84 days ~10% still remained on the HA. When citric acid was used to desorb Co from HA, between 45-50% remained sorbed to HA for all aging periods. HCl removed ~75% sorbed Co after all aging periods.

6.3.2. Ferrihydrite dissolution

The ability of each desorption agent to dissolve ferrihydrite is presented in Fig. 6.3. DIW did not release Fe into solution with the aqueous Fe concentration remaining at 0 ppm for all samples regardless of the length of ageing. EDTA partially dissolved ferrihydrite, with ~100 ppm Fe being in solution after being added to ferrihydrite that had been aged for up to 84 days. Citric acid dissolved the most ferrihydrite with the most aqueous Fe being in solution after being added to all aged ferrihydrite samples. When the ferrihydrite had been aged for 1 day, citric acid released ~600 ppm Fe(aq) into solution. However, when added to 7 day old ferrihydrite, less was dissolved, with only ~350 ppm being present in solution. When added to 28 and 84 day old ferrihydrite, citric acid again released ~600 ppm of Fe(aq) into solution. HCl showed a similar trend to citric acid, but dissolved less ferrihydrite. When added to ferrihydrite that had been aged for 1 day, ~450 ppm Fe(aq) was released into solution, and when added to 7 day old

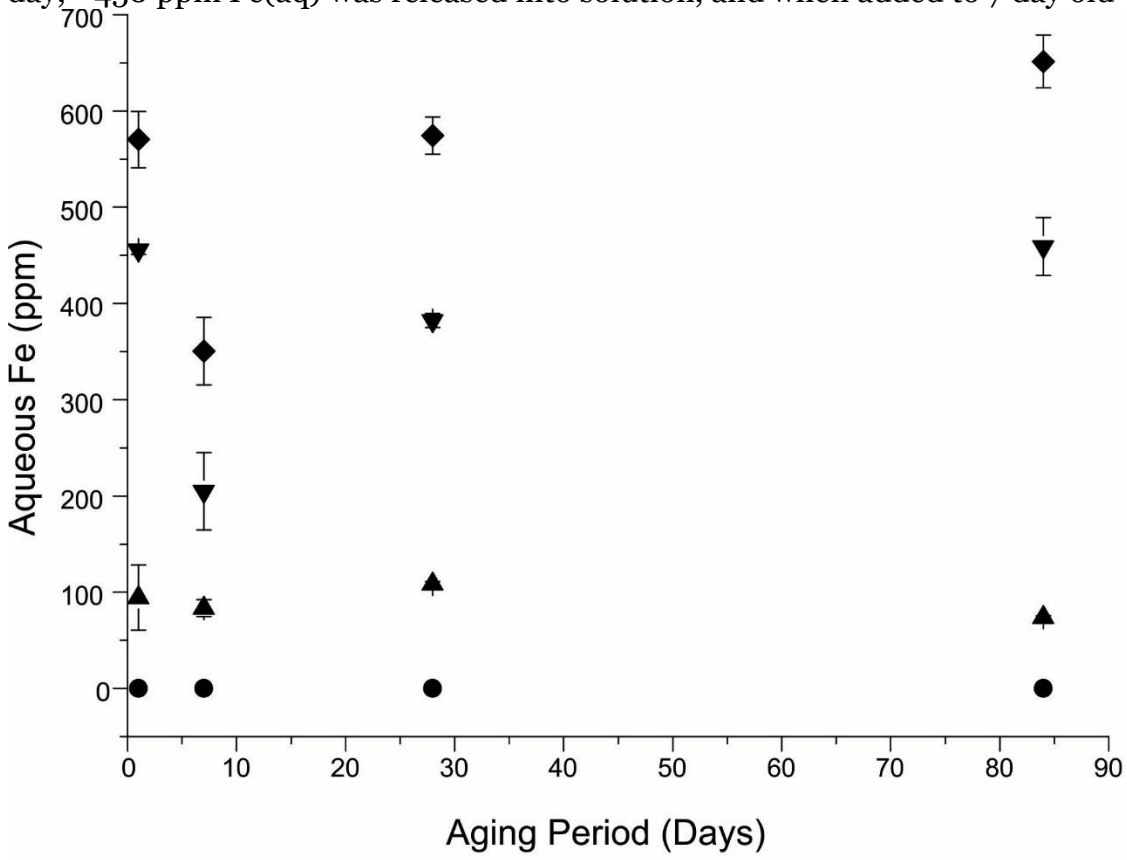

Figure 6.3: Cobalt release from ferrihydrite as a function of the ferrihydrite age and of desorption agents: DIW (circles), EDTA (upwards triangle), citric acid (diamonds) and HCl (downwards triangles).

ferrihydrite only ~200 ppm was released. HCl added to 28 and 84 day old ferrihydrite released ~400 ppm Fe(aq) into solution.

6.3.3. Ferrihydrite XRD analysis

The XRD peaks for ferrihydrite at 1, 7, 28, and 84 days old are shown in Fig 6.4. Scans after 1, 7, and 28 days all showed the characteristic 2 broad peaks at ~35° and ~62° 2θ of 2-line ferrihydrite. The scan of 84 day old ferrihydrite shows narrower peaks on top of the broad ferrihydrite peaks at 21°, 33°, 36°, and 37° 2θ. These are characteristic of goethite.

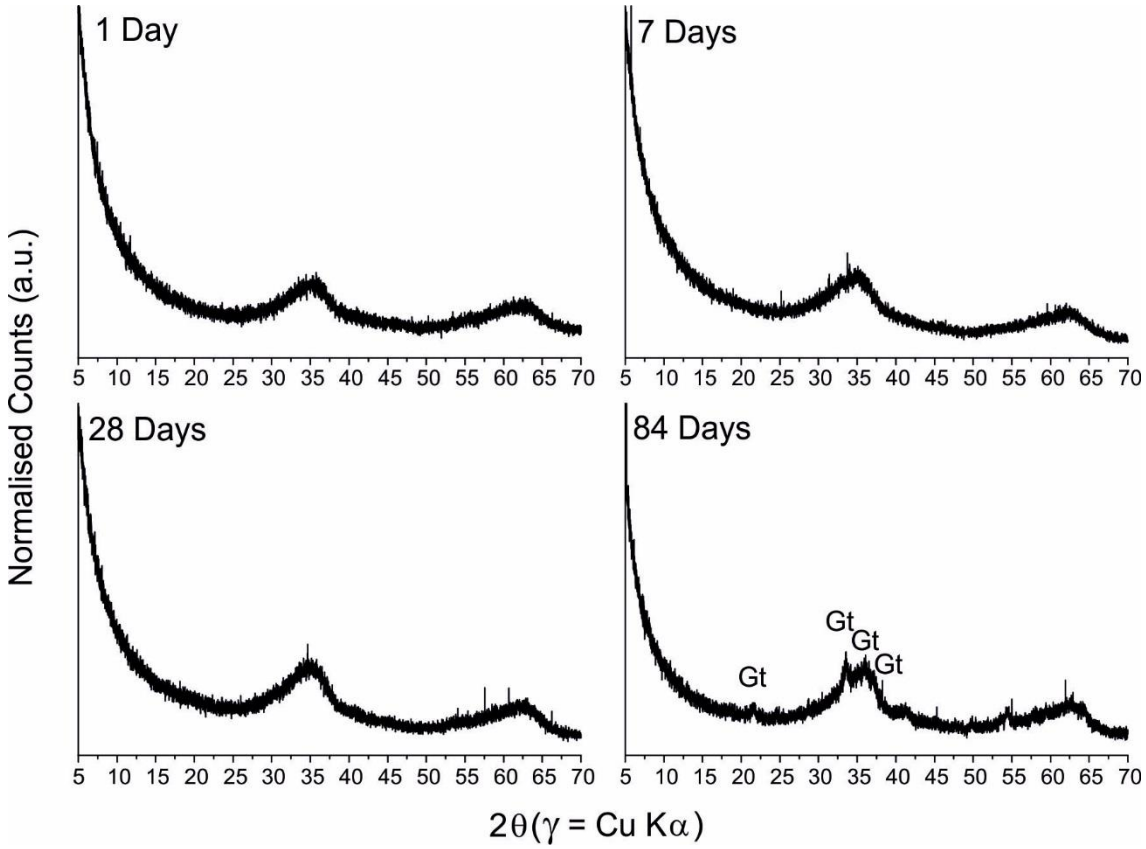

Figure 6.4: XRD spectra of ferrihydrite after being aged for 1, 7, 28, and 84 days. Spectra for 1, 7, and 28 days show the characteristic 2 broad peaks at ~35° and ~62° 2θ for 2-line ferrihydrite, whereas the 84 day aged spectra shows goethite peaks.

6.4. Discussion

6.4.1. Effect of ageing on sorption

Cobalt sorption to ferrihydrite and humic acid remained constant at ~100% for all of the ageing periods up to 84 days (Fig. 6.1.). This suggests that the sorption reactions reach equilibrium in 24 hours or less and do not change over a 84 day period.

Sorption to kaolinite was affected by the length of the ageing period. After 1 day, sorption was at ~65% which increased to ~75% after 7 days and then ~80% at 28 days where it remained stable until 84 days. This could be caused by the sorption reactions being slower when Co sorbs to kaolinite. However, the error bars for the 4 data points do overlap and so it is possible that Co sorption remains stable for 84 days, with some error caused by slight differences in the pH in the repeat experiments done in this study (Table 6.1). This is because near to the main sorption edge small changes in pH can result in significant changes in the percentage sorption observed. This is due to the sorption edge occurring over an extremely narrow pH range.

Previous studies of Co sorption to kaolinite have found that there are two uptake stages: the first of which occurs over a matter of minutes, and the second that takes place over several hundred to thousands of hours (Thompson et al., 2000; Bhattacharyya and Sen Gupta, 2007). This has been explained simply as being because initially cations are sorbing to an empty surface and the rate of adsorption is high. But as more cations form complexes with the surface they have to compete with each other for surface sites, decreasing the rate at which they can be taken up by the mineral surface (Bhattacharyya and Sen Gupta, 2007). Between 1 and 100 hours (~4 days), Co sorption to kaolinite increased regardless of the initial Co concentration.

Table 6.1: The average pH values for each sorbent phase after the sorption ageing period and after Co had been desorbed for 24 hours. The ± symbol provides the standard deviation of the dataset for each value.

Sorbent	Sorption ageing period (days)	Desorption Agent	pH after ageing	pH after desorption
Ferrihydrite	1	DIW	8.41 ± 0.11	7.39 ± 0.02
		EDTA	8.51 ± 0.14	10.20 ± 0.22
		Citric Acid	8.48 ± 0.09	2.56 ± 0.19
		HCl	8.47 ± 0.14	2.33 ± 0.09
	7	DIW	8.44 ± 0.25	7.25 ± 0.19
		EDTA	8.37 ± 0.14	10.03 ± 0.24
		Citric Acid	8.52 ± 0.07	2.54 ± 0.07
		HCl	8.51 ± 0.13	2.3 ± 0.05
	28	DIW	8.2 ± 0.07	7.09 ± 0.21
		EDTA	8.12 ± 0.10	9.64 ± 0.62
		Citric Acid	8.15 ± 0.09	2.78 ± 0.57
		HCl	8.20 ± 0.21	2.56 ±0.62
	84	DIW	7.58 ± 0.06	6.60 ± 0.18
		EDTA	7.63 ± 0.07	10.01 ± 0.16
		Citric Acid	7.63 ± 0.06	2.53 ± 0.17
		HCl	7.62 ± 0.01	2.28 ± 0.17
Kaolinite	1	DIW	8.13 ± 0.33	7.41 ± 0.18
		EDTA	8.15 ± 0.34	9.12 ± 0.13
		Citric Acid	8.13 ± 0.19	2.63 ± 0.03
		HCl	8.13 ± 0.27	2.24 ± 0.48
	7	DIW	7.93 ± 0.03	7.28 ± 0.30
		EDTA	7.94 ± 0.08	9.34 ± 0.16
		Citric Acid	7.93 ± 0.11	2.65 ± 0.02
		HCl	7.88 ± 0.12	2.14 ± 0.16
	28	DIW	7.73 ± 0.16	7.48 ± 0.21
		EDTA	7.67 ± 0.17	8.77 ± 0.31
		Citric Acid	7.71 ± 0.14	2.58 ± 0.01
		HCl	7.70 ± 0.09	2.01 ± 0.03
	84	DIW	7.71 ± 0.10	6.90 ± 0.34
		EDTA	7.74 ± 0.09	8.44 ± 0.09
		Citric Acid	7.69 ± 0.07	2.66 ± 0.07
		HCl	7.69 ± 0.07	2.05 ± 0.05
Humic Acid	1	DIW	8.51 ± 0.03	8.50 ± 0.02
		EDTA	8.64 ± 0.04	8.13 ± 0.02
		Citric Acid	8.54 ± 0.04	2.88 ± 0.03
		HCl	8.57 ± 0.02	2.16 ± 0.10
	7	DIW	8.14 ± 0.03	8.18 ± 0.04
		EDTA	8.12 ± 0.04	9.03 ± 0.12
		Citric Acid	8.08 ± 0.02	2.94 ± 0.13
		HCl	8.08 ± 0.02	2.16 ± 0.10
	28	DIW	7.49 ± 0.02	7.78 ± 0.07
		EDTA	7.51 ± 0.05	7.98 ± 0.04
		Citric Acid	7.53 ± 0.04	2.88 ± 0.13
		HCl	7.50 ± 0.10	2.19 ± 0.13
	84	DIW	7.37 ± 0.01	7.56 ± 0.07
		EDTA	7.39 ± 0.08	9.00 ± 0.05
		Citric Acid	7.33 ± 0.03	2.91 ± 0.11
		HCl	7.31 ± 0.07	2.22 ± 0.17

After 100 hours, Co sorption remained stable. (Thompson et al., 1999; 2000). Therefore it is probable that the initial increase in Co sorption in this study between 1 and 28 days is due to a similar slow uptake mechanism occurring in these experiments, and after this sorption remains stable.

6.4.2 Desorption of cobalt from soil constituents

6.4.2.1 Ferrihydrite

All desorption agents (apart from DIW) showed a decrease in desorption effectiveness with a longer sorption equilibration time. EDTA showed the biggest decrease in effectiveness, dropping from 90% removal after 1 day of sorption, to 20% removal after an 84 day sorption equilibration period. Citric acid showed the highest removal of Co from the ferrihydrite surface after all sorption equilibrium periods, apart from after 1 day sorption ageing period where EDTA, citric acid, and HCl all removed ~90% Co. It has been shown previously that increasing the sorption equilibration time decreases the amount of sorbed cations that can be released for iron oxy(hydr)oxides due to incorporation into a slowly restructuring iron oxide (Ainsworth et al., 1994; Ford et al., 1997). Therefore my results further confirm those found in the literature.

XRD analysis of ferrihydrite after 1, 7, 28, and 84 days sorption is shown in Fig. 6.3. This shows that ferrihydrite remained as ferrihydrite for up to 28 days. Between 28 and 84 days, the ferrihydrite began to transform into goethite, evidenced by the goethite peaks present in the spectrum. During the transformation of ferrihydrite to goethite adsorbed Co was likely to have become incorporated into the mineral, explaining why the desorption agents removed less surface Co after 84 days.

This process has been studied with other transition metals (e.g. Cd, Pb,) and it has been shown that ferrihydrite undergoes structural reordering that can result in sorbed metals becoming incorporated into crystalline structural sites (Spadini et al., 1994; Ford et al., 1997). This results in desorption agents not able to remove metals incorporated into the solid and so results in less metal released back into solution. Therefore, I propose that sorbed Co becomes structurally incorporated into the ferrihydrite structure as it ages therefore making it difficult for the desorption agents to release it.

This hypothesis works in the case of EDTA, as Fig 6.2 shows that desorption decreases as the ferrihydrite is aged for longer, and Fig. 6.4 shows that EDTA dissolves minimal amounts of ferrihydrite (~100 ppm Fe(aq) was present in solution after addition of EDTA) and therefore cannot bind to the Co incorporated into the ferrihydrite structure. EDTA is able to remove Co from the ferrihydrite surface by binding to the Co in the reaction:

$$S\text{-}Co + EDTA \rightleftharpoons S + Co\text{-}EDTA \quad (6.1)$$

where S represents the surface functional group (Bermond and Ghestem, 2001). EDTA has a chelating effect on cations bound to mineral surfaces and thus Co preferentially binds to the EDTA. This creates strong soluble metal-ligand complexations that increase the mobility of cations in soils, leading to the ability to remove metals from the soil completely (Kim et al., 2003). This is likely to account for the high desorption of Co after 1 and 7 days of sorption, but after this time Co becomes incorporated into the mineral and EDTA is not able access Co^{2+} incorporated into the ferrihydrite (and goethite) structure to remove the incorporated Co.

Citric acid and HCl were used as desorption agents to lower the pH, as that has been shown to trigger desorption (Ainsworth et al., 1994). They reduced the pH to ~2.75 and ~2.25, respectively. Despite HCl creating a system with a lower pH, when the 2 desorption agents no longer desorb equal amounts of Co after an 84 day sorption period, citric acid desorbs the most Co. This suggests that another mechanism is taking place other than simply reducing the pH thereby causing the variable charge sites to turn positively charged.

Both citric acid and HCl dissolve large amounts of ferrihydrite (~600 ppm and ~400 ppm, respectively) and this would cause more of the structurally incorporated Co to be released. This is shown in Fig. 6.2, as citric acid releases more Co back into solution than HCl over all sorption equilibrium periods. This implies that the main mechanism resulting in citric acid and HCl releasing Co into solution is the dissolution of the ferrihydrite mineral.

6.4.2.2 Kaolinite

Unlike ferrihydrite, there was no decrease in desorption with longer sorption equilibrium periods for all desorption agents. DIW released ~15% sorbed Co,

which was most likely outer-spherically bound to the permanent charge sites on the Si face (Chapter 4). Outer-sphere bonds are much weaker than inner-sphere bonds and so it is possible that a simple diffusion effect resulted in the outer-spherically bound Co being released from the kaolinite surface. A desorption agent that makes use of the competitive effect to remove ions from the mineral surface (e.g. $CaCl_2$) would likely have been more effective at removing the outer-spherically bound Co.

As with ferrihydrite, EDTA chelates cations that are sorbed to the mineral surface. This creates soluble metal-ligand complexes that are released into solution. However, only ~50% of Co sorbed to kaolinite was desorbed (Fig. 6.2). This contrasts the ability of EDTA to desorb 100% of Cd associated with kaolinite surfaces (Hong and Pintauro, 1996). However it is possible that Co has a higher affinity to kaolinite than Cd, which is implied by Co starting to sorb to kaolinite at pH 7, while Cd starts at pH 8 (Spark et al., 1995). It is also possible that Co multinuclear complexes that form on the kaolinite surface (Chapter 4) help to stabilise Co on the surface, forming stronger bonds than would be created by an EDTA-Co complex. These strong bonds and a high affinity for kaolinite would result in less binding to EDTA and so less Co is released back into solution.

Desorption of Co from kaolinite has been studied by lowering the pH of the solution using HNO_3 and the amount desorbed was found to decrease with increasing sorption periods (Thompson et al., 2000). The only time periods where there was minimal change in desorption were 103 (4 days) and 2664 hours (111 days). For shorter (between 2 and 121 hours) and longer (426 and 6778 hours) periods of time there were large decreases in the amounts of desorption. This contrasts with the results in Fig 6.2, where there was little change in the amount of Co desorbed by either citric acid or HCl after they were used to decrease solution pH. This difference could be due to the NO_3^- anion forming strong bonds with the sorbed Co and releasing it back into solution (Thompson et al., 2000).

6.4.2.3 Humic acid

As with kaolinite, there was limited effect of the length of the sorption equilibration period on the desorption of Co from humic acid. DIW released negligible amounts of Co back into solution, suggesting that Co binds to humic

acid via strong bonds. At high pH (~7 - 8, at which desorption using DIW water took place) Co is bound to humic acid via multinuclear bidentate inner-sphere complexes (Chapter 4). These bonds are therefore too strong for Co to be released back into solution by a dilution effect.

EDTA desorbed ~80% of Co for all sorption equilibration periods and was the most effective at releasing Co from the humic acid out of the 4 desorption agents that were studied. EDTA has previously been found to be effective at desorbing cations from humic acids, as it has desorbed 91% of sorbed Co, 98% Zn, and 88% Mn (Rashid, 1974). This was explained as being caused by weak bonds between these metals and the humic acid. However, Co sorbs to humic acid via strong inner-sphere complexes (Chapter 4) which suggests that Co-EDTA bonds are stronger than Co-HA. As EDTA induced desorption does not decrease with increased sorption time (Fig. 6.2), this implies that Co^{2+} remains on the surface and there are no reactions involving humic acid over 84 days that results in Co becoming inaccessible to desorption by EDTA

Both citric acid and HCl are likely to have desorbed Co simply by lowering the pH of the system. As HCl decreased the pH more than citric acid (to pH values ~2.25 and ~2.9, respectively) it is likely that this caused more Co to be desorbed by HCl. It is possible that repeated washing with either citric acid or HCl could progressively remove more Co from the humic acid as a new equilibrium would form between Co sorbed to the humic acid and the fresh acid solution, potentially desorbing more Co.

6.4.3 Implications for remediation

The length of sorption equilibration time had no effect on the amount of Co desorbed from kaolinite and humic. However, it did have an impact on Co release from ferrihydrite, with the most Co being desorbed after 1, 7, and 28 days sorption. After 28 days sorption, citric acid and HCl were most effective in removing Co from ferrihydrite. Therefore, I recommend decontamination to be carried out within 28 days of a contamination event where the soil contains high amounts of iron oxides. Although, the experiments carried out are not truly representative of a natural soil, making this a conservative recommendation. Natural ferrihydrite in soils will have already aged *in situ* and transformation can be slower due to the presence of other sorbed cations (Jambor and Dutrizac, 1998). Therefore it is possible that experiments using natural Fe-rich soils may exhibit slower incorporation than observed in these experiments. In soils that are high in kaolinite/ clay and/ or humic substances decontamination can be carried out at any time up to 84 days (3 months).

There are drawbacks to using citric acid and HCl in soil washing approaches. The use of these will produce an acidic solution with high Fe(aq) and Co^{2+} concentrations that will need to be treated prior to discharge, increasing the cost of this decontamination technique. However, neutralisation of this solution would result in the precipitation of a Fe-oxy(hydr)oxide, which provides surface sites for the sorption of Co at pH levels above 7. This would make it possible to recover the desorbed Co for safe disposal, and after separation of the solids this would leave a Co free, neutral pH aqueous phase suitable for discharge into the sewer system.

It is possible that repeated washing with EDTA, citric acid, or HCl could desorb more Co from the sorbent phase. If this were to occur even after long sorption equilibration periods then it could result in decontamination that is just as effective as immediate decontamination. This would remove the necessity of immediate decontamination, despite using more resources and increasing the cost.

6.5. Conclusion

There was no decrease in sorption when Co was left in equilibrium with the sorption phase for 84 days, with ferrihydrite and humic acid showing no change in that period. Kaolinite showed a slight increase in Co sorbed between 1 and 28 days. Less Co was desorbed from ferrihydrite with increases in the sorption equilibrium period, implying that it was incorporated into the mineral structure as the ferrihydrite transformed into goethite. EDTA was the most effective in removing Co from humic acid, was equally good as citric acid and HCl in desorbing Co from kaolinite, and released the same amount of Co from ferrihydrite as citric acid and HCl up to 7 day sorption equilibration period. Therefore to avoid mixing desorption agents in the soil, it is recommend to use EDTA to decontaminate soils that contain a mixture of the 3 phases within 7 days of the decontamination event.

6.6 References

Ainsworth C. C., Pilon J. L., Gassman P. L., Van W. G. and Sluys D. (1994) Cobalt, Cadmium, and Lead Sorption to Hydrous Iron Oxide: Residence Time Effect. *Soil Sci. Soc. Am. J.* **58**, 1615–1623.

Backes C. A., McLaren R. G., Rate A. W. and Swift R. S. (1995) Kinetics of cadmium and cobalt desorption from iron and manganese oxides. *Soil Sci. Soc. Am. J.* **59**, 778–785.

Bermond A. and Ghestem J. P. (2001) Kinetic Study of Trace Metal EDTA-Desorption from Contaminated Soils. In *Heavy Metals Release in Soils* (eds. H. Magdi Selim and D. L. Sparks). CRC Press, London.

Bhattacharyya K. G. and Sen Gupta S. (2007) Adsorption of Co(II) from Aqueous Medium on Natural and Acid Activated Kaolinite and Montmorillonite. *Sep. Sci. Technol.* **4215**, 3391–3418.

Elliott H. A. and Brown G. A. (1989) COMPARATIVE EVALUATION OF NTA AND EDTA FOR EXTRACTIVE DECONTAMINATION OF P b -P O L L U T E D SOILS*. *Water, Air Soil Pollut.* **45**.

Ford R. G., Bertsch P. M. and Farley K. J. (1997) Changes in transition and heavy metal partitioning during hydrous iron oxide aging. *Environ. Sci. Technol.*

Harvey E. J. (2015) *Record of RWM Decontaminants Expert Workshop.*,

Hong J. and Pintauro P. N. (1996) DESORPTION-COMPLEXATION-DISSOLUTION CHARACTERISTICS OF ADSORBED CADMIUM FROM KAOLIN BY CHELATORS. *Water, Air Soil Pollut.* **86**.

Jackson M. L. (1969) Chemical Compopsition of Soils. In *Chemistry of the Soil* (ed. F. E. Bear). American Chemical Society, London.

Jambor J. L. and Dutrizac J. E. (1998) Occurrence and Constitution of Natural and Synthetic Ferrihydrite, a Widespread Iron Oxyhydroxide. *Chem. Rev.* **98**.

Kim C., Lee Y. and Ong S. K. (2003) Factors affecting EDTA extraction of lead from lead-contaminated soils. *Chemosphere* **51**.

McLaren R. G., Backes C. a., Rate A. W. and Swift R. S. (1998) Cadmium and Cobalt Desorption Kinetics from Soil Clays: Effect of Sorption Period. *Soil Sci. Soc. Am. J.* **62**, 332.

McLaren R. G., Lawson D. M. and Swift R. S. (1986) Sorption and desorption of cobalt by soils and soil components. *J. Soil Sci.* **37**, 413–426.

Rashid M. A. (1974) ABSORPTION OF METALS ON SEDIMENTARY AND PEAT HUMIC ACIDS. *Chem. Geol.* **13**, 115–123.

Schwertmann U. and Cornell R. M. (2003) *Iron oxides: Structure, Properties, Reactions, Occurrences and Uses.*, Wiley-VCH.

Spadini L., Manceau A., Schindler P. W. and Charlet L. (1994) Structure and Stability of Cd2+ Surface Complexes on Ferric Oxides 1. Results from EXAFS Spectroscopy. *J. Colloid Interface Sci.* **168**, 73–86.

Spark K. M., Wells J. D. and Johnson B. B. (1995) Characterizing trace metal adsorption on kaolinite. *Eur. J. Soil Sci.* **46**, 633–640.

Tadesse B., Donaldson J. D. and Grimes S. M. (1994) Contaminated and polluted land: A general review of decontamination management and control. *Chem. Technol. Biotechnol.* **60**.

Thompson H. A., Parks G. A. and Brown G. E. (1999) Dynamic interactions of dissolution, surface adsorption, and precipitation in an aging cobalt(II)-clay-water system. *Geochim. Cosmochim. Acta* **63**.

Thompson H. A., Parks G. A. and Brown G. E. (2000) Formation and Release of Cobalt(II) Sorption and Precipitation Products in Aging Kaolinite–Water Slurries. *J. Colloid Interface Sci.* **222**, 241–253.

Wendling L. A., Ma Y., Kirby J. K. and McLaughlin M. J. (2009) A Predictive Model of the Effects of Aging on Cobalt Fate and Behavior in Soil. *Environ. Sci. Technol* **43**.

Chapter 7: Conclusions

7.1 Summary

Cobalt has the potential to be released into the environment either in its stable or radioactive forms because of its use in industry and its presence in low level radioactive waste. Therefore, it is important to understand how it reacts with common phases found in soils, such as iron oxides, clay minerals, and organic matter. This detailed scientific understanding is essential for the effective remediation of areas contaminated with Co.

The aim of this thesis was to understand the sorption behaviour of Co in soil environments to aid efforts for clean-up after a contamination event. As a result I chose to investigate Co sorption to ferrihydrite, kaolinite, and humic acid as these sorption processes are likely to dominate Co behaviour in oxic soils and sediments, and these phases represent the dominant sorption surfaces present in soils and sediments. This thesis has presented a comprehensive study of the sorption behaviour of Co^{2+} to a number of different materials (pure soil constituent phases, and composite phases) at a macro- and microscopic level and how this differs in different environmental conditions, whether this behaviour can be accurately modelled in a thermodynamic surface complexation model, how closely Co sorption to soils is representative of sorption to the pure phases, and how effectively a range of desorption agents can reverse sorption after different sorption equilibrium periods.

7.2 Major Findings

Chapter 4 studied the key sorption controlling phases in soils and composite materials. It presented the initial macroscopic results of Co sorption to ferrihydrite, kaolinite, and humic acid, and ferrihydrite-humic acid and kaolinite-humic acid composites. Sorption to each of these phases was generally low (<50%) below pH 6, implying high mobility of Co in these environments. The exception was humic acid, to which sorption was ~100% by pH 4 in environments with low ionic strength (10^{-3} mol L^{-1}) and by pH 6 in high ionic strength conditions (10^{-1} mol L^{-1}). Additionally, the kaolinite-humic acid composite with

2.2 wt% C reached 50% Co sorption by pH ~4.5 and was at ~100% at pH 6. Therefore, in these environments the mobility of Co is low.

EXAFS analysis of these systems provided novel information on the coordination environments of Co sorbed to the 5 phases. It was determined that at low pH (<6.5) sorption to kaolinite and humic acid – and therefore, the kaolinite-humic acid composite – Co formed outer-sphere complexes with the sorbent surface. These are weak bonds that are highly dependent on other ions in solution and therefore it is possibly easy to remove Co sorbed via these complexes. Above pH 6.5, Co formed binuclear bidentate inner-sphere complexes with all of the sorbents under investigation, including ferrihydrite. These are strong bonds that are difficult to break and Co would be less likely to be desorbed. This was the first time that Co sorption to ferrihydrite was studied using EXAFS spectroscopy and therefore provided novel understanding regarding the local environment of Co sorption to an iron oxide.

Additionally, this was the first time Co sorption to ferrihydrite, kaolinite, and humic acid had been studied by STEM. While the ferrihydrite and humic acid systems showed that Co nanoparticles did not form, the kaolinite system showed Co concentrated along one side of the kaolinite particles. Where the Co is present is likely due to highly reactive edge sites that are created when the crystallites break apart.

Ultrafiltration data compared to filtration at 0.22 μm showed that above pH 5, humic acid became solvated and the Co bound to this humic acid phase was dispersed in solution. This provides a potential transport vector for contamination in organic rich environments at pH values above 6 where ~90% sorption would be expected.

The knowledge gained from these methods was used to develop a thermodynamic surface complexation model. The end-member systems were able to be modelled well. For the composite systems, the relevant end-member models were combined assuming a linear component additivity approach and these model fits did not match the EXAFS results, and therefore systems that more closely reflect a true soil system cannot be modelled with an additivity approach.

Chapter 5 continued as an extension of the work completed in Chapter 4. Co was sorbed to 3 different soils with varying C contents – peat, agricultural, and sediment. Sorption to peat soil was greater than that to the other 2 soils, which behaved identically to each other: low sorption below pH 6, and then an increase until 100% sorption is reached at pH 8. The surface complexation model developed in Chapter 4 was tested with these soils. The overall sorption behaviour to peat, agricultural soil and sediment were able to be modelled using the previously constructed humic acid, ferrihydrite-humic acid, and kaolinite models, respectively. However, the models lacked accurate details about the processes involved, so while Co sorption to these natural soils are comparable to sorption to humic acid, ferrihydrite-humic acid composite and kaolinite they are not perfect representations.

Chapter 6 used the knowledge gained in the previous chapters to inform decontamination methods after aging. The effect of ageing on Co sorption to ferrihydrite, kaolinite, and humic acid, was investigated, as well as the effectiveness of 4 desorption agents after different sorption equilibration periods. Ageing did not have an impact on Co sorption to ferrihydrite and humic acid, both of which remained at 100% sorbed for the full 84 day sorption equilibrium. However, Co sorption to kaolinite increased between 1 day and 28 days and then remained stable. Co desorption from ferrihydrite decreased with longer sorption equilibrium period, and XRD spectra show that this is likely due to Co becoming incorporated into the mineral as ferrihydrite transforms into goethite. Therefore, Co mobility decreases with time in environments where ferrihydrite is present.

EDTA was found to desorb the most Co after up to 84 days sorption equilibration period for humic acid and kaolinite. EDTA forms strong chelating bonds that are capable of breaking the inner-sphere complexes binding the Co to the sorbents. However, for ferrihydrite citric acid released the most Co back into solution after up to 84 days sorption equilibration, though EDTA was equally effective at mobilising Co after a 7 day sorption equilibration period due to Co not having been incorporated into the ferrihydrite structure yet.

This implies that for the most effective decontamination, and to avoid mixing decontaminants, the soil should be treated with EDTA within 7 days of the contamination event. This method also will not destroy the soil as much as using

citric acid or HCl (the two desorption agents that dissolved the most ferrihydrite) as little ferrihydrite was dissolved.

7.3 Future Work

Future work in this area should focus on building a complete understanding of cobalt sorption to soil phases. Initially, using the work in this thesis as a starting point, this could be carried out by producing a ferrihydrite-kaolinite-humic acid composite and modelling the Co sorption data. The data could be compared to the Co sorption to natural soils to determine whether the sorption behaviour is similar and whether this composite is a good approximation to sorption to the natural soils. The ferrihydrite-kaolinite-humic acid model could then be adjusted for the correct ratios of the phases in the natural soils and continue the work in Chapter 5 in determining whether a simple model can accurately predict sorption to the complex natural system.

Further work in this area could consist of producing sorption edge data for Co interactions with other common clay minerals such as muscovite, chlorite and montmorillonite, and more stable iron oxides like goethite and Si incorporated ferrihydrite (as this is how ferrihydrite is most commonly found in natural environments (Berquó et al., 2007)). This sorption edge data could then be modelled and the models combined with each other and the models developed in this thesis. It would then be possible to test whether a combination of these soil phases is a good approximation for Co sorption to a range of natural soils, based on the characterisation of the soils under use.

Continuing on from the work carried out in Chapter 4, research should be conducted into the interactions between humic acid and minerals in order to determine why sorption to the composite phases as not additive. This could be carried out using microscopic techniques such as (S)TEM and EXAFS to initially gain an image of how the humic acid coated the surface of the minerals – and possibly whether it is possible to determine where on the composites Co sorbed, as this could show whether Co was preferentially sorbed to one phase of the composite more than the other. EXAFS could then be used to determine the local structure of carbon atoms bound to the mineral phase and potentially investigate the type of bonds between the two phases.

It would be interesting to carry out this work with a range of similar heavy metals. It has already been found that Cu sorbs to iron oxide-organic composites additively (Otero-Fariña et al., 2018) and so it would be interesting to study how other heavy metals (e.g. Zn, Mn, Cr and Ni) behave in similar systems, and why.

The desorption studies carried out in Chapter 6 can be developed further by next investigating the effectiveness of the same desorption agents (DIW, EDTA, citric acid and HCl) on desorption of Co from mineral-organic composites and natural soils. These experiments would be carried out in the same way but with the different sorbent material. Again, this is a way of building up the scientific knowledge from a simple to more complex system to determine whether the basic understanding is a good approximation of the more complex system.

To further test the effectiveness of the desorption agents it would be possible to study the effects of repeated washing cycles. This would be carried out by sampling the solution after the desorption period, removing the solution and replacing it with the initial desorption agent. Doing this would create a new equilibration gradient and could potentially remove more Co from the solid.

Developing this work further with the context of a nuclear contamination event, it would be interesting to carry out the ageing studies using ^{60}Co to investigate whether the radiation emitted affects the chemical bonds and could make decontamination more or less effective. This would be particularly interesting in the case of Co sorbing to organics such as bacteria in the soil as the radiation could damage the bacteria in ways that affect Co binding to it.

7.4 References

Berquó T. S., Banerjee S. K., Ford R. G., Penn R. L. and Pichler T. (2007) High crystallinity Si-ferrihydrite: An insight into its Néel temperature and size dependence of magnetic properties. *J. Geophys. Res. Solid Earth* **112**.

Otero-Fariña A., Peacock C. L., Fiol S., Antelo J. and Carvin B. (2018) A universal adsorption behaviour for Cu uptake by iron (hydr)oxide organo-mineral composites. *Chem. Geol.*